# EFFECT OF PROCESS PARAMETERS ON MICROSTRUCTURE AND PROPERTIES OF SPARK PLASMA SINTERED Al-SiC NANOCOMPOSITES

BY

ISMAILA KAYODE ALIYU

A Thesis Presented to the

DEANSHIP OF GRADUATE STUDIES

**KING FAHD UNIVERSITY OF PETROLEUM & MINERALS**

DHAHRAN, SAUDI ARABIA

In Partial Fulfillment of the
Requirements for the Degree of

# MASTER OF SCIENCE

**In**

MECHANICAL ENGINEERING

MAY 2013

KING FAHD UNIVERSITY OF PETROLEUM & MINERALS

DHAHRAN- 31261, SAUDI ARABIA

## DEANSHIP OF GRADUATE STUDIES

This thesis, written by **Ismaila Kayode Aliyu** under the direction of his thesis advisor and approved by his thesis committee, has been presented to and accepted by the Dean of Graduate Studies, in partial fulfillment of the requirements for the degree of **MASTER OF SCIENCE IN MECHANICAL ENGINEERING.**

**Thesis Committee**

Dr. Saheb Nouari
(Advisor)

Dr. Zuhair Mattoug Gasem
Department Chairman

Dr. Nasser Al-Aqeeli
(Member)

Dr. Salam A. Zummo
Dean of Graduate Studies

Dr. Syed Fida Hassan
(Member)

1/10/13
Date

**DEDICATION**

أَعُوذُ بِاللهِ مِنَ الشَّيْطَانِ الرَّجِيـم،

بِسْمِ اللهِ الرَّحْمَـنِ الرَّحِيـمِ،

**قُلْ إِنَّ صَلَاتِي وَنُسُكِي وَمَحْيَايَ وَمَمَاتِي لِلَّهِ رَبِّ الْعَالَمِينَ**

**سورة الأنعام، الآية١٦٢**

I seek refuge with Allah from the accursed Satan,

In the name of Allah, the Entirely Merciful, the Especially Merciful

**Say, "Indeed, my prayer, my rites of sacrifice, my living and my dying are for Allah, Lord of the worlds.**

Surat Al-'An`ām (The Cattle), verse 162

# ACKNOWLEDGEMENT

Alhamdulillah, I thank Allah, for giving me the strength, means and skills to carry out this work. I thank my parents for guiding and sponsoring me to acquire basic and further education. Also, I say thanks to my wife, children and the rest of my family members for their patience and support. I commend King Fahd University of Petroleum and Minerals (KFUPM) and the Ministry of Higher Education (MoHE), Saudi Arabia for awarding me the scholarship to undertake this degree. My appreciation also goes to Advanced Manufacturing Technology Program (AMT-P), NASENI, Jalingo, Nigeria for their support.

My Advisor; Dr Nouari Saheb, Associate Professor, Department of Mechanical Engineering, KFUPM, has helped me a lot to develop my research skills; hence, I acknowledge him. I also acknowledge the contributions of Dr. Nasser Al-Aqeeli, Dean of Scientific Research, KFUPM, and my thesis committee member, to my thesis success. I express my gratitude to Dr. Syed Fida Hassan, Associate Professor, Department of Mechanical Engineering, KFUPM, and my thesis committee member. He gave me valuable advices and suggestions.

My profound gratitude goes to Dr. Abbas Saeed Hakeem, Research Scientist, Center of Excellence in Nanotechnology, KFUPM. He gave me adequate technical assistance that allowed me to use the Scanning Electron Microscope and the Spark Plasma Sintering machine successfully. He also offered me lots of valuable advices. Also, I acknowledge the assistance of Dr. Mohammed Nasiruzzaman Shaikh and Mr. Akolade Idris. I thank

Mr. Mohammad Latif Hashmi and Mr. Sadaqat Ali for their support I got in the Materials Science Laboratory.

I thank Abdullah Kachala and Abdullah Khalil for their advices and suggestions. Siddiqui Muhammad Usama, Mohammad Khwaja, Zafar Iqbal Fateh Muhammad, Abdul Azeem Mohammed and Muhammad Luqman also deserve my gratitude for their help.

Financial support for this work from Deanship of Scientific Research (DSR) through research project number IN121008 is highly acknowledged.

Finally, I express my gratitude to anyone I didn't mention that has assisted or contributed to the success of this research in one way or the other.

# TABLE OF CONTENTS

# LIST OF TABLES

# LIST OF FIGURES

# ABSTRACT (ENGLISH)

Full Name : Ismaila Kayode Aliyu

Thesis Title : Effect of Process Parameters on Microstructure and Properties of Spark Plasma Sintered Al-SiC Nanocomposites

Major Field : Mechanical Engineering

Date of Degree : May, 2013

The inadequacy of metals and alloys in providing both strength and stiffness to a structure has led to the development of metal matrix composites (MMCs) where rigid ceramic reinforcements are embedded in ductile metal or alloy matrix. MMCs combine metallic properties i.e. ductility and toughness with ceramic characteristics i.e. high strength and modulus. These composites are extensively used in automobile and aerospace applications because of their attractive physical and mechanical properties. Further improvement of the properties of MMCs was possible using nano-size reinforcement and/or matrix; this led to the development of metal matrix nanocomposites (MMNCs). However, there are challenges associated with processing nanocomposites with the desired properties. These challenges include uniform distribution/dispersion of the nano-size reinforcement and grain growth of the matrix phase. Ball milling (BM), a powder metallurgy processing technique, which involves cold welding, fracturing and rewelding of powder particles, is being used to achieve a uniform distribution of the nanoreinforcement phase. Also, spark plasma sintering (SPS), a binder less process, which does not require a pre-compaction step, has been shown to be effective none-

conventional sintering method for obtaining fully dense materials with preserved nanostructure. Although, few published works reported the synthesis of Al-SiC nanocomposites using BM and SPS, the process was not fully investigated and effect of all critical sintering parameters i.e. compaction pressure, heating rate, sintering temperature, and sintering time on Al-SiC nanocomposites properties was not fully analysed. Hence, the main objective of this research work is to study the effect of BM and SPS process parameters on the microstructure and properties of Al-SiC metal matrix nanocomposites. Aluminium based nanocomposites containing 1, 5 and 10 wt% SiC were mechanically milled between 0 and 28 hours. Milling for 24 hours led to crystallite size reduction of the aluminium phase and homogeneous dispersion of the SiC nanoreinforcement which was maintained even after sintering. Spark plasma sintering experiments were carried out on the milled powders at a pressure from 20 to 50 MPa, and heating rate from 100 to $300^0$C/min. Maximum density and hardness were obtained at 50 MPa and $200^0$C/min. These values were kept constant while temperature was varied from 500 to $600^0$C and holding time from 5 to 15 min in the second phase of experiments where a sintering temperature of $600^0$C and a sintering time of 10 min. led to better densification and improved properties. A unique needle like structure that resulted in high strength was observed for composites sintered at 50 MPa and 10 min. Compression tests were carried on samples, which showed good combination between densification and properties, at compression rate of 1mm/min. Al -10 wt% SiC had the highest strength with a 200% increase above base material.

# ملخص الرسالة ABSTRACT (ARABIC)

**الاسم الكامل : إسماعيل كايودي عليو**

**عنوان الرسالة : تأثير عوامل التلبيد عن طريق شرارة البلازما على البنية المجهرية وخواص المواد المركبة النانوية من اللألومنيوم المدعوم بكربيد السيلكون**

**التخصص : الهندسة الميكانيكية**

**تاريخ الدرجة العلمية : مايو ٢٠١٣**

نظرا لعدم إمتلاك المعادن وسبائكها الخواص الميكانيكية الكافية لإستعمالها في تطبيقات كثيرة تم تطوير المواد المركبة ذات الأساس المعدني المدعومة بطور خزفي حيث تجمع هذه المواد بين مواصفات المعادن و مواصفات المواد الخزفية. هذه المواد المركبة تستخدم كثيرا في صناعة وسائل النقل مثل السيارات و الطائرات لما تتمتع به من خواص فيزيائية و ميكانيكية عالية. هذه الخواص يمكن تحسينها أكثر إذا كان الطور الخزفي الداعم ذا أبعاد من رتبة النانو حيث أدى هذا إلى تطوير المواد المركبة النانوية. رغم أن إنتاج ومعالجة هذه المواد المركبة النانوية لازل يواجه مجموعة من الصعوبات مثل تكتل الطور الخزفي الداعم و نمو حبيبات الطور المعدني الأساسي مما يؤثر على خواصها فإن استخدام طريقة المعالجة بالبودرة و الطحن الميكانيكي أظهر نتائج متميزة في تحضير مواد مركبات نانو متجانسة. من جهة أخرى أظهرت طرق التصنيع الغير تقليدية مثل التلبيد عن طريق شرارة البلازما قدرة عالية على التحكم بنمو الحبيبات والحد منه. ويمكن تلخيص أهداف هذا البحث في دراسة تأثير عوامل الطحن الميكانيكي و التلبيد عن طريق شرارة البلازما على البنية المجهرية و الخواص الميكانيكية للألومنيوم المدعوم بطور خزفي نانوي هو SiC. تم تحضيرمركب نانوي من الألومنيوم المدعوم ب 1, 5, 10 % وزنا من SiC عن طريق الطحن لمدة تتراوح بين 0

و 28 ساعة. وجد أن الطحن لمدة 24 ساعة أدى إلى تقليص البعد الحبيبي للألومنيوم بالإضافة إلى التوزيع المتجانس للطور الداعم. في المرحلة الأولى تم تلبيد العينات المحضرة عن طريق شرارة البلازما تحت ضغط بين 20 و 50 ميجا باسكال, و معدل تسخين بين 100 و 300 درجة مئوية لكل دقيقة. وجد أن أعلى كثافة تم تحصيلها هي عند معدل تسخين 200 درجة مئوية لكل دقيقة و ضغط 50 ميجا باسكال. هذه القيم تم إبقائها ثابتة عندما تغيير درجة الحرارة ما بين 500 و 600 درجة مئوية وزمن التلبيد بين 5 و 15 دقيقة في المرحلة الثانية من التجارب. عند إستخدام 600 درجة مئوية و 10 دقائق وجد أن معدل التلبيد أزداد و الخواص الميكانيكية تحسنت. كما لوحضت بنية مجهرية مميزة على شكل إبر مما أدى إلى خواص عالية للعينات التي تم تلبيدها لمدة 10 دقائق عند ضغط قدره 50 ميجا باسكال.

# CHAPTER 1

# INTRODUCTION

The increasing need for metallic materials with better physical and mechanical properties to satisfy current applications in aerospace, automobiles etc. has led to continuous metals development. In the history of metals exploration, alloys were first developed from two or more different metals. Later on, composite materials were synthesized from metals and alloys. They are referred to as Metal Matrix Composites (MMCs) obtained by embedding a rigid ceramic reinforcement in a ductile metal or alloy matrix. Developed to a micro scale, MMC is currently evolving from a micro scale to a nanoscale. The dimension of one or more of the constituent materials of a Metal Matrix Nanocomposite (MMNCs) should be less than 100nm. MMNC has been explored and observed to be a means of developing metal matrix composite with improved and desired physical and mechanical properties [1-5]. For instance, the strength of Al reinforced with 1 vol% nanoscale $Si_3N_4$ is higher than that of Al reinforced with 15 vol% microscale SiC particles [6]. The success of MMNCs development has helped tremendously the automobile and aerospace industries due to their high specific strength, low coefficient of thermal expansion, high thermal conductivity, and low weight. However, challenges such as the dispersion of the reinforcement in the matrix and grain growth are faced in obtaining the composites with excellent properties.

There are two parent categories of synthesis that researchers have so far adopted in composites fabrication. In in-situ, the reinforcement is formed as a product of chemical reaction of the raw materials used while ex-situ involves external addition of reinforcement [7]. The ex-situ method is further divided into Liquid state (casting) and solid state (powder metallurgy) processing. In the liquid state processing, composite development and reinforcement distribution are achieved by one of die casting, mechanical stirring, squeeze casting, spraying, ultrasonic cavitation and infiltration [7, 8]. Casting is cheap however there are lots of drawbacks in its application for metal matrix nanocomposite development. Problems such as contamination and non-uniform dispersion were faced during a casting that involved the use of ultrasonic wave for dispersing SiC in Al and Mg [9, 10]. Also liquid state processing method can lead to the formation of unwanted and brittle phases like $Al_4C_3$ and Si, in the case of Al-SiC composite [11, 12] due to processing at elevated temperature. Other problems associated with liquid state dispersion and synthesis method include porosity and poor wettability of reinforcement with liquid matrix [7, 12-15]. The solid state processing which involves powders grinding then sintering has been found useful in solving these problems. Conventional powder metallurgy techniques include cold isostatic pressing (CIP), hot isostatic pressing (HIP), hot pressing, hot extrusion and hot rolling [8, 16]. Nonconventional solid state processing includes microwave sintering (MW) and spark plasma sintering (SPS). The SPS process has emerged the best method of consolidating powders after milling. The process involves simultaneous application of pulse DC current and uniaxial pressure. With this, a heating rate as much as $1000^0$C can be achieved [17].

This enables short sintering time and fully dense composite material [18] with minimum grain growth and preserved nanostructure. The process does not require the use of binders nor pre-compaction. Khalil [18] sintered Al 6061 alloy using HIP, MW, SPS and furnace sintering (FS) and found that the highest density (100%) was obtained from SPS sample. Powder metallurgy techniques require a pre-powder preparation by mechanical milling. With mechanical milling, uniform dispersion, grain refinement and prevention of unwanted phase formation can be achieved. Rostamzadeh and Shahverdi [11] stated that this can improve the mechanical properties of the composite. Csanády used SPEX 9000 and a Frisch Pulverisette 4 mill to achieve uniform dispersion of Pb in Al matrix[19].

Nanoparticle reinforcements such as SiC, TiC, $Al_4C_3$, WC, TaC, $TiB_2$, $AlB_2$ AlN, and $Al_2O_3$ have been used with metals like Al, Co, Cu, Fe, Mg, Mo, Ni, Ti and W to produce MMNC [7, 20]. It is know that Al is an ideal candidate in metal matrix nanocomposite for its excellent properties such as light weight, low melting point [21], high corrosion resistance, great formability etc. This has allowed its wide range application in aerospace, high temperature and pressure need, turbines, aircraft, building materials, desalination machined components and automobiles for quite a long time. SiC has excellent mechanical properties such as high hardness, strength, modulus of elasticity wear resistance, oxidation resistance and corrosion resistance [14, 22, 23]. It has been found very good for Al reinforcement; SiC is thermodynamically stable and has good wettability with Al [22-24]. However, Al-SiC development has not been fully explored despite the potentials of SiC nanoparticles to improve the properties of Al matrix.

The development of metal matrix nanocomposite is still in its embryonic stage. Al-SiC nanocomposites have been synthesized using MM and SPS however, only very little work has been done in this area. The challenges mentioned earlier were not overcome and the SPS process parameters effects on sintered composite were not fully investigated. These are some of the main reasons hindering the commercialization of metal matrix nanocomposite. In the present work, SiC will be uniformly dispersed in Al matrix by the use of MM, then sintered in an SPS machine. This will help to avoid agglomeration of reinforcement, grain growth and unwanted phase formation during sintering. Also the process parameters will be varied to account for adequate investigation of their effects on sintered composites.

# CHAPTER 2

# LITERATURE REVIEW

## 2.1 Metal Matrix Composites and Nanocomposites

Metal matrix composites (MMCs) involve the dispersion of hard ceramic and brittle component in a ductile metal matrix in order to obtain a composite material with high strength, hardness, wear resistance, thermal stability and corrosion resistance[2]. Additional properties of MMCs include high specific stiffness, high plastic flow strength, creep resistance and good oxidation [12]. These improved properties have resulted in MMCs being extensively used in industries such as aerospace and automobile industries. In order to further improve the properties of composites due to increasing quality demand, efforts have been made to develop Metal matrix nanocomposites (MMNCs). An MMNC is a composite whose one or more of its constituent has a particle size less than 100nm [4]. Possible distributions of the reinforcement in the matrix [14] can be seen in Fig. 2.1. The open hexagons represent the matrix grains while the open and filled circles represent the reinforcement phase(s). The reinforcement phase is distributed along the grain boundaries of the matrix phase in Fig. 2.1 (a), but it is inside the matrix grains in Fig. 2.1 (b). The reinforcement phase is both inside the grains and along the grain boundaries in Fig. 2.1 (c) while in Fig. 2.1 (d), both the matrix and reinforcement grains (filled hexagons) are uniformly distributed An implication of using nano scale particles is a change of the physics of synthesis at nano scale and consequently introduction of

ample synthesis challenges. These challenges include poor interfacial bonding, excessive agglomeration of reinforcement, unwanted phase formation and grain growth during sintering. Unlike conventional MMCs, the commercialization of MMNCs is limited due to the mentioned challenges. However if these challenges can be overcome, MMNCs have the potential of providing property improvement over MMCs. Saberi et al [12] studied the role of nano-size SiC on lattice strain and grain size of Al/SiC nanocomposite. They compared micro and nano scale SiC reinforced composites and found that the crystallite size of nano scale SiC reinforced matrix was smaller after milling both for 10 hours. This indicates that nano sized reinforcement serves as better grinding medium than micro sized ones resulting to higher strength.

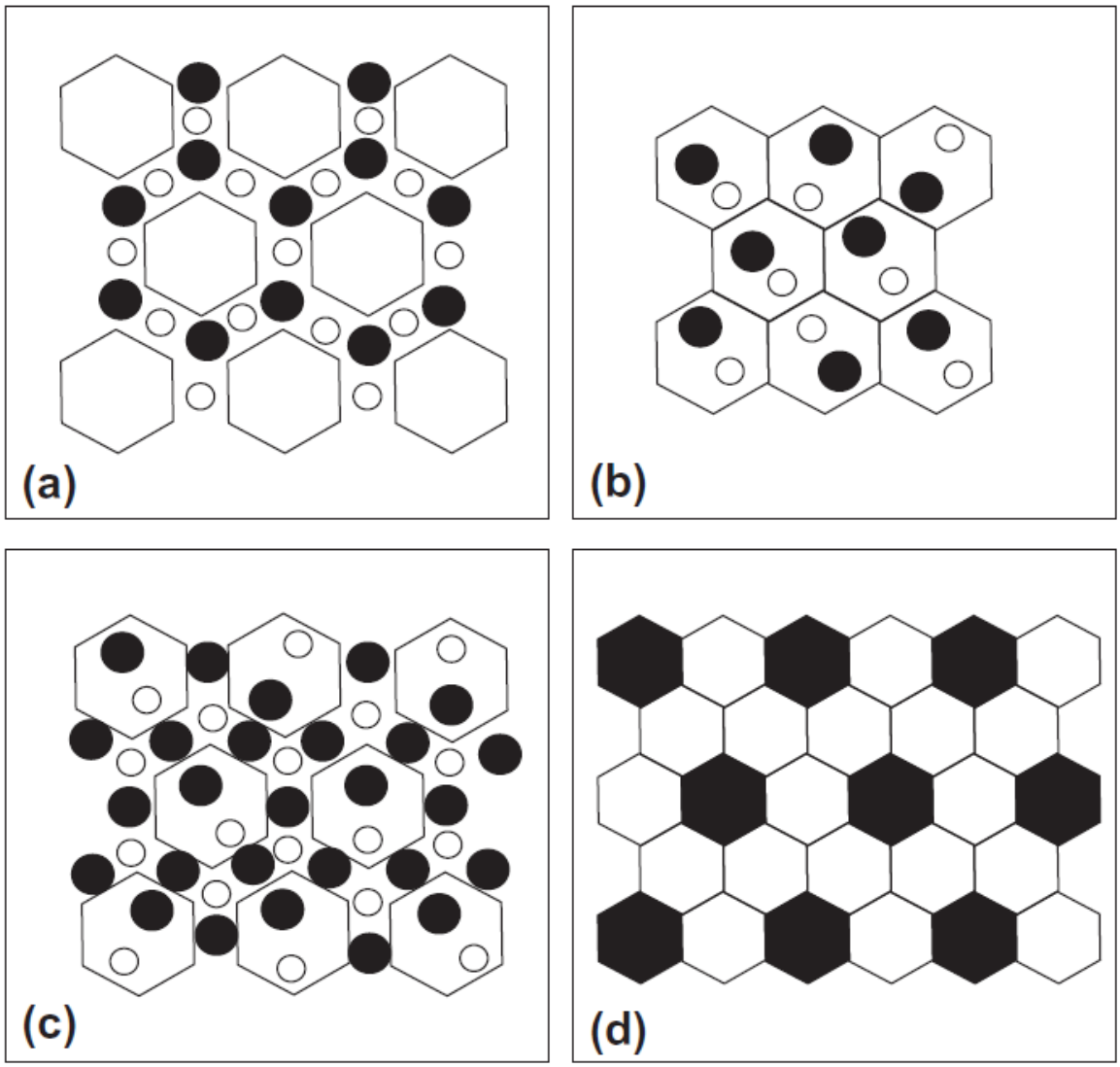


Fig. 2.1 Possible distribution of the matrix and reinforcement phases in a nanocomposite [14].

The main challenges faced in the development of MMNCs include:

- Agglomeration and non-homogenous dispersion of reinforcement in the matrix [5].
- Reaction between the interfaces (bonding) is not clear; this affects strengthening. To obtain high strength, interfacial bonding should be strong [5, 8].
- Cost of the development of MMNCs [5].
- Grain growth during sintering [8].

The MMNCs that have been successfully synthesized include Al-$B_4C$, Mg-SiC, Al-CNT, Cu-CNT, Ti-SiC (prepared using powder metallurgy), Al-SiC, Mg-SiC, Al-$Al_2O_3$, Al-CNT, Mg-$Y_2O_3$, Al-Diamond, and Zn-SiC (prepared using solidification processing) [1]. Ti and Ni alloys reinforced with Al2O3, SiC particulates and whiskers [12] and Al-Cu-SiC were also synthesized [25].

## 2.2 Mechanical Milling

### 2.2.1 The Process

Mechanical milling (MM) is a ball milling process in which powders placed in vials are subjected to high energy impact by balls [26]. It is a non-conventional alternative solid state means of producing advanced nanomaterials. MM helps to obtain desired structures, compositions, physical and mechanical properties. It enables material production at a lower temperature i.e. the bottom of the phase diagram. It is also referred to as mechanical alloying (MA) by some researchers whereas others consider both to be a type of ball milling. They state that MA involves milling of powders of different materials in

which alloy formation is expected at the end while MM refers to milling of powders of similar metals or alloys or compounds. Reactive milling refers to a milling in which a chemical reaction occurs during the milling. This can lead to formation of ultra-fine dispersed particles [27]. With ball milling, ranges of materials such as metastable, amorphous, nano crystalline, metal-ceramic composites metal composites and novel materials can be produced [27-29].

### 2.2.2 Principles and Mechanism of Mechanical Milling

Mechanical milling is a non-equilibrium method of synthesizing materials. It involves bringing a material into a metastable state and then tailoring it to the desired structure and properties. It shares the similarity of "energizing and quenching" concept with techniques like rapid solidification process, vapour deposition, ion implantation and plasma processing [30].

Fig. 2.2 illustrates how an external energy is used to put the material in an energy level beyond the metastable state. Then by one of these methods, the material passes through metastability to equilibrium state. MA can take the material much farther from equilibrium than couple of other methods such as Solid state quenching, Rapid solidication and Mechanical cold working [30].

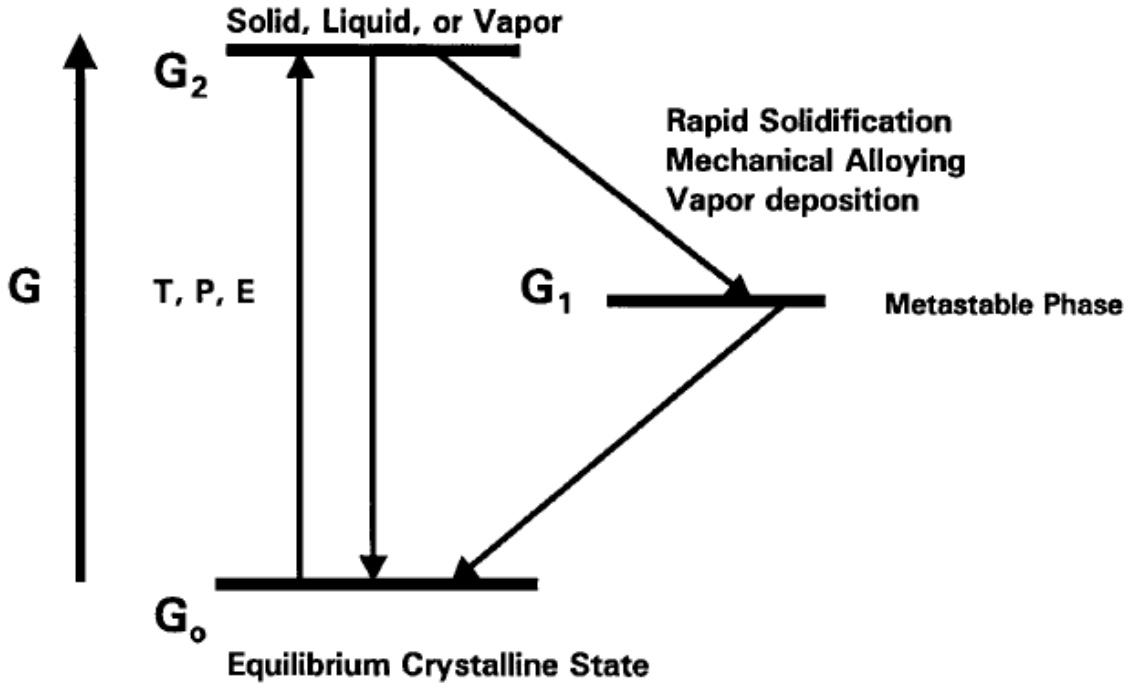


Fig. 2.2 The basic concept of ``energize and quench'' to synthesize non-equilibrium materials [30].

The major events that take place during ball milling are continuous repetition of particles fracturing, plastic deformation and cold welding [27, 31] resulting to further particles fragmentation. The possibility of ball milling process to continue depends on two factors:

1. The rate of cold welding must balance the rate of particle fracturing.
2. Average particle size should be relatively coarse.

The main objective of mechanical milling is to prepare powders for sintering process. In cases where the powder is a mixture or composites, it performs the function of blending the powders properly to give even distribution before sintering is done [30]. In terms of microstructure the process of ball milling can be divided into four stages.

**Initial stage**: This involves flattering of particles due to collision as shown in Fig. 2.3. Wide range of particle size is present. It may also be partly due to alloy nature (hard or ductile). In this stage chemical composition of particles varies within and between particles. The step isn't sufficient to achieve homogenous size and shape distribution. This is due to duration; as a result homogeneity is only expected in further steps [26].

**Intermediate stage:** In this step, welding becomes significant. Layered structure (Lamellae) is obtained due to fracturing and subsequent cold welding. The structure of the powder gets refined [26].

**Final stage**: There is more particles refinement in this stage. Rather than layered structure, homogenous particles at the macroscopic scale are obtained. This implies that equilibrium between fracturing and welding has occurred and a true alloy has been formed. The chemical composition attained is also homogenous [26].

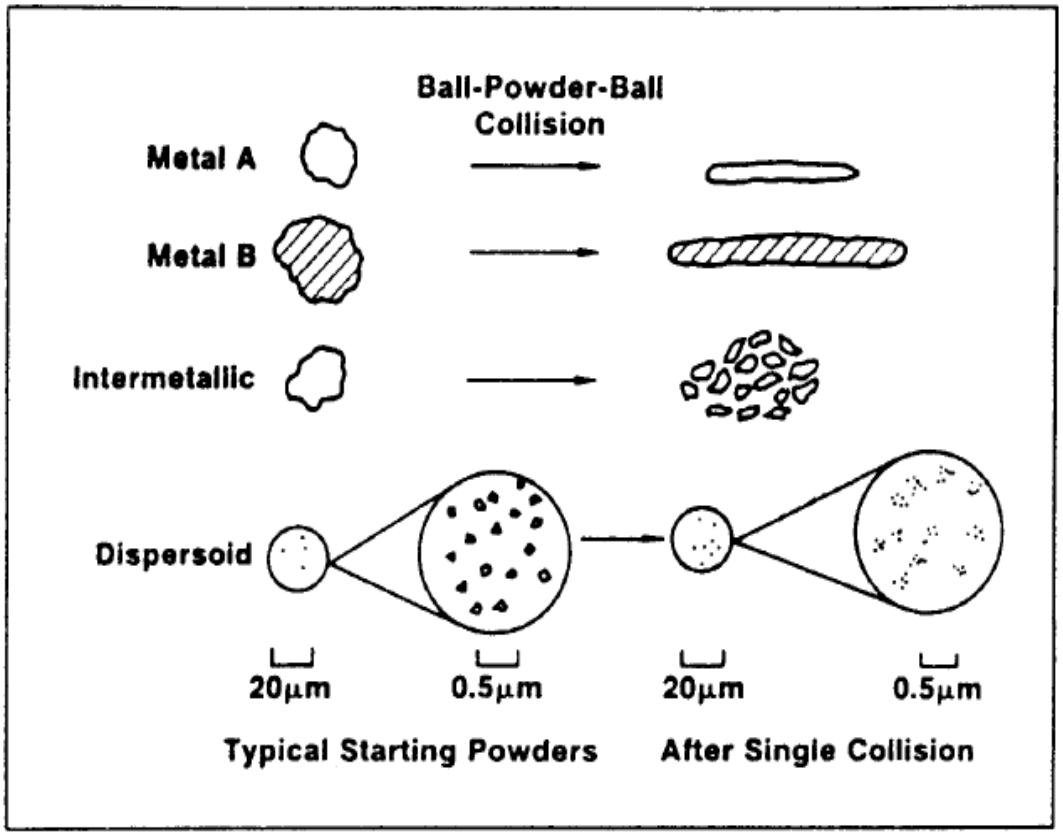


Fig. 2.3 Shape and size change for different types of milling system after collision [31].

Finer welded particles require greater force to fracture them. As a result of this, during alloying, particles either undergo fracturing or welding depending on the predominant force (the force required to cold weld or the force required to de-agglomerate and fracture) until there is equilibrium when none will further occur. The balance between these two forces determines the average particle size of the powder. Eventually, the powder becomes so fine that it is no longer lamellae and homogenous chemical composition is attained [26].

**Completion stage:** During this stage, the powder particles are extremely deformed and no further improvement can be obtained by alloying. Thus, an alloy with composition similar to the starting constituents is formed. Microscopes with resolutions higher than optical or scanning electron microscopes are needed for the resolution of the lamellae [26].

During MM, as the mill rotates the vial, grinding balls collide with each other and with the wall of the vial. In the process, an amount of powder is trapped between any two colliding balls or a colliding ball and the vial wall as seen in Fig. 2.4. Impact force plastically deforms the powder leading to fracture. The new surface created causes ease of welding resulting in particle size increase [30]. This is the case for ductile materials. Brittle materials have to be milled for relatively longer time before they can behave ductile; welding together. The structure of the powder is flake like at this stage and hence further fragmentation occurs with continuous ball collision. If the predominant force is fracture, there will be continuous decrease in particle size. This cause increase in number

of layers in a particle and consequence decease in interlayer spacing. The efficiency of particle size reduction is low; therefore energy not used for particle size reduction, elastic or plastic powder particles deformation is lost as heat [30].

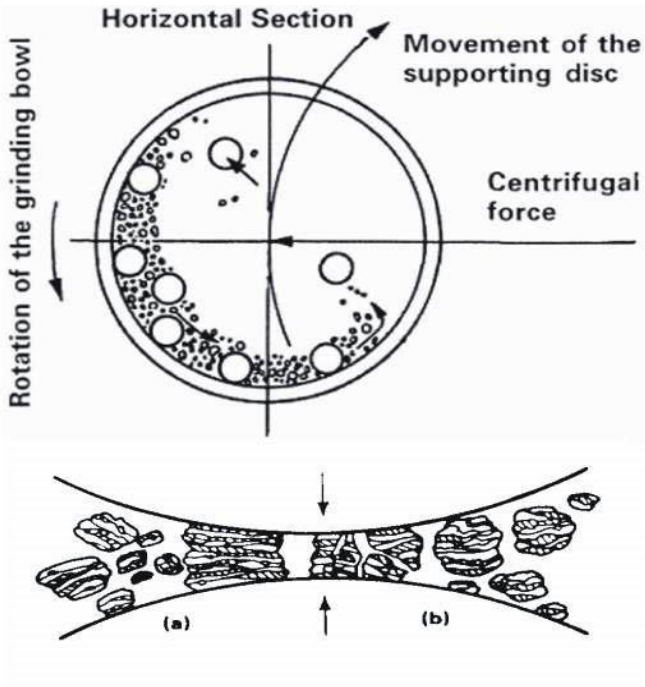


Fig. 2.4 Scheme of ball movement within high energy mill showing ball-powder-ball collision of powder mixture during mechanical alloying [32]

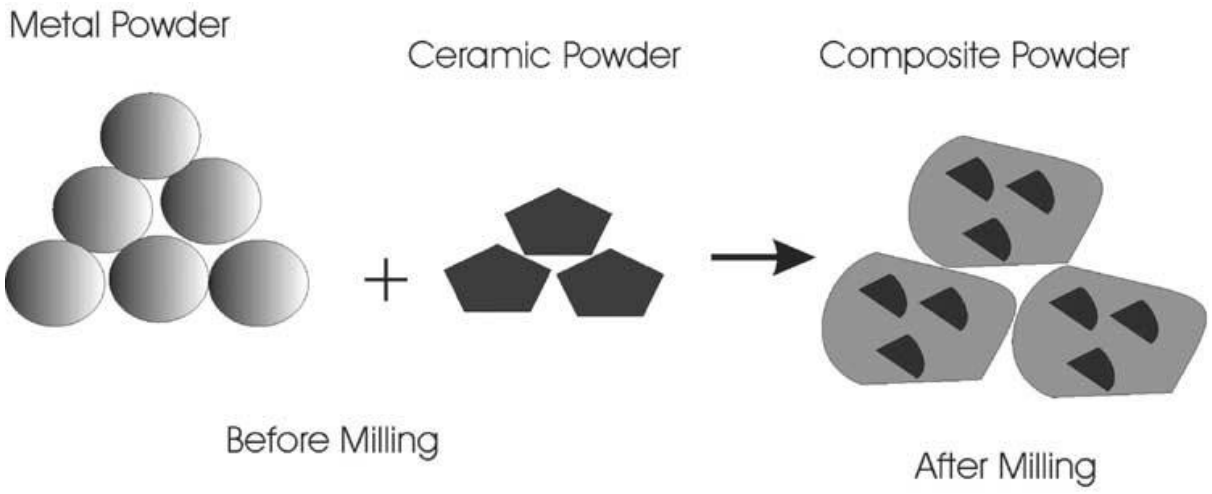


Fig. 2.5 Schematic diagram showing the formation of composite powder after high-energy mechanical milling [29].

During milling, steady-state is attained when rates of welding and fracturing balance each other. At this stage, the rate of particle size growth by agglomeration equals the rate of particle size reduction by fracturing. Each particle then has composition similar to the starting powder and strain energy is accumulated to saturation. This can be seen in Fig. 2.6. The deformation occurring during ball milling causes defects like dislocations, vacancies, stacking faults, grain boundaries. These defects and temperature rise during milling help to increase diffusion for attainment of true alloying. The relationship between particle size reduction and milling time is approximately logarithmic. There are three possible systems during ball milling of two powders; (i) ductile-ductile, (ii) ductile-brittle, and (iii) brittle-brittle systems. It will be expected that alloying will not occur for brittle-brittle system due to the absence of ductility that enhances cold welding. But alloying in such systems have been reported in some case [30]. This is because at very small particle size the powder start behaving ductile [30].

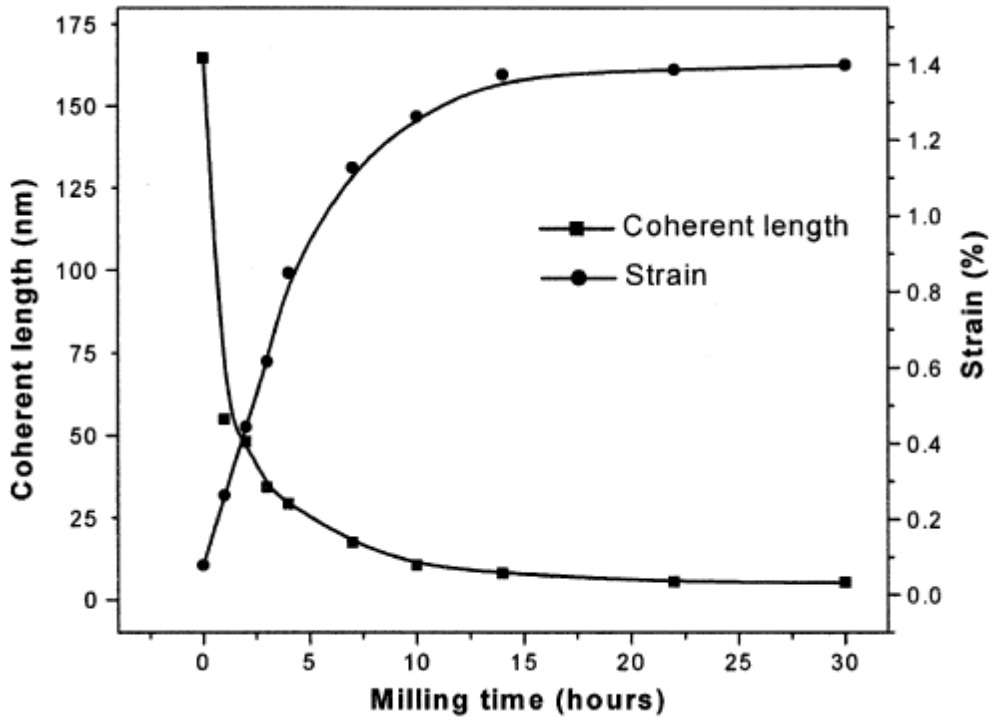


Fig. 2.6 Coherent length and strain vs. milling time [33].

### 2.2.3 Milling Parameters

**Type of mill:** The characteristics to be considered when selecting a mill type for a particular ball milling(type, quantity of powder, and the final constitution required) include; capacity, speed of operation, ability to control the operation by varying the temperature of milling and the extent of minimizing powders contamination. According to Suryanarana [30], the SPEX shaker mills are used for alloy screening purposes. The Fritsch Pulverisette planetary ball mills or the attritors are used to produce large quantities of powder.

**Milling container:** Vials should be made of strong materials like hardened steel, tool steel, hardened chromium steel, tempered steel, stainless steel, tungsten carbide cobalt composite, tungsten carbide lined steel [34] or bearing steel. Some other materials are used for special ball milling purpose.

**Milling speed:** The higher the mill's speed, the higher is the energy input into the powder. However excessive speed can cause balls to pin to the walls of the grinding container minimizing force exerted on powder. Also, temperature may rise beyond a desired value if there is no diffusion requirement for homogenization. This could cause decomposition of non-equilibrium phase formed [30]. High temperatures can also cause grain growth and powder contamination. Speed of milling also accounts for formation of amorphous or crystalline structure.

**Milling time:** Time just enough for the milling of a powder based on the milling condition should be adopted. More milling time can increase powder contamination.

Factors that affect milling time include type of mill used, the intensity of milling, the ball-to-powder ratio, and the temperature of milling [30]. Fig. 2.6 shows that powder particle size is inversely proportional to milling time and becomes steady at a time. The steady state is the appropriate milling end time.

**Grinding medium:** The density and size of the milling balls affect the end product of the powder; higher density will have greater impact on the powder. Difference in size can mean difference in formation of solid solution or mixture, crystalline or amorphous phases [30] etc.

**Ball-to-powder weight ratio (BPR):** This is the mass ratio of milling balls to milled powders sometimes called charge ratio CR. In practice various ratios are used such as 10:1, 50:1 up to 100:1 mills with higher capacity are the ones that than accommodate higher ratio[2]; The higher the BPR, the faster the milling.

**Extent of filling the vial:** The vial should not be too full. This reduces the effect of milling. 50% filling is recommended [30].

**Milling atmosphere:** Milling container should be evacuated or filled with an inert gas such as argon or helium to avoid powder contamination by reacting with the milling atmosphere. Care should be taken while choosing a milling atmosphere due to the possibility of contamination. The atmosphere also is found to affect the final structure of the powder in terms of formation of amorphous phase in the presence of a particular atmosphere.

**Process control agent PCA:** It is used to minimize the effect of cold welding. This helps to prevent or minimize agglomeration. This reduces milling time and/or gives finer

particles. Examples of PCAs include stearic acid, hexane, methanol, and ethanol. A liquid PCA is preferable to solid; a homogeneous distribution of particle size can easily be attained with liquid PCA. The impurity induced by PCA in the powder is rated with a term called yield. A high yield refers to low impurity. Hence PCA that gives the minimum impurity is desired.

**Temperature of milling:** The milling temperature has effect on the milled powder due to diffusion enhancement. Different milling temperatures cause variation in solid solubility levels, or type of phase formed. The extent of solid solubility was reported to decrease at higher milling temperatures [30]. Researchers have investigated the effect of varying milling temperature on milling outcomes and found that at higher temperatures, the root mean square (rms) strain decreases while grain size increases. Also, it was found that higher milling temperature enhances the formation of amorphous phase in some powders.

**Powder contamination and prevention/minimization**

There is a possibility of powder contamination especially when reactive metal powders like Titanium and zirconium are milled. The level of contamination depends on the milling time, the milling intensity, the atmosphere in which the powder is milled, and difference in the strength/hardness of the powder and the milling medium [30]. Major sources of impurities include oxygen and Nitrogen, from the atmosphere and/or PCAs used, and iron from the steel grinding medium and the steel container [30]. Also impurities can result from chemical impurity of the starting powders. The amount of contamination increases with milling time. Contamination can be minimized by using

similar material as the powder for the vial and milling medium. Generally harder materials should be used for the milling medium and the vial. Vials should be adequately sealed to avoid atmospheric contamination. Use of vacuum or inert gas and Teflon seal can help to achieve this. PCA choice and milling condition should be such that it doesn't react with milled powders.

## 2.3 Mechanically Milled Al-SiC Nanocomposites

El-Daly et al. [35] ball milled and characterized SiC reinforced aluminium matrix nanocomposites using non-destructive technique. Three powder composites (Al containing 2.5, 7.5 and 12.5 vol. % SiC) were ball milled at a Speed of 320rpm and BPR of 20:1, 10:1 w for 10 h under argon atmosphere. The characterization of the milled powder was done using SEM and TEM to check the microstructure. XRD (Cu Kα radiation ($\lambda = 0.15406$ nm) operated at 30kv and 25mA along with The Williamson–Hall method was used to analyse the particle size and lattice strain accumulation. XRD chart showed no peak for $Al_4C_3$ and Si but FCC Al and Hexagonal SiC [35], after milling meaning there was no solid-state reactions between Al and SiC in all compositions during milling [35]. XRD analysis also showed that SiC content enhanced crystallite size reduction during milling; 97.9 nm was obtained for Al-12.5 vol. % SiC compared to other lower compositions, 2.5 vol. %, 175.6nm milled for same amount of time. EDS analysis was used to confirm the absence of $Al_4C_3$ and Si after 10h ball milling and show there was uniform distribution of the reinforcement in Al matrix although small amount of clustering was observed in some local areas.

In order to prepare powder samples for sintering, Zhang et al [36] milled two Al- 20 vol% SiC composite powders with same Al matrix size (6μm) but different reinforcements sizes (12μm and 45μm). Alumina balls were used instead of steel to avoid excessive SiC size reduction. BPR of 8:1, turn table speed of 240rpm and vial relative speed ratio of 2 were used. The 10 h milling was done in argon atmosphere using ethanol as the PCA. SEM micrograph showed that milled powders have rounded morphology and uniformly distributed SiC. Zhang et al observed that size reduction was prevalent in the case of Al - 45 μm SiC than Al- 12 μm SiC. This is because larger SiC is more difficult to embed in Al and therefore experiences more fracturing [36].

Yadav [8] ball milled Pure Al and SiC nanocomposite. The milling process parameters included BPR of 5:2, acetone as the PCA, Polyacrylic as the dispersive agent, a speed of 500rpm and milling time of 30 minutes. Al-SiC of three compositions were milled; 5, 10 and 20 wt%. EDS results showed that ball milling gave uniform dispersion of SiC in Al.

Al-5% vol SiC nanocomposite powders was mechanically milled at a Speed of 300 rpm and BPR of 15:1 from 0 to 25 h under argon atmosphere [11]. 1.5 wt. % stearic acid was used as the process control agent. At intervals of 5 hours, samples were taken and characterized using SEM, EDS, XRD TEM and X-ray mapping. The Williamson–Hall method was used to obtain the crystallite size and the lattice strain. Secondary phases were not formed, rather peaks broadened as time increased. Near-spherical nanostructured composite powder with a uniformly distributed reinforcing phase in a laminated aluminium matrix was obtained [11].

Saberi et al [12] milled micros and nano scale SiC reinforced Al for up to 10 h at 36.2 Hz and 10:1 BPR. In comparison with base Al, two volume fractions were investigated; Al - 2.5% vol. and 5% vol. SiC. XRD was used to check the effect of SiC particle size, secondary phase content and milling time on the particle size and lattice strain of Al matrix. There was a decrease in crystallite size and lattice strain accumulation over the milling time. The analysis was done using Williamson hall's method [12]. XRD analysis showed peak broadening and absence of peaks for reactive products like $Al_4C_3$ and Si. Saberi et al showed that the grain size decreased with milling time and that it resulted from crystallite defects and energy accumulation. This further resulted in sub grain formation in order for dislocation to move to lower energy. The grain size of Aluminium matrix reinforced with nano-size SiC becomes much lower than that of the one reinforced with micron-size SiC at the end of milling (10 h).

Gujba [16] fabricated silicon carbide reinforced aluminium matrix nanocomposites. The dispersion of the reinforcement and the reduction of powder composite grain size were done by mechanical milling. Composite of compositions 5, 12 and 20 wt. % nano-SiC particles (20 - 40 nm) were milled at a speed of 200 rpm and 10:1 BPR for 5, 12 and 20 h. Milling atmosphere was argon. The characterization of the milled powder was carried out using XRD for crystallite size and lattice strain analysis and SEM for microstructure analysis. SEM analysis of the powder showed that powder particles change from spherical shape to flake like and then to equiaxed structure. Grain size also decreased with milling time and it was found that the higher the reinforcement content the higher the grinding effect. Also, EDS showed that some SiC particles were embedded in the Al

particles and SiC was homogenously distributed. The best hardness was observed for composite whose reinforcement composition is 12wt%SiC while 20 h of milling gave the minimum crystallite size.

Finally Mostaed et al. [37] performed the mechanical alloying of Al–4.5 wt.% Cu/SiC composite powders in a high-energy P-6 planetary ball mill. They found that SiC particles sizes were less than 100nm after 5 h of milling.

## 2.4 The Spark Plasma Sintering Process

### 2.4.1 The Process

Sintering is the high-temperature treatment that causes particles to join, gradually reducing the volume of pore spaces between them [38]. It is a diffusion assisted process for synthesizing refractory materials, with high melting points that cannot be easily casted, based on the knowledge of advanced material science. However it is also suitable for processing of metal alloys, intermetallic, and metal–ceramic composites [39]. Sintering is one of the steps of Powder Metallurgy used to consolidate powder particles to eliminate pores between the particles [38]. Pores exist between particles at initial compaction. Because these particles are at higher energy wishing lower energy, atoms diffuse to the point of contact between any two given particles resulting in bonding between the particles and shrinkage of pores. The more successful a sintering operation is, the more reduced (or eliminated) is the porosity fraction. This is referred to as densification. It is caused by lattice diffusion of atoms from bulk of the particles into the neck region. The extent of densification depends on sintering time, temperature, initial

powder density, sintering mechanism, average powder particle size and size distribution of the powder particles [38, 40]. Liquid phase sintering occurs when a small amount of liquid forms during sintering and assists densification [38]. This is because diffusion in liquid is greater than in solid. The driving force for solid state sintering is the reduction in the total surface area of powder particles and consequently decrease in total free energy of the material [38, 40].

There are two major categories of sintering namely conventional and non-conventional sintering [41-44]. Conventional sintering includes: HIP, CIP and Tube furnace sintering, while non-conventional sintering includes: SPS, plasma activated sintering (PAS), Electro-consolidation and MW [41-44].

The differences between conventional and non-conventional sintering are that non-conventional sintering [41-45]:

i. is faster; shorter sintering time. This implies higher heating and cooling rate
ii. gives better microstructure and better densification (can be fully dense).
iii. results in better mechanical properties due to high heating rate that prevents grain growth.
iv. doesn't need pre-sample compaction to obtain green density.
v. is a relatively new sintering method.

SPS which is the main interest here falls under resistance sintering RS (one of the two categories of electric current assisted/activated sintering (ECAS). SPS has also been referred to as field assisted sintering (FAST) [44], pulsed electric current sintering

(PECS) [42], or plasma activated sintering (PAS) [46]. SPS is a sintering process that involves simultaneous application of pulsed electrical high energy, low voltage, spark pulse current and pressure directly on sintered material [42]. The process should not be confused with some other types of RS. The criteria with which RS processes can be differentiated include apparatus used and type of wave form of the applied current [39].

ECAS has really advanced in recent time due to its numerous advantages [39] such as:

1. faster heating rate
2. flexibility and controllability of the sintering parameters[8]
3. lower sintering temperature; helps to avoid grain growth
4. shorter holding time; helps to avoid grain growth and prevent undesired phase transformation.
5. consolidation of difficult-to-sinter-powders
6. elimination of the need of sintering aids,
7. no need of cold compaction,
8. less sensitivity to initial powders characteristics
9. marked comparative improvements in the properties of materials consolidated [39].
10. sintered parts of uniform density, close or equal to theoretical density can be produced
11. no problem of environmental control, since the process is fast.
12. overall process time is short implying high productivity; benefit of quality product at faster time is an economic good.

### 2.4.2 Principles and Mechanism of Sintering

SPS has something common to conventional hot pressing in that the precursors are loaded in a die and a uni-axial pressure is applied during the sintering. But, in SPS the heat source is from within and outside. A current (DC, pulsed DC, or AC) is passed through the electrically conducting pressure die and, in appropriate cases, also through the sample from beginning to the end of the process to produce heat by joule effect [39, 43]. This makes the sintered material to be heated from both outside and inside. The high energy pulses produced by pulsed DC current is concentrated at the point of inter-granular bonding [47]. The pulse current can be as high as 10000A with pulse duration of about 10ms at cycle of 2-2.5ms ON-OFF [48]. Some researchers have claimed that in addition to joule heating effect, spark plasma is generated by the pulse DC current between particles. The high energy pulses produced by pulsed DC current as earlier mentioned is concentrated the point of inter-granular bonding. They claim that it causes high local heating with temeperatures in the order of $10{,}000^{0}$C resulting in optimum thermal and electrolytic diffusion [47]. This, in addition to cleansing effect, results in the special qualities of spark-plasma sintered samples. However, whether plasma is formed or not, has not been well established [49, 50]. Hulbert et al. [51] conducted a study to verify the generation of plasma using up to three techniques. They couldn't detect any plasma formation.

In SPS, the sintering temperature can be up to 2000 ℃ which is 200 – 500 lower than conventional sintering. During SPS, temperature rises to a sintering temperature which is

held for an amount of time and then cooling occurs to room temperature. This takes place at a fast rate ranging from 5 to 20 minutes [47]. During this period, vaporization, melting and sintering takes place.

With the aid of SPS, efficient sintering is attained even at low power consumption [47]. Particle growth is minimized since the applied heating is restricted to contacting surfaces. This explains the mechanism of necking as shown in Fig. 2.9. Local heat generated between particles surfaces causes vaporization and the melting of the surfaces of the powder particles helping diffusion to bond the adjacent surfaces to form necks. The necks gradually develop and plastic transformation progresses during sintering, resulting in a dense sintered powder.

In order to carry out SPS, the powder is placed in a graphite die which serves as a container. The graphite die contains the two punches which are in contact with graphite and stainless steel blocks protecting the electrodes [46, 52]. This set up is shown in Fig. 2.8. The sample temperature is measured by various means ,e.g. using optical pyrometer, thermocouple, etc. taking the temperature of the die and the sample throughout the process. During the SPS process, spark plasma is created by a pulse direct current in a graphite die [46], implying the name of the process. However, the plasma is a low energy one resulting from the lack of gap between the die and the sample and is, probably, the reason for problems in plasma identification [46].

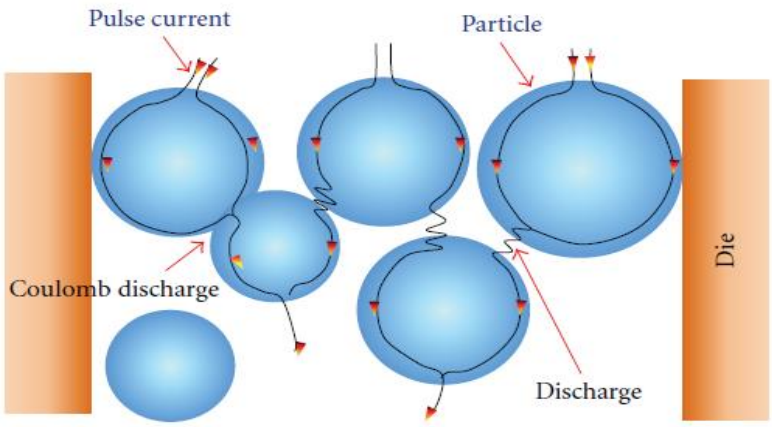


Fig. 2.7 DC pulse current flow through the particles [53, 54]

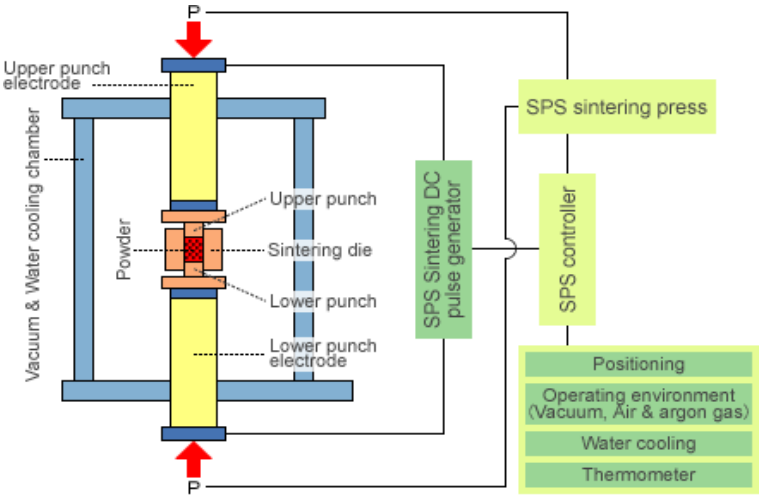


Fig. 2.8 Spark plasma sintering set up [47]

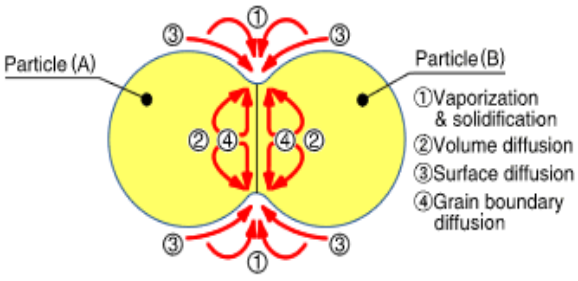


Fig. 2.9 Material transfer path during sintering [47]

### 2.4.3 Sintering Parameters

**Sintering pressure**

Spark plasma sintering is one of the pressure assisted sintering methods. Pressure is applied through the upper and the lower punches to assist densification of specimens. Khalil et al. [53] reported that the densification of specimens is less sensitive to the applied pressure during sintering of Al2124 and Al6061 alloys by SPS. With respect to the effect of pressure, they concluded that, the relationship between applied pressure and specimen's properties is not well defined [53]. In contrast, it has been reported by many researchers that pressure plays a great role in achieving dense sintered sample. Ohser-Wiedemann et al. [55] observed that the density of spark plasma sintered molybdenum is enhanced by pressure. They stated that densification is extremely fast when pressure is involved. It allows low sintering temperature which in turn minimizes grain growth. Table 2.1 shows that increase in pressure caused increase in relative density of sintered specimen at any temperature.

Table 2.1 Density of sintered composites [55].

| Pressure (MPa) | Relative density at $1600^0$C (%) | Relative density at $1800^0$C (%) | Relative density at $1900^0$C (%) |
|---|---|---|---|
| 29 | 89.4 | 92.1 | 92.4 |
| 57 | 94.4 | 95.3 | 95.3 |
| 67 | 95.0 | 95.7 | 95.8 |

Pressure sintering resulted in better densification than the one without applied pressure at equal sintering temperature [56]. Pressure contributes mechanically by rearranging the particles and destroying agglomerates. However the effect of pressure is not significant if the particle size is very small (e.g. 6 nm) until higher value of pressure is applied (e.g. 35MPa) [56]. Also it has been shown that relative densities of sintered zirconia increased with applied pressure until a limiting value is attained [17]. A study [57] explained the principles by which pressure assists to enhance densification during spark plasma sintering as follow; In SPS, material properties such as electrical resistivity, thermal conductivity, density and specific heat capacities of the die, punch and sample determine how the process proceeds [57]. These properties produce a coupling effect on the sintering process between the physical fields (including stress/strain) involved at the interfaces between the sample, the die, the spacers and the punches. The external pressure affects current distribution, bulk and interface heat generation and heat flow across the contact interfaces. There is electrical and thermal resistance at the interfaces. It was reported by previous researchers that vertical interface (between sample and die) resistance is higher than horizontal one [57]. Graphite was SPSintered at several pressures from 5 to 80 MPa while other parameters were kept constant. Temperature difference between the die outer surface and the sample edge was taken [57]. It was found that as pressure increases the difference decreases. This implies that at higher pressure, there is lower thermal resistance, better bulk material conductivity and better joule heating. Less temperature difference in the sample enhance densification,

homogeneous microstructure and minimal residual stresses after sintering [57]. The external pressure really affects the overall temperature distribution in the elements of SPS. And eventually higher pressure gives better densification

**Sintering temperature**

Sintering proceeds mainly by diffusion. As a result sintering temperature plays a vital role. However, excessive temperature causes grain growth. As a result there is need to identify or obtain the maximum temperature that gives optimum densification and as well gives minimum grain growth. Chai et al. [58] studied the effect of sintering temperature on the mechanical property and microstructure of melt-spun TiAl alloys. The alloy was sintered at 1200, 1260 and $1300^0$C. They found that the hardness and density was the same for the three temperatures but the microstructure and phases present changed with temperature. In [59], the relationship between density and temperature was formulated as;

$$\rho = s\,(T/T_m) + b \qquad \text{Eqn. 2.1}$$

Where, ρ is relative density, s temperature sensitivity, $T$ and $T_m$ are sintering and melting temperature respectively and $b$ is the intercept on density axis. It shows that densification increases with sintering temperature. However, the temperature sensitivity determines whether density will be affected by sintering temperature or not. If temperature sensitivity is high material's density will dependent on temperature, otherwise the opposite results. Metals have been reported to have lower temperature sensitivity than ceramics [59]. Also, it can be seen from Table 2.1, extracted from [55], that densification

increases with sintering temperature. Marginal density was observed at $450^0$C when Al2124 and Al6061 alloys were sintered by SPS at 400, 450 and $500^0$C [53]. This agrees with other reports earlier mentioned indicating that there is a maximum temperature suitable for maximum densification and minimum grain growth.

**Sintering time**

Sintering time is also desired to be minimal to avoid grain growth. However Wang et al [60] reported that density increased with increase in sintering time. The required time to sinter a given material depends on the heating rate; high heating rate implies short sintering time. At constant sintering parameters (i.e. pressure, temperature and heating rate), increase in time increases densification to a limiting value after which there will be grain growth [17].

**Heating rate**

The heating rate in spark plasma sintering is higher than the conventional sintering contributing to fast sintering time associated with SPS. There is a significant difference from the conventional sintering [56] as heating rates can go as high as high as $1000^0$C/min. in a work carried out by Stanciu et al, a non-conducting, $Al_2O_3$ and a conducting material MoSi2 were sintered at same condition, varying heating rate between 50 and 700◦C/min [61]. It was found that this didn't affect the density of both materials but grain size of alumina decreased [62] while that of MoSi2 remained unchanged. A study [63] also reported that there was strong effect of heating rate (50 to $200^0$C/min.) on grain size reduction during sintering of alumina whereas effect on density was little and then negative. Yadav [8] reported that higher heating rates can be used to restrain

powders grain growth. It was also observed that reduced particle size enhanced the heating rate effect on consolidation of aluminum.

## 2.5 Spark Plasma Sintered Al-SiC Nanocomposites

It has been found that SiC is a good and suitable Al matrix reinforcement. This is because of its outstanding properties such as high hardness, wear resistance, high specific modulus, oxidation resistance, high strength, high corrosion resistance, and thermodynamic stability with Al[2, 12]. SiC is also reported to have good wettability with Al [24]. As a result of Al-SiC's attractive physical and mechanical properties, it has found wide applications including but not limited to aerospace, automobiles industry, electronic heat sinks, automotive drive shafts, ground vehicle brake rotors, jet fighter aircraft fins, explosion engine components etc. [12]. El-Daly et al. [35] used spark plasma sintering to fabricate mechanically milled SiC pure Al matrix nanocomposites. Compositions such as Al - 2.5, 7.5 and 12.5 vol. % Nano-SiC in graphite die and punches were sintered at $550^0$C and 50MPa for 1 hr. in 4 Pa vacuum condition. A maximum densification of 96.3% was obtained for the 7.5 vol. % composition; densification increased with composition but fell after 7.5 vol. %. The composite with the highest composition gave the highest micro hardness of 7.1 GPa. Also, the reinforcement improved the Young's modulus (75.57 – 100.23GPa) and strength (shear modulus 21.9 – 29.5 GPa) of the sintered composite. El-Daly et al. attributed composite strengthening to grain refinement, strong interfacial bonding, dislocation strengthening and impurity level. Grain growth was not investigated after sintering. Their SEM analysis showed that there

was good interfacial bonding between the matrix and the reinforcement. Other inferences include absence of $Al_4C_3$ phase, void or cracks between matrix and reinforcement. All of these were suggested to be the reasons for good interfacial bonding which gave rise to strength.

Using pure Al as matrix, Zhang et al [36] sintered two mechanically alloyed Al- 20 vol% SiC composite powders with same Al matrix size (6μm) but different reinforcements sizes (12μm and 45μm). The powders were sintered in vacuum at 30MPa and $590^0$C for 10 min. heating rate was $50^0$C /min but furnace cooling was adopted. Zhang et al. [36], in one instance, reported that no micro voids were seen in the optical micrographs of SPS composites but in another said that many fissures and micro voids were presented in the surface of the SiC particles. However, the micrograph showed uniform distribution of SiC. The Al- 12 μm SiC resulted in better densification of 99.3% than Al - 45 μm SiC with 99.1%. XRD was used to verify that secondary phases were not formed after sintering. Compressive test results showed that the Al- 12 μm SiC composite has higher young modulus, 104 GPa and proof stress, 273 MPa than the Al- 45 μm SiC composite with 104 GPa and 228MPa respectively. This was attributed to higher densification and lesser defect in Al- 12 μm SiC composite.

Yadav [3] studied the spark plasma sintering of Aluminium Matrix composites. Pure Al and SiC nanocomposite is among the composites he fabricated. Ball milled Al - 5, 10 and 20 wt% SiC powders were spark plasma sintered in a $10^{-2}$ Torr. vacuum at 600°C, 40MPa and 100°C /min heating and cooling rate. He inferred from SEM images of sintered Al-SiC that there was weak interfacial bonding between Al and SiC because there was

scratches during polishing. The relative density of Al-SiC composites was found to decrease as the reinforcement content increase from a value approximately 100% for Al - 5 wt% SiC downward. The observed porosity was attributed to the higher melting point (~2700 °C) of SiC [8]. However, the micro hardness of Al-SiC composites increased with the increase in the content of reinforcement from 74 to 87 HV. The wear analysis implies that SiC content enhanced wear property of the composite.

In order to further study the processing of pure Al matrix nanocomposite and due to limited work on the synthesis of pure Al matrix SiC nanocomposite, a review of the SPS of pure Al CNT nanocomposite by H. Kwon et al [64] was also carried out. Al and 5 vol.% CNT was placed in 15 mm die and sintered by SPS at 600°C, 50MPa and 40°C /min heating for 20 minutes. The 5 vol. % composite gave better densification of 96.1%. The summary of the reviewed research works along with pure Al metal matrix nanocomposites $Al–TiB_2$ and $Al/ Al_4C_3$ are given in Table 2.2

.

Table 2.2 Spark plasma sintered aluminium nanocomposites

| S/N | Materials | (temp, press. time & H.R | Properties ( & HV) | Optimum parameters | grain growth | | Note/ remark | Ref. |
|---|---|---|---|---|---|---|---|---|
| 1 | Al-SiC (2.5, 7.5, 12.5 vol% ) | $550^0$C<br>50MPa<br>60 min<br>0 | 96.3<br>7.1 GPa | 12.5 vol% | Not checked | | Process parameters were not varied aside vol% | [35] |
| 2 | Al-SiC (20vol%) | 590<br>30<br>10<br>50 | 99.3 | Not applicable | Not checked | | Process parameters were not varied. | [36] |
| 3 | Al-SiC (5, 10, 20wt%) | 600<br>40<br>10<br>100 | 99.9<br>87 | 20 wt.% | Not checked | | Process parameters were not varied aside wt.%. ρ of composite decreased with SiC but hardness increased | [8] |
| 4 | Al–$TiB_2$ | 550<br>35<br>0 | 95.2<br>206 | Not applicable | XRD | Not signifi cant | Diameter of sintered sample is 40mm. total sintering time= 10min | [65] |
| 5 | Al/ $Al_4C_3$ | 500<br>100<br>10<br>3.3 | 292 | Not applicable | Not checked | | Diameter of sintered sample is 13mm | [66] |
| 6 | Al-CNT (1, 5 vol.%) | 600<br>50<br>20<br>40 | 96.1 | 5 vol.% | SEM | Not signifi cant | Process parameters were not varied aside vol%. Diameter of sintered sample is 15mm | [64] |

Table 2.3 Spark plasma sintered aluminium alloys based nanocomposites

| S/N | Materials | (temp, press. time & H.R | Properties ( & HV) | Optimum parameters | grain growth | | Note/ remark | Ref. |
|---|---|---|---|---|---|---|---|---|
| 1 | Al2124 | 400 - 500 | 99.9 | 35Mpa, 450$^0$C | Optical microscope | Increase with pressure | Pressure and times were paired. Pressure increase didn't give +ve but -ve effect. | [53] |
| | | 35 | | | | | | |
| | | 20 | 108 | | | | | |
| | | 100 | | | | | | |
| 2 | Al2124 | 400 - 500 | 100 | 500$^0$C | Not checked | | Only sintering temperature was varied. ρ increased with sintering temperature to a limiting value. | [67] |
| | | 35 | | | | | | |
| | | 20 | 117.1 | | | | | |
| | | 100 | | | | | | |
| 3 | Al-SiC (6 & 10 % wt.) | 500 | ~ 100 | 10 wt.% | Not checked | | Process parameters were not varied aside vol% | [68] |
| | | 50 | | | | | | |
| | | 3 | 280 | | | | | |
| | | 300 | | | | | | |
| 4 | Al-7Si-0.3Mg - SiC (5, 12 & 20 % wt.) | 400 - 500 | 98 | | | | Temp & content varied. ρ decreased with SiC content. Hardness dropped after SiC exceeded 12 wt% | [16] |
| | | 35 | | | | | | |
| | | 20 | 74.82 | | | | | |
| | | 100 | | | | | | |
| 5 | Al- $B_4C$ (20 wt.%) | 450 - 525 | 99.2 | 500$^0$C, 5min, | XRD | Rise with temp. and dwell time increase | 525$^0$C was used only for 15s. dwell time. Effect of time is more at low temp 2. HV increased with temp at medium dwell time. 3. at higher temps short sint Time is required. | [69] |
| | | 50 | | | | | | |
| | | 0.25 - 5 | 244 | | | | | |
| | | 100 | | | | | | |

Reported works on the investigation on the effect of pressure on sintered composite properties are very limited. Especially pressure and heating rate have not been varied to see how it affects the properties of spark plasma sintered nanocomposite. In a work by Khalil et al [53] that checked the effect of pressure, pressure and time were paired and they claimed that pressure effect didn't give significant property improvement. Most variation done was on the amount of reinforcement in the matrix. Temperature and time also have small amount of variation in the reviewed literatures. For this reason, the literature review was extended to cover other metal matrix nanocomposites. The summary is given in Table 2.4 that relates process parameters with the properties of the sintered composites.

Table 2.4 Spark plasma sintered metal alloys

| S/N | Materials | (temp, press. time & H.R | Properties ( & HV) | Optimum parameters | grain growth | | Note/ remark | Ref. |
|---|---|---|---|---|---|---|---|---|
| 1 | Pure molybdenum powder | 850-2000 | 96.1 | 57MPa,1900 $^0$C | Optical microscope | Increase with temp from 0.56$T_m$ | ρ increased with press. & temp till 57MPa & becomes const. H.R rate has no effect. | [55] |
| | | 29, 57, 67 | | | | | | |
| | | 3 | 2057MPa | | | | | |
| | | 130 - 360 | | | | | | |
| 2 | Pure molybdenum powder | 1200 - 1950 | 99.5 100 | 1650$^0$C, 5min | | rises with increase in tem. & sint. time. | 99.5% ρ for const t of 5min at varying temp. 100% density for const temp of 1850 at varying time | [70] |
| | | 77 | | | | | | |
| | | 5 - 30 | 161 | | | | | |
| | | 700 | | | | | | |
| 3 | melt-spun TiAl alloys | 1200-1300 | 4.098g/cm3 | 1260$^0$C | SEM | Increase after 1260$^0$C | Beyond 1260$^0$C G. growth occurs. Limiting ρ obtained at 1200 $^0$C. increase above this affected phase compositn. | [58] |
| | | 50 | | | | | | |
| | | 10 | 280 | | | | | |
| | | 100 | | | | | | |

## 2.6 Objectives

The review has shown that only few works have been published on mechanical milling and spark plasma sintering of Al-SiC nanocomposites.

In most reported works, the process was not fully investigated and critical sintering parameters effect on properties of the nanocomposite was not adequately studied.

Therefore, the main objective of this research work is to study the effect of BM and SPS process parameters (milling time, compaction pressure, heating rate, sintering temperature, and sintering time) on the microstructure and properties of Al-SiC metal matrix nanocomposites. Homogenous Al-SiC metal matrix nanocomposites with improved mechanical properties will be developed with a set of best process parameters.

# CHAPTER 3

# MATERIALS AND EXPERIMENTAL PROCEDURES

## 3.1 Raw Materials

Pure Aluminium powder (99.88% purity and 33 μm average particle size) purchased from Alpoco Ltd. was used as the composites' matrix. Chemical composition and particle size distribution of the powder are presented in Table 3.1 and Table 3.2 respectively.

Table 3.1 Chemical composition of pure aluminium powder

| Elements | Al | Fe | Si | Ti | Ga | Ni | Cu, Mn, Pb, Zr, Zn, Cr |
|---|---|---|---|---|---|---|---|
| wt. % | 99.88 | 0.074 | 0.024 | 0.006 | 0.006 | 0.005 | 0.001 each |

Table 3.2 Particle size distribution of aluminium powder

| Size (μm) | % |
|---|---|
| 63 | 0 |
| 53 | 1 |
| 45 | 11 |
| 38 | 11.4 |
| < 38 | 76.6 |

$SiC_{\beta}$ (97.5% purity and particle sizes ranging from 45 - 55 nm) obtained from Nanostructured and Amorphous Materials was used as the reinforcement. The SiC is a β phase type with zinc blende cubic structure. Four compositions of raw powders

composites from the as received Al and SiC were prepared. They include; pure Al, Al - 1wt% SiC, Al - 5wt% SiC and Al - 10wt% SiC. In volume percent, the respective composite samples are Al, Al – 0.8vol% SiC, Al – 4.2vol% SiC and Al – 8.5vol% SiC.

## 3.2 Experimental Procedures

### 3.2.1 Mechanical Milling

MM was used to uniformly disperse SiC particles in Al matrix and obtain fine grains of composite powders. Planetary ball mill (Model: Pulverisette 5, provided by Fritsch GmbH, Germany) shown in Fig. 3.1 was used. The vials and balls used are made of hardened stainless steel [2, 20, 37, 68]. With stainless steel, materials transfer is avoidable. Each ball has an average mass of 3.9g. Three different composite powders were milled with the same milling conditions. They include Al - 1wt% SiC, Al - 5wt% SiC and Al - 10wt% SiC. Approximately, half of each vial was filled with powders and balls. Powders were milled for 28 hours at 200rpm and 10:1 BPR [12, 16, 20, 35]. Milled samples were taken out of the vials at 2, 5, 10, 12, 15, 20, 24 and 28 hour of milling for characterization. This is to closely monitor the change of powder properties with milling time and ensure attainment of steady state and uniform dispersion of SiC in Al matrix. Hourly, milling is paused for 30 minutes to avoid excessive heat accumulation from kinetic energy. To avoid excessive cold welding, 2 wt% stearic acid, at the beginning of the milling and 1 wt% acid after 10 h of milling, were used as the process control agent, PCA [2, 11, 12, 20]. The milling was done under argon atmosphere to avoid powders contamination as done in previous research works [2, 16, 20, 35].

Fig. 3.1 Fritsch planetary ball mill

### 3.2.2 Scanning Electron Microscopy

JEOL (model JSM 6460) and Tescan Lyra-3 (Czech Republic) (Fig. 3.2) scanning electron microscopes were used to examine the morphology and microstructure of the as received and milled powders. SEM was also used to analyse sintered samples microstructures. The analysis was carried out at high voltages (15 and 20kV) and high vacuum. Sample preparation is a very important step in achieving excellent SEM analysis. To prepare samples for SEM analysis, small amount of powder samples were placed on carbon tape. Sintered samples were mounted and polished using Handimet 2 Roll Grinder. After achieving smooth surface, etching was done using keller's reagent to reveal the grains and their boundaries [67]. Samples were then gold coated for adequate conduction. Elemental compositional mapping was carried out using X-ray energy dispersive spectrometer (EDS) of the SEM to examine the level of SiC distribution in Al matrix [2, 11, 16, 71] of milled and sintered samples. Constant number of frames was maintained throughout for ease of comparison. SEM images and X-ray mapping of the fractured surface were also taken.

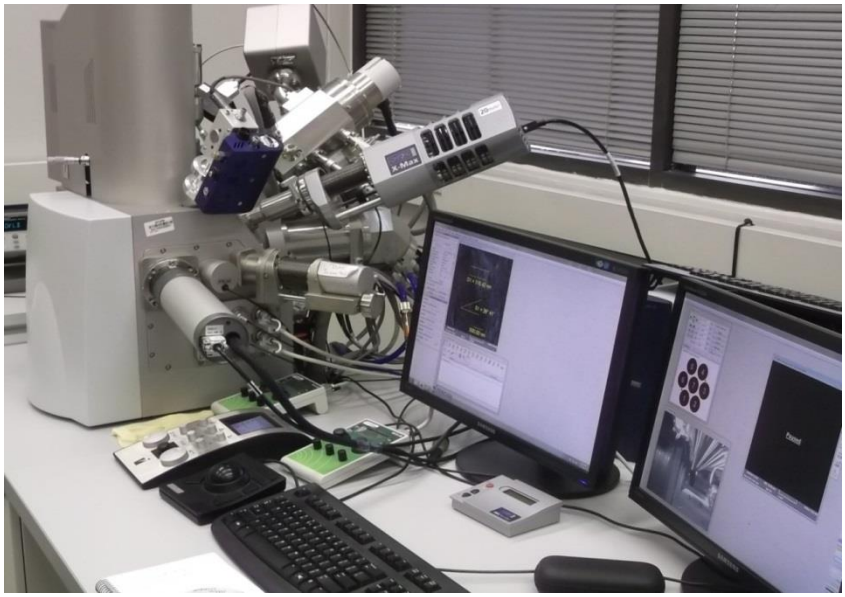

Fig. 3.2 Field emission scanning electron microscope

### 3.2.3 X-Ray Diffraction

X-ray Diffraction analysis was carried out using Bruker x-ray diffractometer model D8 ADVANCE, with Cu-Kα radiation whose wavelength is 0.15418 nm. Diffraction angle ($2\theta$) used ranged from 20 to 120, at a step increment of 0.02 with a count time of 1s. Annealed and milled powders were characterized to examine their crystallite size and strain variation with increase in milling time and presence or absence of secondary phase. Also XRD analysis was carried out on sintered samples to compare crystallite sizes and investigate formation of secondary phase.

The analysis of crystallite size and strain was done using Williamson Hall method [2, 11, 35] given in Eqn. 3.1.

$$B\cos\theta = \frac{k\lambda}{d} + \eta\sin\theta \qquad \text{Eqn. 3.1}$$

Where $\eta$ is the lattice strain accumulated, $k$ is a constant that ranges from 0.8 to 1.0 [16], $\theta$ is diffraction angle, $\lambda$ is X-ray wavelength and $B$ is the full width at half-maximum (FWHM) of the diffraction peak after instrument correction. $B$, the peak broadening resulting from size effect, was obtained from Eqn. 3.2.

$$B^2 = {B_{obs}}^2 - {B_i}^2 \qquad \text{Eqn. 3.2}$$

Where $B_{obs}$ is the FWHM obtained for the milled samples which includes size, strain and instrument peak broadening effect. $B_i$ is the FWHM obtained from the XRD of the pure Al annealed at $350^0$C for 3 h. The peak broadening due to strain and instrument

constitutes $B_i$. $B\cos\theta$ was plotted against $\sin\theta$ for each specimen a straight line is obtained with the slope being $\eta$ and the intercept $\frac{\lambda}{d}$.

### 3.2.4 Spark Plasma Sintering

Milled composite powders (Al-SiC) and as received pure un-milled Al were sintered using spark plasma sintering machine, type HP D 5/2, model SE – 607 from FCT group, Systeme GmbH (Fig. 3.3). The machine is capable of sintering at high heating rate (specification; 5 - $400^0$C/min). The pure un-milled powder was sintered in order to study the effect of sintering parameters on its properties and to serve as reference for the sintered and milled composite powders. For every sample, about 4.3g of powders was filled into 20 mm graphite die with a graphite sheet lining. This is to minimize friction between die walls and the powder and to avoid the sample from sticking to the die after sintering. To avoid powders running out of die during sintering a tight fit was made between die graphite sheet and the punch. Initial force of 3kN was applied. Force application rate of 5mm/min was used for most of the samples. 4:1 pulse pattern was used; 10 ms pulse time with 2 pulses before pause duration of 5ms. The sintering was done in ultra-high vacuum of 0.4 hPa. The sintering temperature was measured using a K-type thermocouple inserted in the graphite die through a drilled hole. Some studies [2, 16, 35] have reported spark plasma sintering of pure Al - SiC at temperatures ranging from 500 to $550^0$C while V. Yadav [8] used $600^0$C as sintering temperature in his work.

Pressure values ranging from 35 to 50 MPa were reported in [2, 8, 16, 18, 35] for pure Al composite spark plasma sintering.

In this work, 36 samples were first sintered to study the effect of heating rate and sintering pressure on properties of sintered nanocomposites at constant temperature of $550^0$C and holding time of 5 min. Pressure was varied between 20 and 50MPa and heating rate between 100 and $300^0$C/min for all the compositions; pure Al, Al containing 1wt%, 5wt% and 10wt% SiC. The best sintering pressure and heating rate were obtained. Then they were kept constant while 32 samples were sintered to study the effect of sintering temperature and time on properties of sintered nanocomposites. Now sintering time was varied between 5 and 15 minutes and temperature between 500 and $600^0$C. Table 3.3 and Table 3.4 illustrate this parametric set up in details.


Fig. 3.3 Spark plasma sintering machine.

Table 3.3 Experimental parameters for studying the effect of sintering pressure and heating rate on properties of sintered nanocomposites

| | SAMPLE | Pressure(MPa) | Temperature ($^0$C) | Time (min) | H.R (K/min) |
|---|---|---|---|---|---|
| Al | | | | | |
| | Al-1 | 20 | 550 | 5 | 100 |
| | Al-2 | 35 | 550 | 5 | 100 |
| | Al-3 | 50 | 550 | 5 | 100 |
| | Al-4 | 20 | 550 | 5 | 200 |
| | Al-5 | 35 | 550 | 5 | 200 |
| | Al-6 | 50 | 550 | 5 | 200 |
| | Al-7 | 20 | 550 | 5 | 300 |
| | Al-8 | 35 | 550 | 5 | 300 |
| | Al-9 | 50 | 550 | 5 | 300 |
| Al-1 wt% SiC | | | | | |
| | Al-1 wt% SiC - 1 | 20 | 550 | 5 | 100 |
| | Al-1 wt% SiC - 2 | 35 | 550 | 5 | 100 |
| | Al-1 wt% SiC - 3 | 50 | 550 | 5 | 100 |
| | Al-1 wt% SiC - 4 | 20 | 550 | 5 | 200 |
| | Al-1 wt% SiC - 5 | 35 | 550 | 5 | 200 |
| | Al-1 wt% SiC - 6 | 50 | 550 | 5 | 200 |
| | Al-1 wt% SiC - 7 | 20 | 550 | 5 | 300 |
| | Al-1 wt% SiC - 8 | 35 | 550 | 5 | 300 |
| | Al-1 wt% SiC - 9 | 50 | 550 | 5 | 300 |
| Al-5 wt% SiC | | | | | |
| | Al-5 wt% SiC - 1 | 20 | 550 | 5 | 100 |
| | Al-5 wt% SiC - 2 | 35 | 550 | 5 | 100 |
| | Al-5 wt% SiC - 3 | 50 | 550 | 5 | 100 |
| | Al-5 wt% SiC - 4 | 20 | 550 | 5 | 200 |
| | Al-5 wt% SiC - 5 | 35 | 550 | 5 | 200 |
| | Al-5 wt% SiC - 6 | 50 | 550 | 5 | 200 |
| | Al-5 wt% SiC - 7 | 20 | 550 | 5 | 300 |
| | Al-5 wt% SiC - 8 | 35 | 550 | 5 | 300 |
| | Al-5 wt% SiC - 9 | 50 | 550 | 5 | 300 |
| Al-10 wt% SiC | | | | | |
| | Al-10 wt% SiC - 1 | 20 | 550 | 5 | 100 |
| | Al-10 wt% SiC - 2 | 35 | 550 | 5 | 100 |
| | Al-10 wt% SiC - 3 | 50 | 550 | 5 | 100 |
| | Al-10 wt% SiC - 4 | 20 | 550 | 5 | 200 |
| | Al-10 wt% SiC - 5 | 35 | 550 | 5 | 200 |
| | Al-10 wt% SiC - 6 | 50 | 550 | 5 | 200 |
| | Al-10 wt% SiC - 7 | 20 | 550 | 5 | 300 |
| | Al-10 wt% SiC - 8 | 35 | 550 | 5 | 300 |
| | Al-10 wt% SiC - 9 | 50 | 550 | 5 | 300 |

Table 3.4 Experimental parameters for studying the effect of sintering temperature and time on properties of sintered nanocomposites

| | SAMPLE | Pressure(MPa) | Temperature ($^0$C) | Time (min) | H.R (K/min) |
|---|---|---|---|---|---|
| Al | | | | | |
| | Al-1 | 50 | 500 | 5 | 200 |
| | Al-2 | 50 | 550 | 5 | 200 |
| | Al-3 | 50 | 600 | 5 | 200 |
| | Al-4 | 50 | 500 | 10 | 200 |
| | Al-5 | 50 | 550 | 10 | 200 |
| | Al-6 | 50 | 600 | 10 | 200 |
| | Al-7 | 50 | 500 | 15 | 200 |
| | Al-8 | 50 | 550 | 15 | 200 |
| | Al-9 | 50 | 600 | 15 | 200 |
| Al-1 wt% SiC | | | | | |
| | Al-1 wt% SiC - 1 | 50 | 500 | 5 | 200 |
| | Al-1 wt% SiC - 2 | 50 | 550 | 5 | 200 |
| | Al-1 wt% SiC - 3 | 50 | 600 | 5 | 200 |
| | Al-1 wt% SiC - 4 | 50 | 500 | 10 | 200 |
| | Al-1 wt% SiC - 5 | 50 | 550 | 10 | 200 |
| | Al-1 wt% SiC - 6 | 50 | 600 | 10 | 200 |
| | Al-1 wt% SiC - 7 | 50 | 500 | 15 | 200 |
| | Al-1 wt% SiC - 8 | 50 | 550 | 15 | 200 |
| | Al-1 wt% SiC - 9 | 50 | 600 | 15 | 200 |
| Al-5 wt% SiC | | | | | |
| | Al-5 wt% SiC - 1 | 50 | 500 | 5 | 200 |
| | Al-5 wt% SiC - 2 | 50 | 550 | 5 | 200 |
| | Al-5 wt% SiC - 3 | 50 | 600 | 5 | 200 |
| | Al-5 wt% SiC - 4 | 50 | 500 | 10 | 200 |
| | Al-5 wt% SiC - 5 | 50 | 550 | 10 | 200 |
| | Al-5 wt% SiC - 6 | 50 | 600 | 10 | 200 |
| | Al-5 wt% SiC - 7 | 50 | 500 | 15 | 200 |
| | Al-5 wt% SiC - 8 | 50 | 550 | 15 | 200 |
| | Al-5 wt% SiC - 9 | 50 | 600 | 15 | 200 |
| Al-10 wt% SiC | | | | | |
| | Al-10 wt% SiC - 1 | 50 | 500 | 5 | 200 |
| | Al-10 wt% SiC - 2 | 50 | 550 | 5 | 200 |
| | Al-10 wt% SiC - 3 | 50 | 600 | 5 | 200 |
| | Al-10 wt% SiC - 4 | 50 | 500 | 10 | 200 |
| | Al-10 wt% SiC - 5 | 50 | 550 | 10 | 200 |
| | Al-10 wt% SiC - 6 | 50 | 600 | 10 | 200 |
| | Al-10 wt% SiC - 7 | 50 | 500 | 15 | 200 |
| | Al-10 wt% SiC - 8 | 50 | 550 | 15 | 200 |
| | Al-10 wt% SiC - 9 | 50 | 600 | 15 | 200 |

### 3.2.5 Optical Microscopy

The microstructure of sintered specimens was studied using optical microscope. Samples were first mounted and polished using Handimet 2 Roll Grinder. After achieving smooth surface, etching was done using keller's reagent [67] soaking each sample in solution for 10 to 20 seconds. Then microstructural images of the samples were taken at a magnification of 200X.

### 3.2.6 Density Measurement

The density of sintered samples was measured using METTLER TOLEDO balance density determination kit. Model AG285 was purchased from METTLER TOLEDO GmbH & weighing Technologies, Switzerland. The process involves weighing the sample in air then in liquid (i.e. water for this experiment). Then Eqn. 3.3 was used to calculate the density of the sample.

$$\rho_o = \frac{A}{A-B} * (\rho_l - \rho_a) + \rho_a \qquad \text{Eqn. 3.3}$$

Where $\rho_o$ is calculated sample density, A and B are weight of sample in air and liquid respectively, $\rho_l$ and $\rho_a$ are density of liquid and air respectively.

The theoretical density of pure Al and SiC are 2.7 g/cm3 and 3.2 g/cm3 respectively.

Hence, the theoretical density of composites $\rho_c$ can be obtained using Eqn. 3.4

$$\rho_c = \rho_m V_m + \rho_r V_r \qquad \text{Eqn. 3.4}$$

Where $\rho_m$ and $\rho_r$ are the densities of matrix and reinforcement respectively, $V_m$ and $V_r$ are the volume fractions of matrix and reinforcement, respectively. With this, the theoretical densities of the composites are obtained and given in Table 3.5. After obtaining the densities of the samples, relative density was calculated using Eqn. 3.5

$$\text{Densfification} = (\rho_c/\rho_{theoretical}) * 100 \quad \text{Eqn. 3.5}$$

Table 3.5 Theoretical density of composites

| Composite | Theoretical density (g/cm$^3$) |
|---|---|
| Al - 1wt% SiC | 2.704 |
| Al - 5wt% SiC | 2.722 |
| Al - 10wt% SiC | 2.744 |

### 3.2.7 Hardness Test

Micro Hardness of sintered specimens was obtained using Vickers's MMT-3 Digital Micro Hardness Tester, Buehler, USA. Ten hardness values were taken from different locations in the specimen using 100 gf load applied for time of 12s. The average of these values was taken as the micro hardness.

Vicker's hardness (HV) is given as;

$$\mathrm{HV} = \frac{0.1891\mathrm{F}}{d^2}$$ Eqn. 3.6

Where, ‘F’ is the applied load and ‘d’ represents the diagonal length of an indent.

### 3.2.8 Compression Test

In order to study the compressive properties of the sintered specimens, specimens with the best set of sintering parameters were machined to a dimension of diameter = 5 mm (± 0.02 mm) and length = 8 mm (± 0.02 mm). Instron 3367 testing machine was used for the compression tests at a compression rate of 1 mm/min. Each unique test was repeated twice to ensure precision.

# CHAPTER 4

# RESULTS AND DISCUSSION

## 4.1 Characterization of Milled Powders

### 4.1.1 Morphology of Powders

The morphology of as received pure Al powder is shown in Fig. 4.1. The powder particles are near spherical elongated and irregular. They show a size distribution that is in agreement with the as received pure Al particle size distribution data. The figure showed that most particles are less than 50μm which is close to the evaluated average size of 33μm. Fig. 4.2 shows the morphology of the as received SiC. It shows several almost spherical nanoparticles that seem agglomerated. The average particle size that can be inferred from the micrograph also agrees with the range of 45 to 55nm from the as received SiC data. The effect of milling on Al- 5wt% SiC nanocomposite powder morphology can be seen in Fig. 4.3. At 2 h. milling time, the powders started flattening due to plastic deformation. This was seen in previous literature [11, 20]. As milling proceeds to 9 h, the powders particles become flake like. This is as a result of plastic deformation caused by high energy impact. As milling gets to 20 h, the particles became flaker and showed reduced size. Flake like morphology has been observed in previous research. The mechanical alloying of Al (42μm) mixed with 1.2, 6, and 8.2 wt% SiC (50nm) for 16 h at 250 rpm [72] resulted in flake like powders. Milling to 24 h caused more fracturing by excessive plastic deformation. Over all, as milling time increased,

particle size of the composite powder decreased due to increase in milling effect. The micrograph of Al -1wt% SiC powders shown in Fig. 4.4 looks similar to that of Al- 5wt% SiC (Fig. 4.3); the shape of the particles is flake like. However the particle size is larger meaning that milling effect is less pronounced in 1 wt% Si Composite. This can be attributed to the SiC amount being less. This agrees with what was reported in previous studies [16, 72, 73]. The more the amount of SiC, the more frequent the interaction between dislocation and hard particles [74] leading to greater milling effect. Similar analogy is observed in Al -10wt% SiC were milling effect is most seen (Fig. 4.5). The SEM images of the three composites show that 24 h is enough to impact adequate milling on the powders.

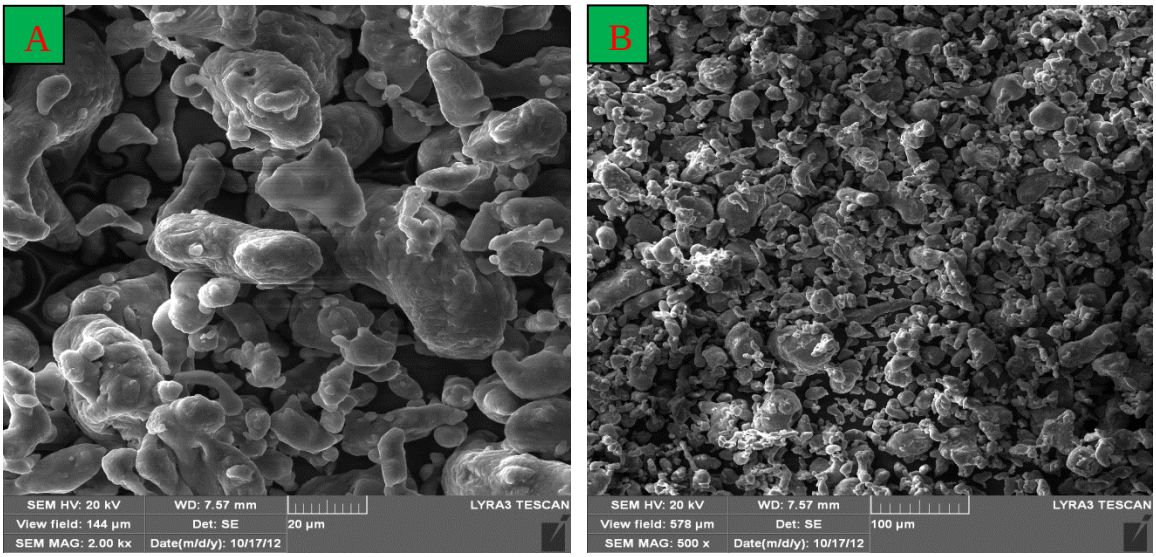


Fig. 4.1 SEM images of as received pure Al powder, (a) 2000 X magrification (b) 500 X magnification

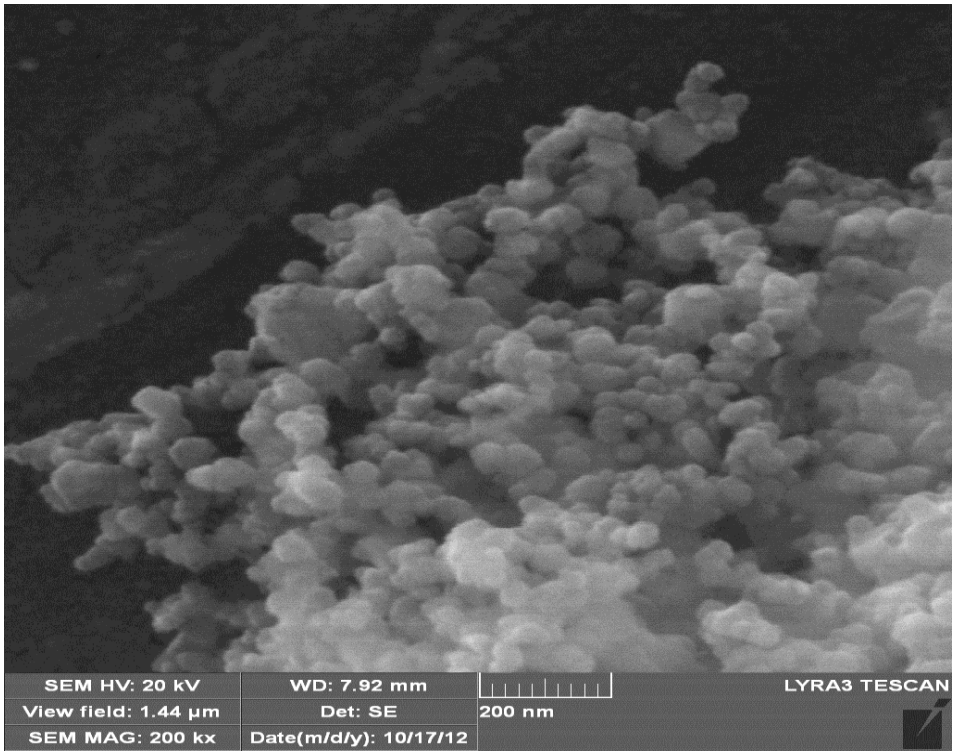


Fig. 4.2 SEM images of as received pure SiC powder at 200,000X magnification

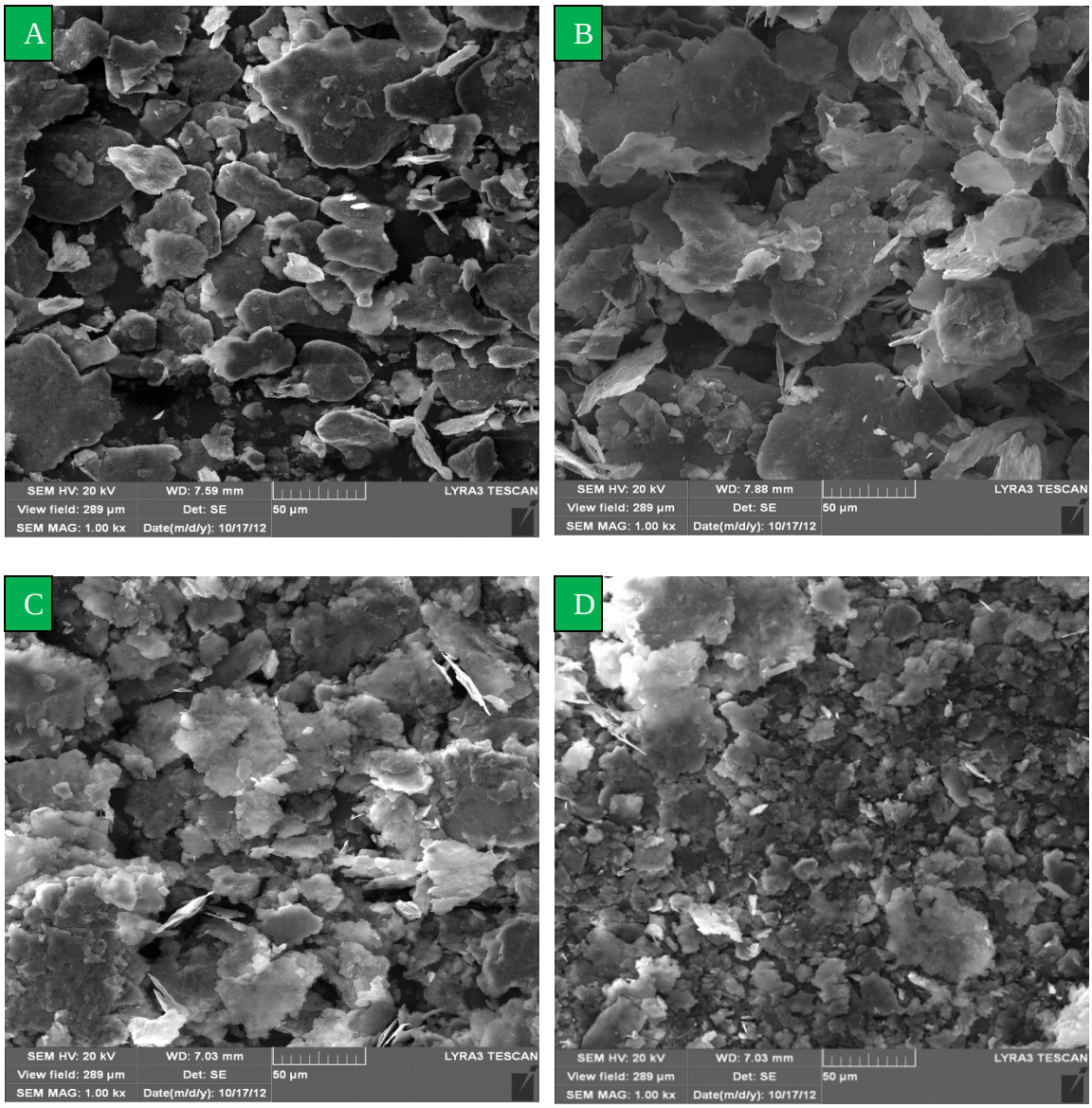


Fig. 4.3 SEM images of Al- 5wt% SiC nanocomposite powders milled for (a) 2h (b) 9h (c) 20h (d) 24h.

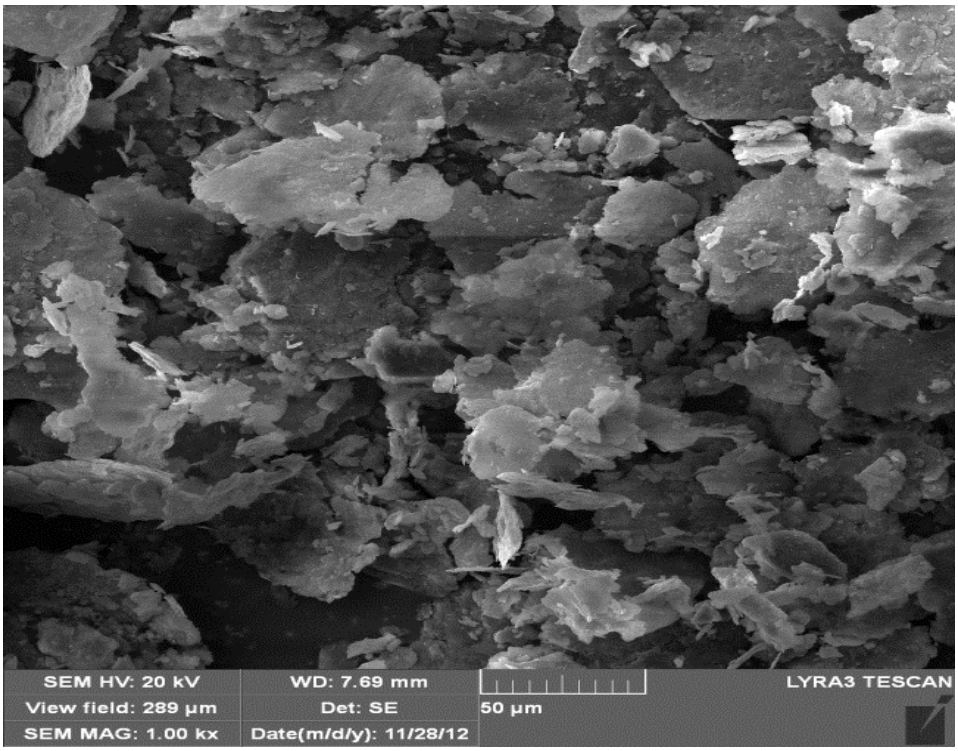


Fig. 4.4 SEM images of Al- 1wt% SiC nanocomposite powders milled for 24h.

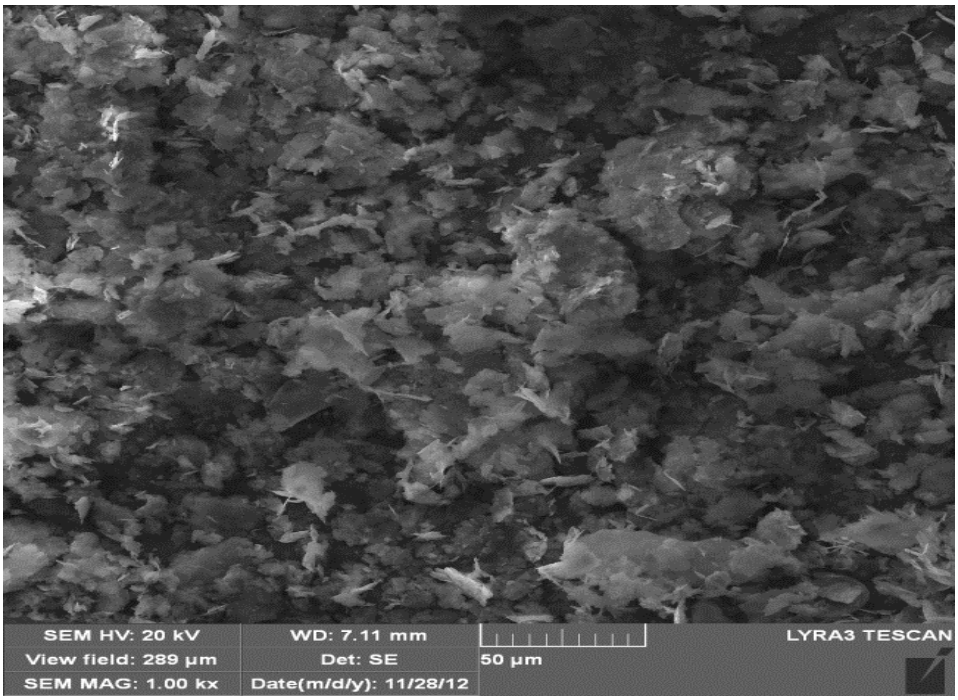


Fig. 4.5 SEM images of Al- 10wt% SiC nanocomposite powders milled for 24h.

### 4.1.2 SiC Dispersion

The x-ray maps of Al - 5wt.% SiC composite powders are shown in Fig. 4.6 and Fig. 4.7 after 9 and 24 h milling respectively. It is obvious that at 9 h there was non-uniform dispersion of SiC, but as milling reached 24 h, SiC has become almost uniformly dispersed. Some studies [11, 37] have used X-ray mapping to establish uniform reinforcement distribution in Al matrix. X-ray mapping of mechanically alloyed Al (42μm) mixed with 1.2, 6, and 8.2 wt.% SiC (50nm) for 16 h [72] showed uniform distribution but with clusters in some locations. The same observation was made for both Al- 1wt% SiC and Al- 10wt% SiC; At 24 h of milling SiC has become well dispersed in the Al matrix. This can be seen in Fig. 4.8 and Fig. 4.9.

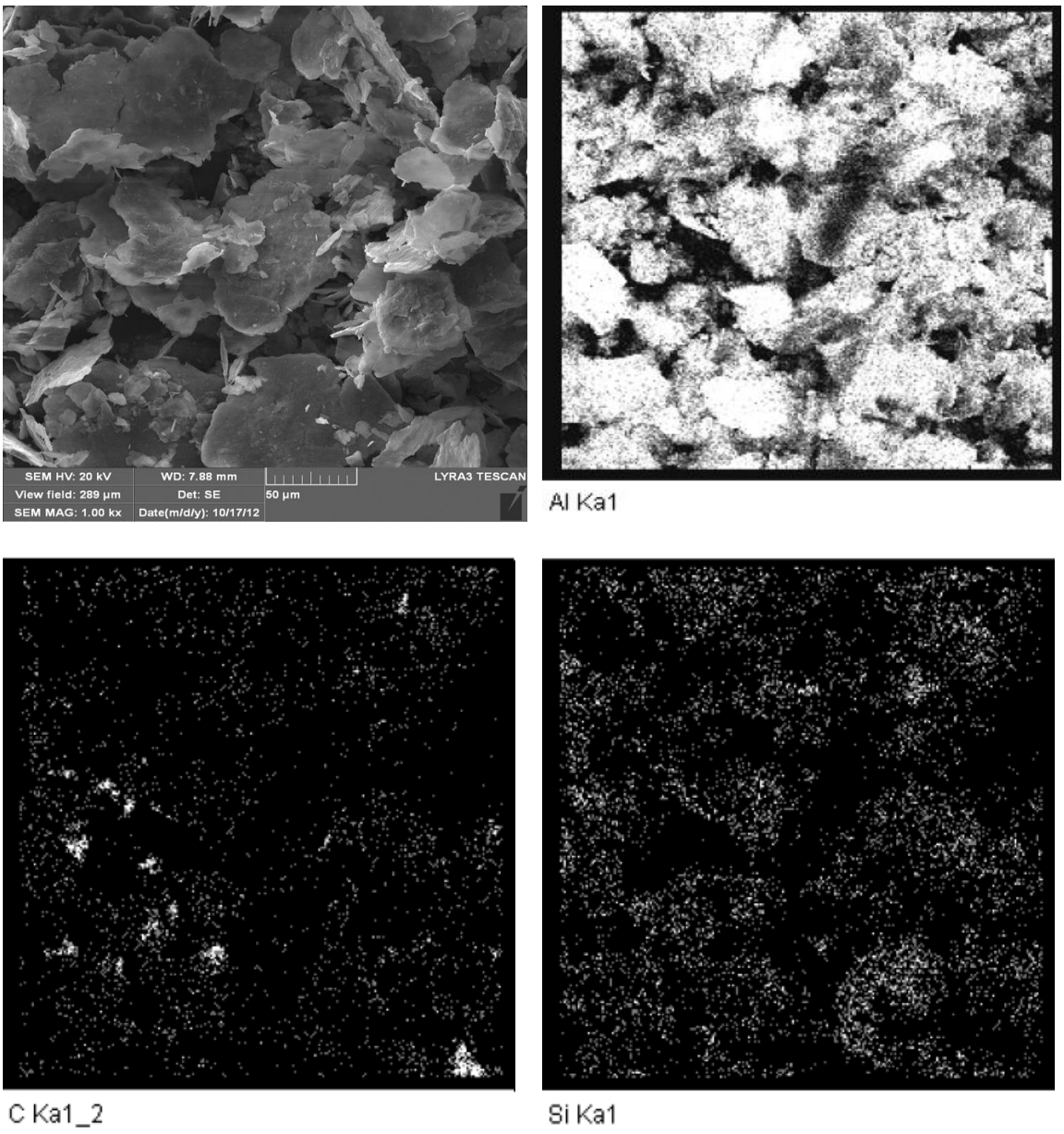


Fig. 4.6 X-ray mapping of Al – 5wt% SiC composite milled for 9 h.

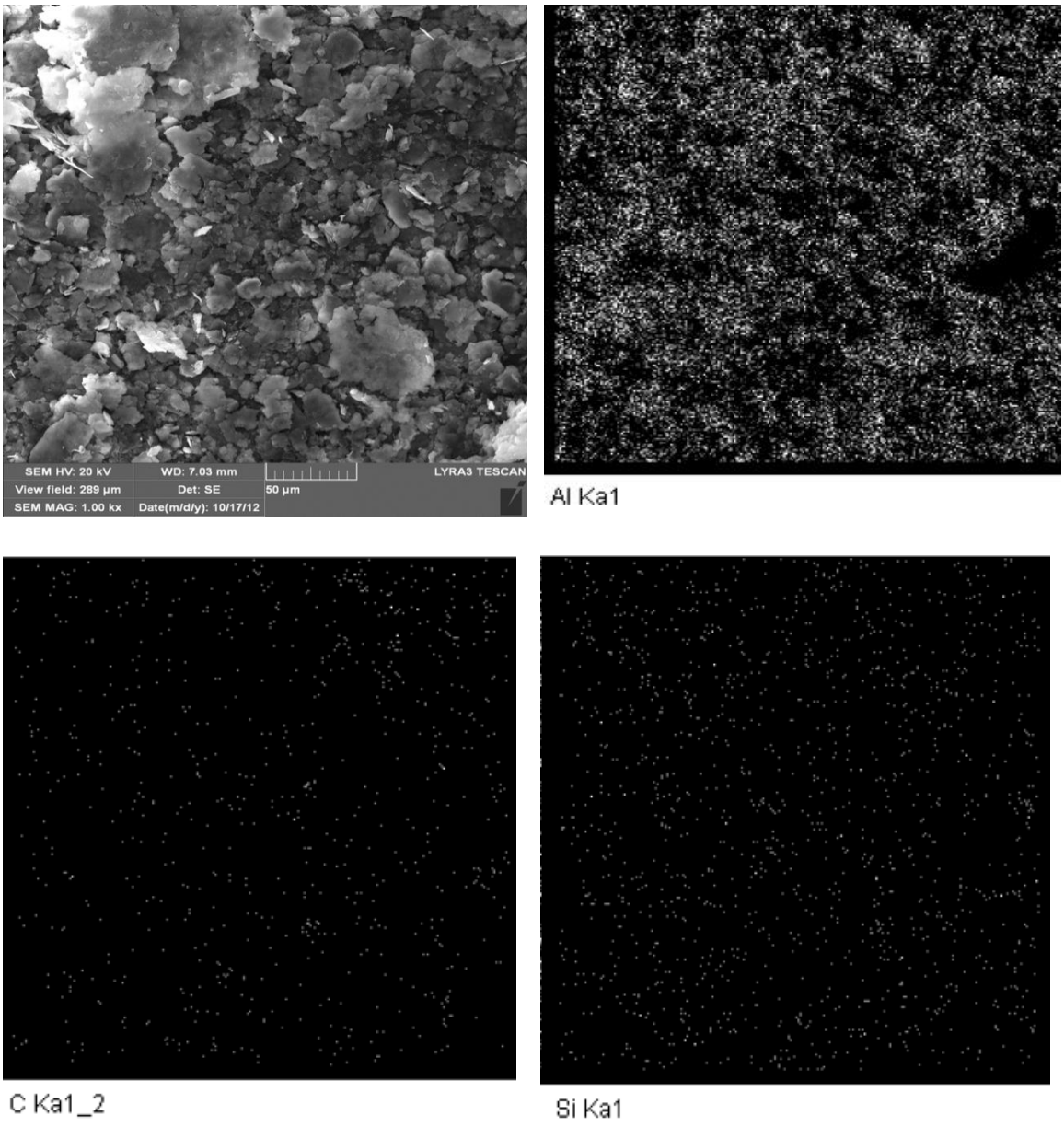


Fig. 4.7 X-ray mapping of Al – 5wt% SiC composite milled for 24 h.

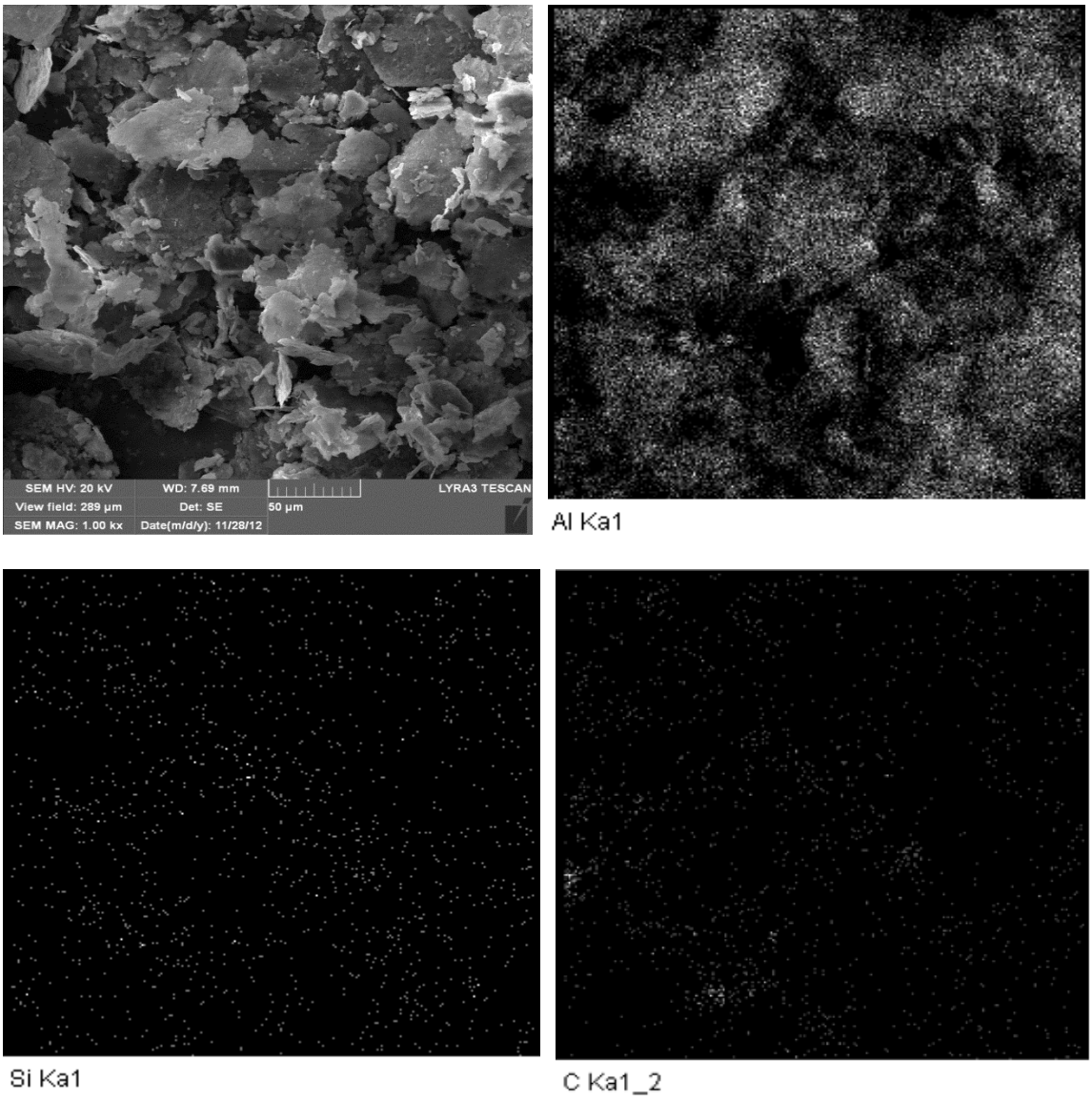


Fig. 4.8 X-ray mapping of Al – 1wt% SiC composite milled for 24 h.

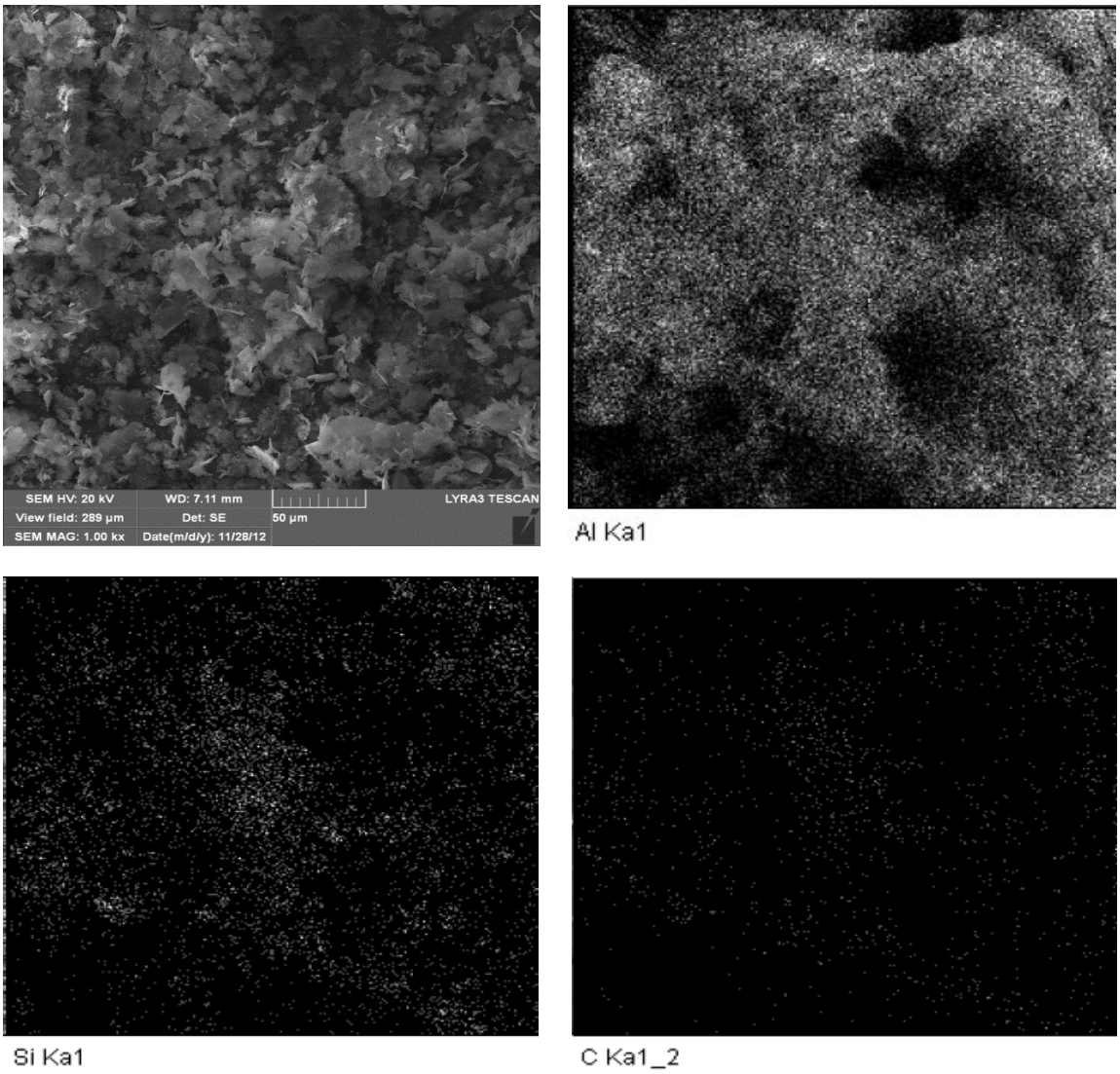


Fig. 4.9 X-ray mapping of Al – 10 wt% SiC composite milled for 24 h.

### 4.1.3 Crystallite Size and Lattice Strain

The XRD spectra of pure Al (annealed and as received), Al - 1wt% SiC, Al - 5wt% SiC and Al - 10wt% SiC milled composite powders with different milling durations are shown in Fig. 4.10, Fig. 4.11 and Fig. 4.12 respectively. Only Al peaks are seen throughout the Al - 1wt% SiC and Al - 5wt% SiC, however a small SiC peak is observed in addition to Al peaks in Al - 10wt% SiC. Peaks of SiC were not seen in the two composites with lower reinforcement because the amount is smaller than can be detected by the XRD machine used. This is in agreement with a study in [73] where XRD spectra of Al -5 vol.% SiC milled for 10 h showed no presence of SiC peaks until the SiC was increased to 10 vol.%. Also in [12], 2.5 vol.% (3 wt%) SiC showed no presence of SiC peaks. Even with increase of SiC to 5 vol.% (5.9 wt%) some charts didn't show SiC peaks, while the SiC peaks of those that did were very small [12]. Similar observation was made in [11, 16, 35]. Any secondary phase peak was not seen in the three charts. This implies that secondary phases were not formed during the high energy milling of Al -5 vol.% SiC for 25 h at 300 rpm [11]. However it can be argued that a phase was formed but not detected due to the detectability of XRD and the smallness of the phase. This can be responded to as follow. The amount of secondary phase, if formed, should increase with increasing amount of SiC. Therefore secondary phase's peak should at least show in the XRD specra of Al - 10wt% SiC. However, none is seen in Fig. 4.12.

There was broadening of peaks and peak intensities reduction as milling time increased except for Al - 1wt% SiC in which the reverse occurred at 12 h. The peaks broadening

are due to crystallite size reduction and strain accumulation. This is in agreement with what was stated or found in [16, 20, 35]. The peak height increase and width reduction observed at 12 h can be attributed to annealing effect as mentioned in the milling of α-$Fe_2O_3$ powder at 250 rpm for 48 h [75]. The three composites showed the broadest and shortest peak at 24 h of milling.

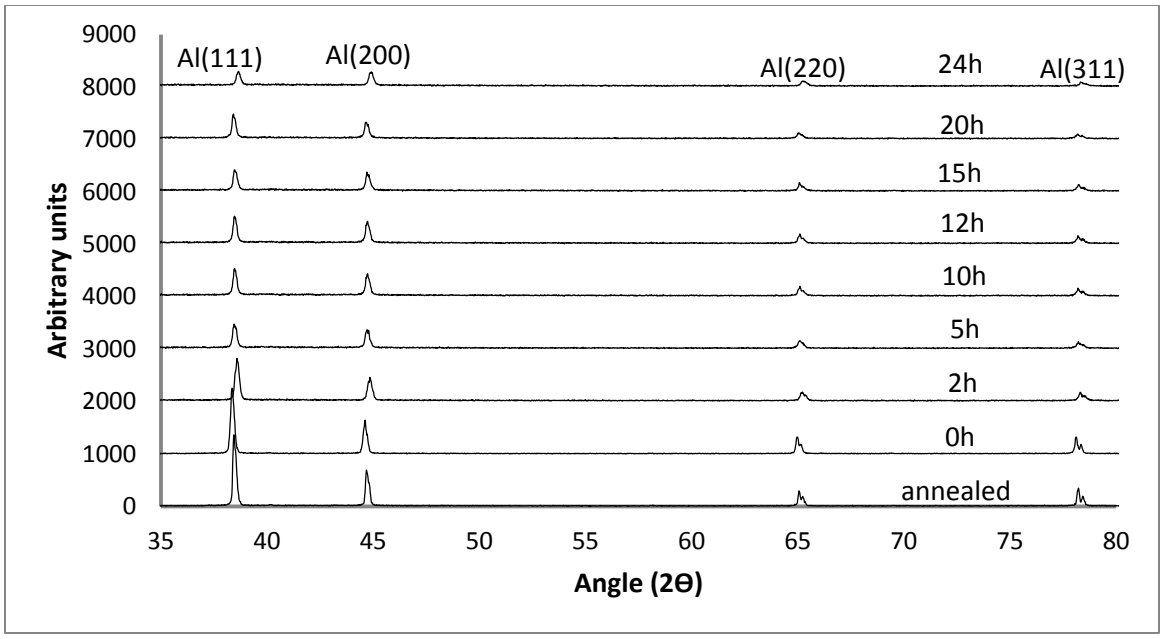


Fig. 4.10 XRD spectra for Al- 1 wt% SiC milled from 0 to 24 h.

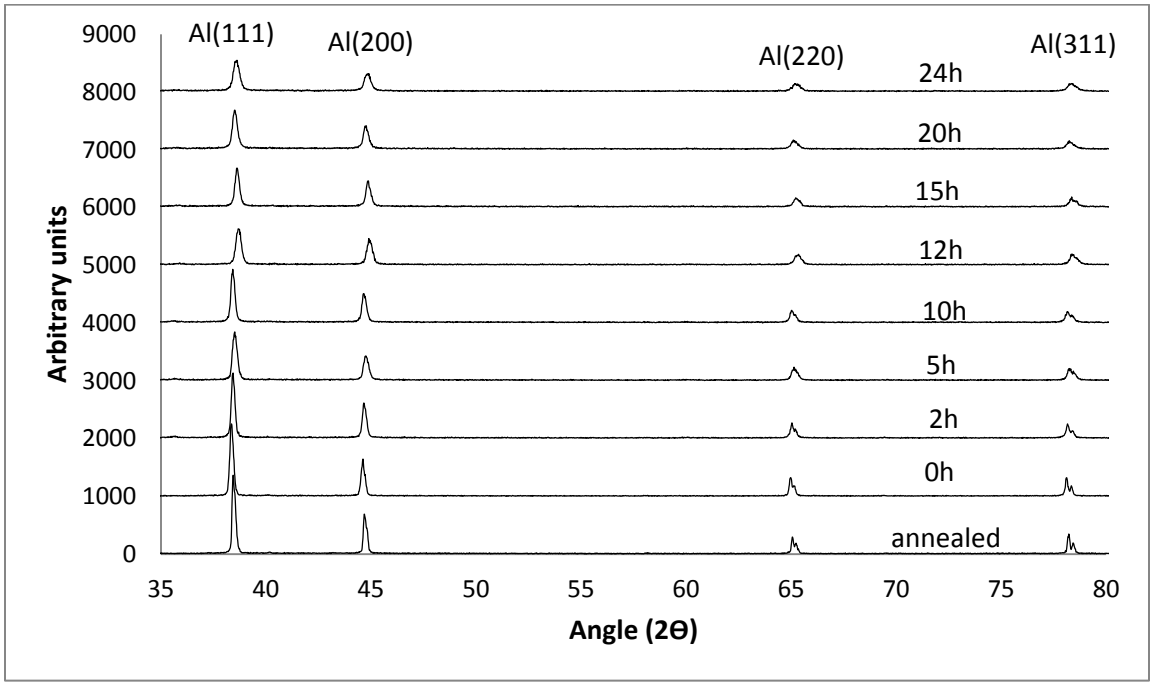


Fig. 4.11 XRD spectra for Al- 5 wt% SiC milled from 0 to 24 h.

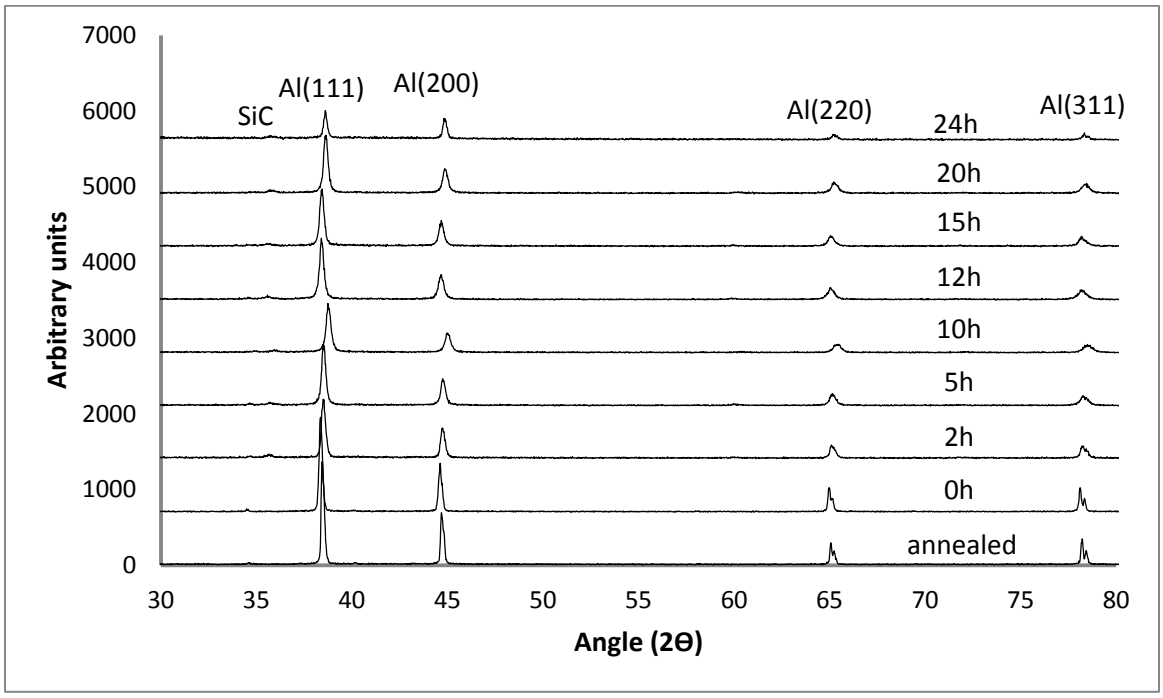


Fig. 4.12 XRD spectra for Al- 10 wt% SiC milled from 0 to 24 h.

This implies that the smallest crystallite size and highest internal strain were attained at 24 h. With similar milling condition, using Williamson-Hall analysis, a trend of size decrease but strain increase with milling time were observed in the three powders composites see Fig. 4.13, Fig. 4.14 and Fig. 4.15. This is in agreement with what was found in previous studies [11, 12, 33, 37]. The crystallite size decrease and lattice strain increase was throughout the milling time except for the Al - 1wt% SiC in which a crystallite size increase was observed at 12 h while strain decreased. See Fig. 4.13. The unexpected increase in crystallite size of Al - 1wt% SiC at 12 h can be due to the fact that SiC amount in Aluminium is very small and Al is ductile. Another justification is the analogy derived from [75] where decrease in strain observed at a particular milling time was attributed to annealing effect during milling. Hence if annealing effect is observable during milling to cause strain decrease then it can also cause crystallite size increase. The XRD chart of Al - 1wt% SiC also showed this as explained earlier. One coherent observation about the Williamson-Hall crystallite size and lattice strain analysis is that for every milling time where crystallite size decrease occurred, lattice strain increased and when there was crystallite size increase in the case of Al - 1wt% SiC lattice strain decreased. Also the observation here agrees with what has been discussed above with the XRD charts. Steady state size and strain variation with time can be seen for the three composites at 24 h of milling, Fig. 4.13, Fig. 4.14 and Fig. 4.15. Khadem [76] obtained similar graph in the milling of Al-SiC nanocomposite.

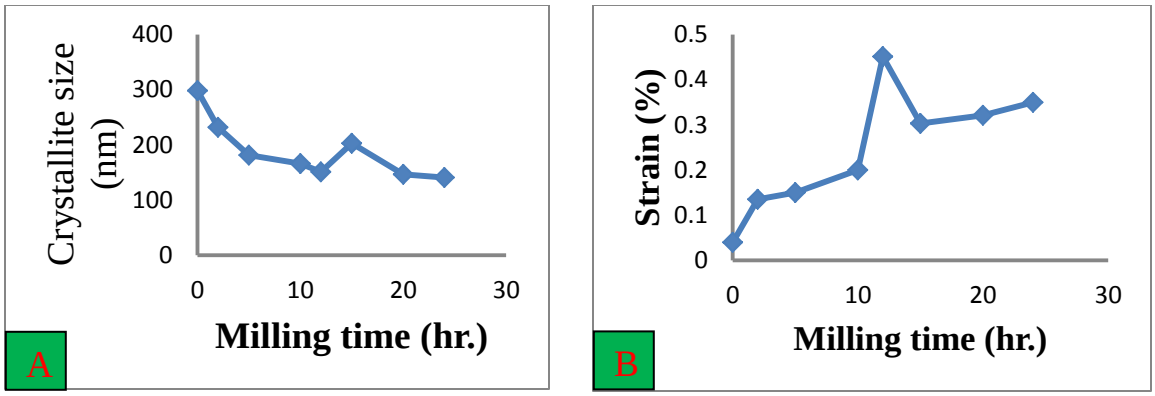


Fig. 4.13 (a) Crystallite size (b) and Strain variation with milling time for Al- 1wt% SiC milled from 0 to 24 h.

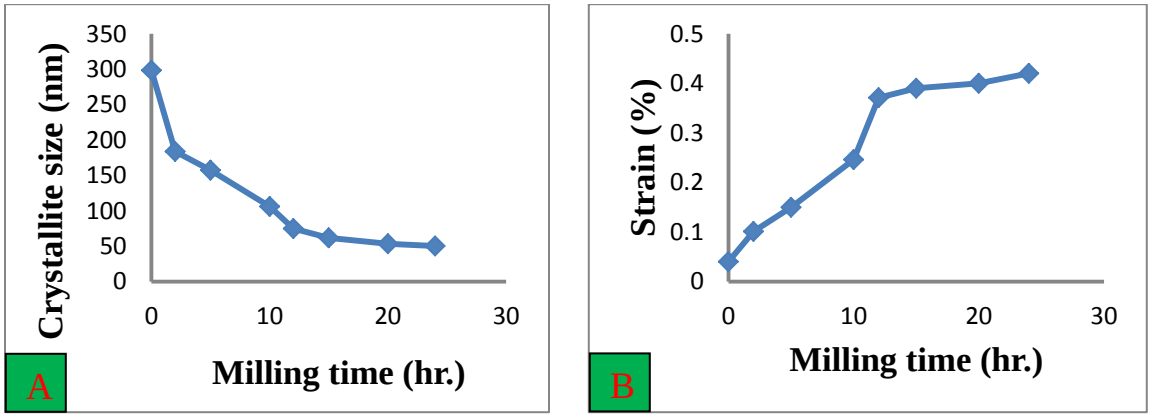


Fig. 4.14 (a) Crystallite size (b) and Strain variation with milling time for Al- 5wt% SiC milled from 0 to 24 h.

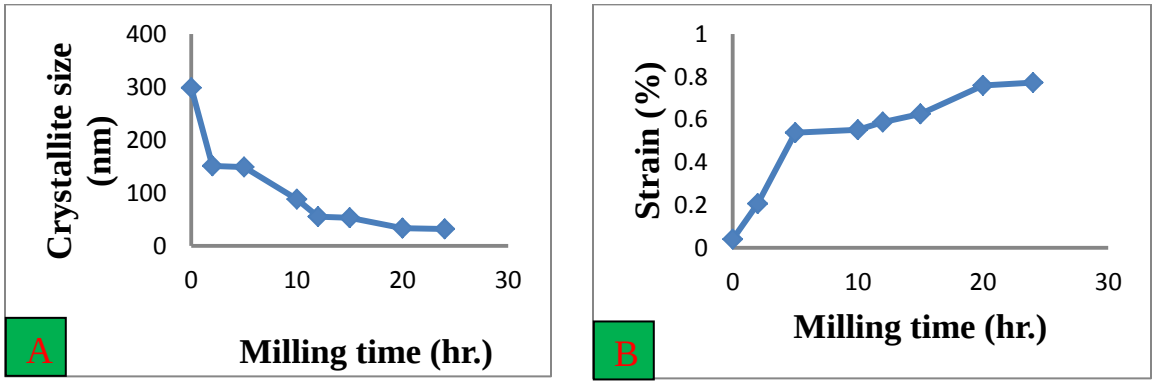


Fig. 4.15 (a) Crystallite size (b) and Strain variation with milling time for Al- 10wt% SiC milled from 0 to 24 h.

In order to compare the milling effect observed in the three composites, their XRD charts have been overlaid in Fig. 4.16. The peaks reduced in height and increased in width with increase in SiC content from 1 to 10 wt % for powders milled at same milling conditions for 24 h. This means that SiC amount enhance the milling effect as reported in [20, 35, 73]. For confirmation, the crystallite size- time graphs of the three composites have been overlaid as seen in Fig. 4.17. The graphs showed that as SiC content increases, the matrix crystallite size decrease with time increase while lattice strain increases. Decreasing from un-milled Al crystallite size of 298.27nm, the final crystallite size of the composites; Al- 10wt% SiC, Al- 5wt% SiC and Al- 1wt% SiC are 31.72, 50.15 and 140.82 nm respectively. 31.72 nm is very small compared to the 97.9nm obtained for Al -12.5 vol.% SiC aftrer 10 h of milling at a speed of 320 rpm reported in [35]. Comparing the final crystallite size of Al- 10wt% SiC with 10 vol.% SiC reinforced Aluminium milled for 10 h at 320 rpm, 90.7nm was obtained [73] and Al -20wt.% SiC milled for 20 h at 200 rpm, 70 – 80nm was obtained [16]. Also a final crystallite size of 50 nm was attained in the milling of Al (μm) mixed with 8.2 wt % SiC (50nm) [72]. The milling was done at 250 rpm 10:1 BPR for 16 h. In this research, similar crystallite size was obtained with less amount of SiC (Al- 5wt% SiC). However the milling time was longer (24 h). Therefore, 16 h is not enough for adequate grain refinement of the composite.

A further comparison is made with Al -.5 vol.% SiC milled for 25 h at 300 rpm, 15:1 BPR [8]. The final crystallite size reached was 45nm. This value is a bit less than the crystallite size obtained for Al- 5wt% SiC in this research, however the amount of SiC is lesser and the Al -5vol.% SiC was milled at higher parameters. This implies that the

adopted combination of milling parameters in this work has helped to achieve adequate refinement of the composite powders. The overall observation on the crystallite size variation with milling time is in agreement with the XRD charts.

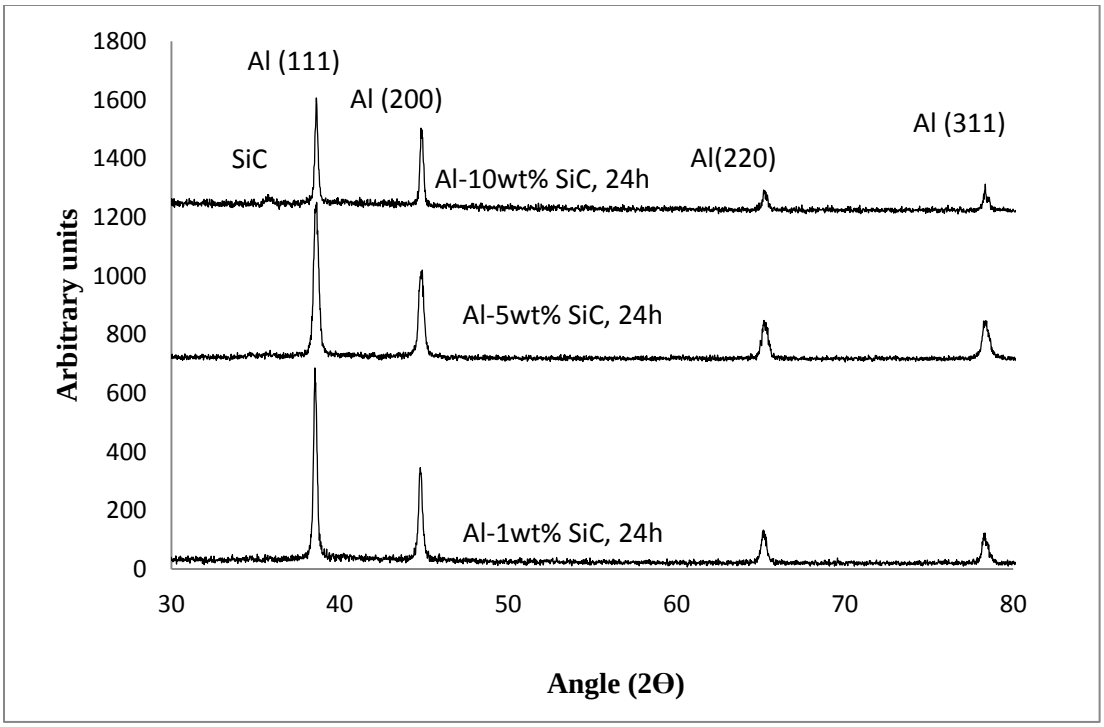


Fig. 4.16 XRD spectra for Al containing 1, 5 and 10 wt% SiC milled for 24 h.

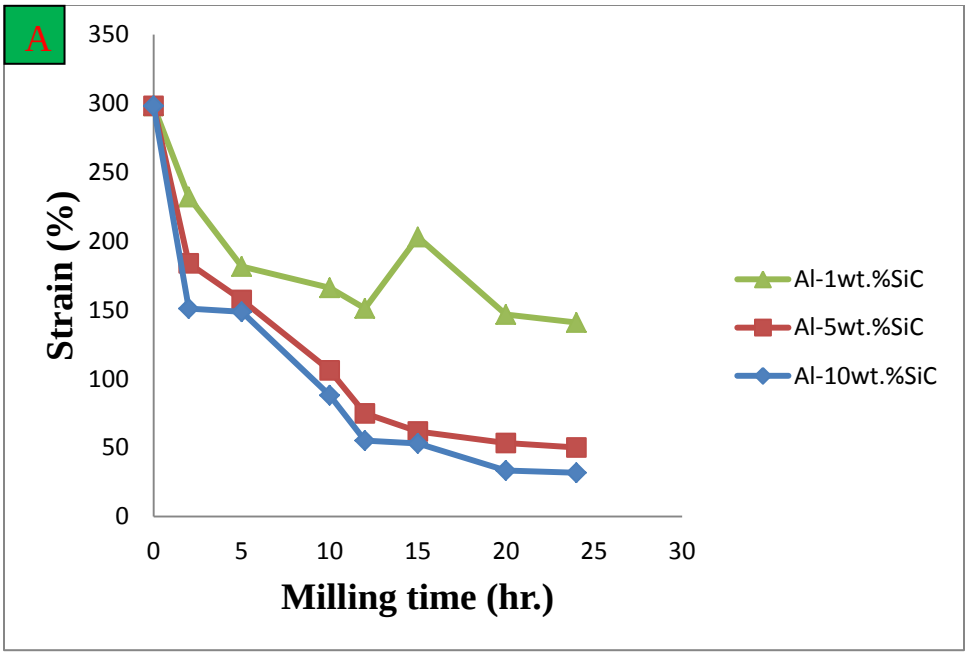


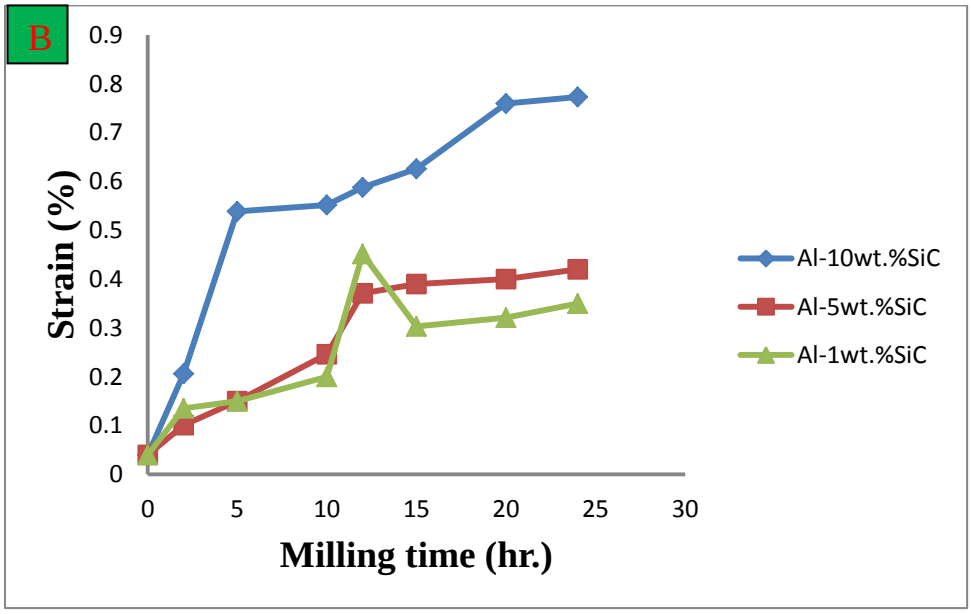


Fig. 4.17 (a) Crystallite size (b) and Strain variation with milling time for Al containing 1, 5 and 10 wt% SiC milled for 24 h.

## 4.2 Characterization of Sintered Samples

### 4.2.1 Effect of Pressure and Heating Rate

This section discusses the effect of pressure on the relative density and then on the microhardness of sintered samples while other sintering parameters were kept constant. Likewise, the effect of heating rate on the relative density and microhardness is discussed. The sintering temperature and time were kept constant at $550^0$C and 5min respectively while pressure and heating rate were varied, one after the other. This is shown in Fig. 4.18 and Fig. 4.25. Increase in pressure from 20 to 50 MPa resulted in tremendous improvement of composites' relative density as can be seen in Fig. 4.18. The relative density of monolithic Al, Al – 1 wt% SiC, Al – 5 wt% SiC and Al – 10 wt% SiC increased from 90.6 to 99.9%, 87.4 to 97%, 87.8 to 94.5% and 86.3 to 92.6% respectively. The rate of this effect at lower pressure range is higher than at higher pressure range for all the composites, (Fig. 4.18). Such behavior was observed in [17, 55, 56]. In the SPS sintering of pure Mo, [55] varying pressure between 29 and 67 MPa, pressure rise enhanced densification till a marginal value was attained at 57 MPa. The observation of Khalil et al. [53] during the SPSintering of Al alloys Al6061 and Al2124 was contrary to this. They carried out the sintering at temperature ranging from 400 to $500^0$C, pressure; 35 to 40 MPa and time varying from 20 to 10 min. At constant temperature of $450^0$C, they noticed that increase in pressure led to decrease in densification as justified by the porosities seen in the microstructure of sintered alloys. However the effect of pressure was not properly studied because each pressure was paired with time and as pressure increase holding time was

decreased (i.e 35 MPa/20 min., 40 MPa/15 min. and 45 MPa/10 min). Definitely the decrease in time as pressure increase led to decrease in densification. There are limited studies, as mentioned in the review, which fully investigated the effect of pressure on properties of sintered composites that is why there are no pure Al reference to compare with. Only temperature effect was investigated in [77, 78] where pressure was kept constant at 50 MPa. Marginal value isn't attained in the sintered composites (density increased continuously with pressure) except for Al – 10 wt% SiC, pressure increase from 35 to 50 MPa didn't result in any significant improvement of relative density. Also a common trend is observed at heating rate of $300^0$C/min; increase in pressure from 35 to 50 MPa only led to very little (less than 1%) density increase. The general effect of density rise with pressure is confirmed by the optical microscopy of the four composites. It can be seen from Fig. 4.19 to Fig. 4.22 a, b and c of each figure that dark spots decreased as pressure increased. This implies that porosity decrease as pressure increase. At higher magnification and contrast, SEM images, Fig. 4.23a, b, d, e and Fig. 4.24a, b, d, e confirms the same argument.

As heating rate of the sintering process was increased from 100 to $300^0$C/min, three different observations were made depending on the set of parameters and the composites. There was significant density rise between 200 and $300^0$C/min for Al -5 wt% SiC. However as can be seen from Fig. 4.18, the rate of increase is slight in most cases for the remaining composites. Even drop in density was observed for Al -10 wt% SiC between 200 and $300^0$C/min. This observation is not the case in a study conducted in [56] which a variation in heating rate from 50 to 700 didn't enhance the relative density of $MoSi_2$.

Likewise Ohser-Wiedemann et al. [55] reported that heating rate didn't enhance the density of pure Mo. No research was found to have treated this with respect to Aluminium. The effect of heating rate on the porosity of sintered samples was also checked using optical microscope (Fig. 4.19 to Fig. 4.22 d, e and f of each figure). For all the composites except Al -10 wt% SiC, dark areas decrease in amount as heating rate increase. An initial decrease and then rise was observed for Al -10 wt% SiC. Both observations confirm what is reported earlier on in Fig. 4.18. SEM images, Fig. 4.23b, c, e, f and Fig. 4.24b, c, e, f confirms the same argument with better image quality.

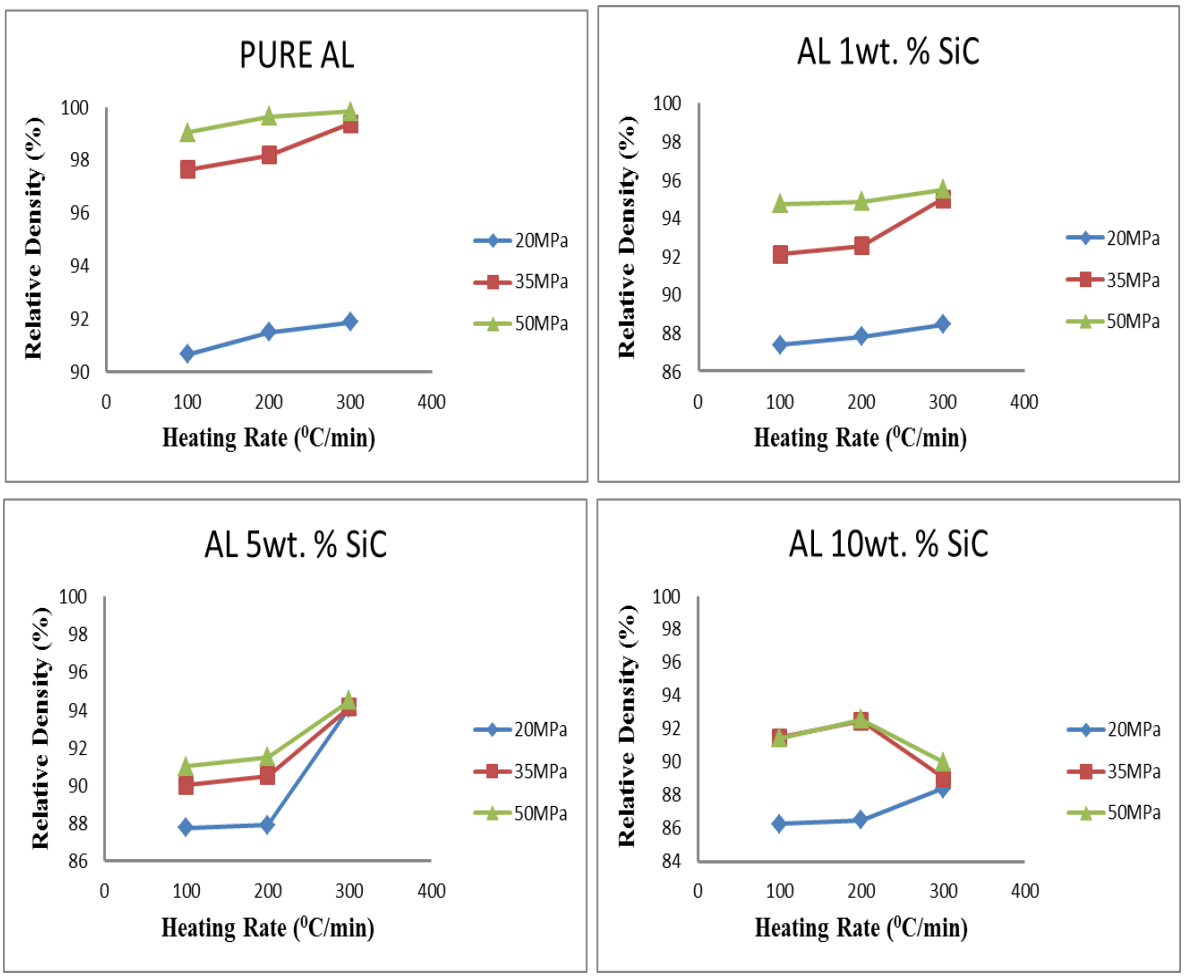


Fig. 4.18 Variation of relative density with heating rate and pressure for monolithic aluminium and aluminium composites reinforced with 1, 5 and 10 wt% SiC.

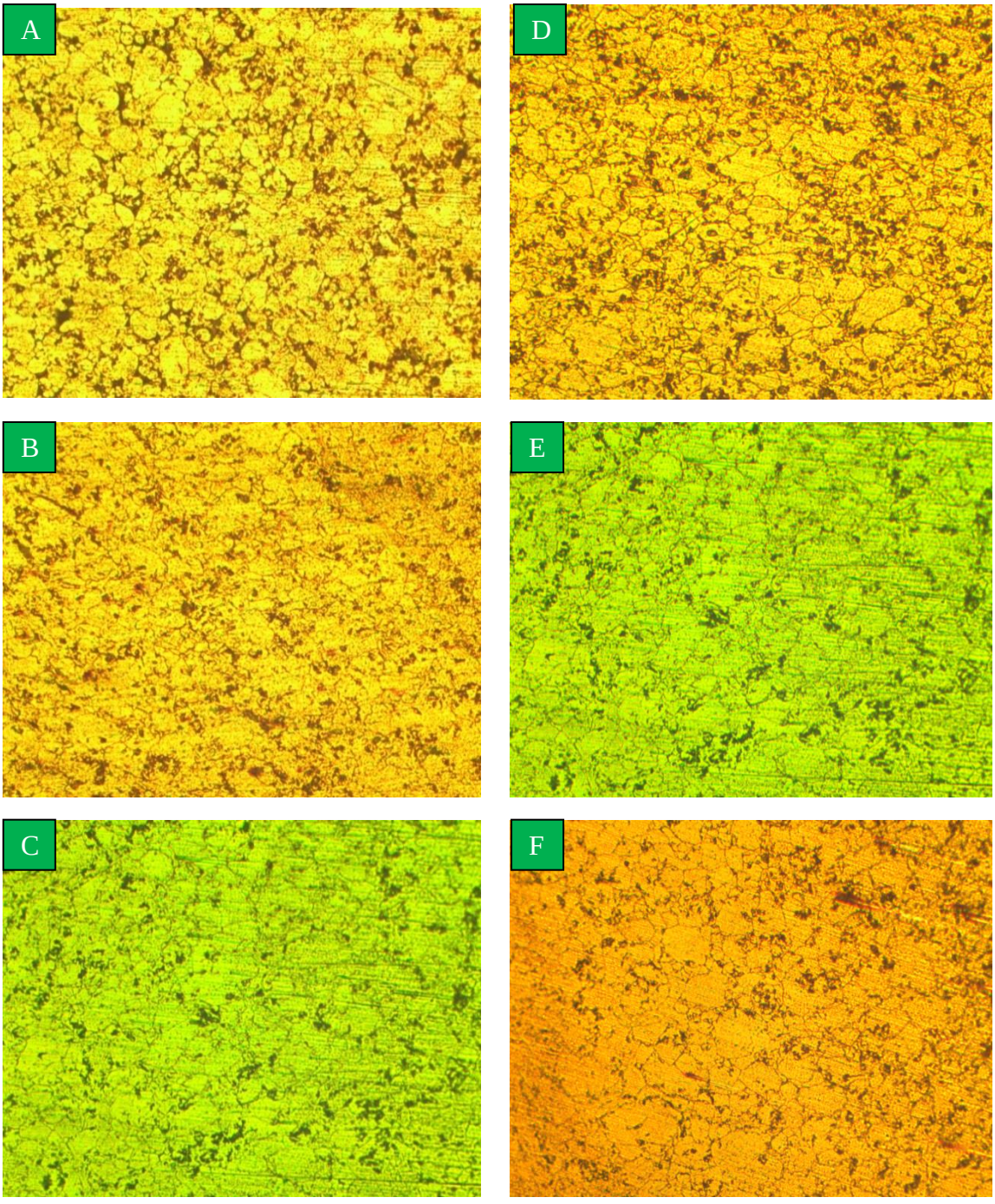


Fig. 4.19 Monolithic aluminium sintered at (a) 20 MPa (b) 35 MPa (c) 50 MPa with other parameters, 550$^0$C, 5 min, 200$^0$C/min kept constant and at (d) 100$^0$C/min (e) 200$^0$C/min (f) 300$^0$C/min with other parameters, 550$^0$C, 5min, 50MPa, kept constant.

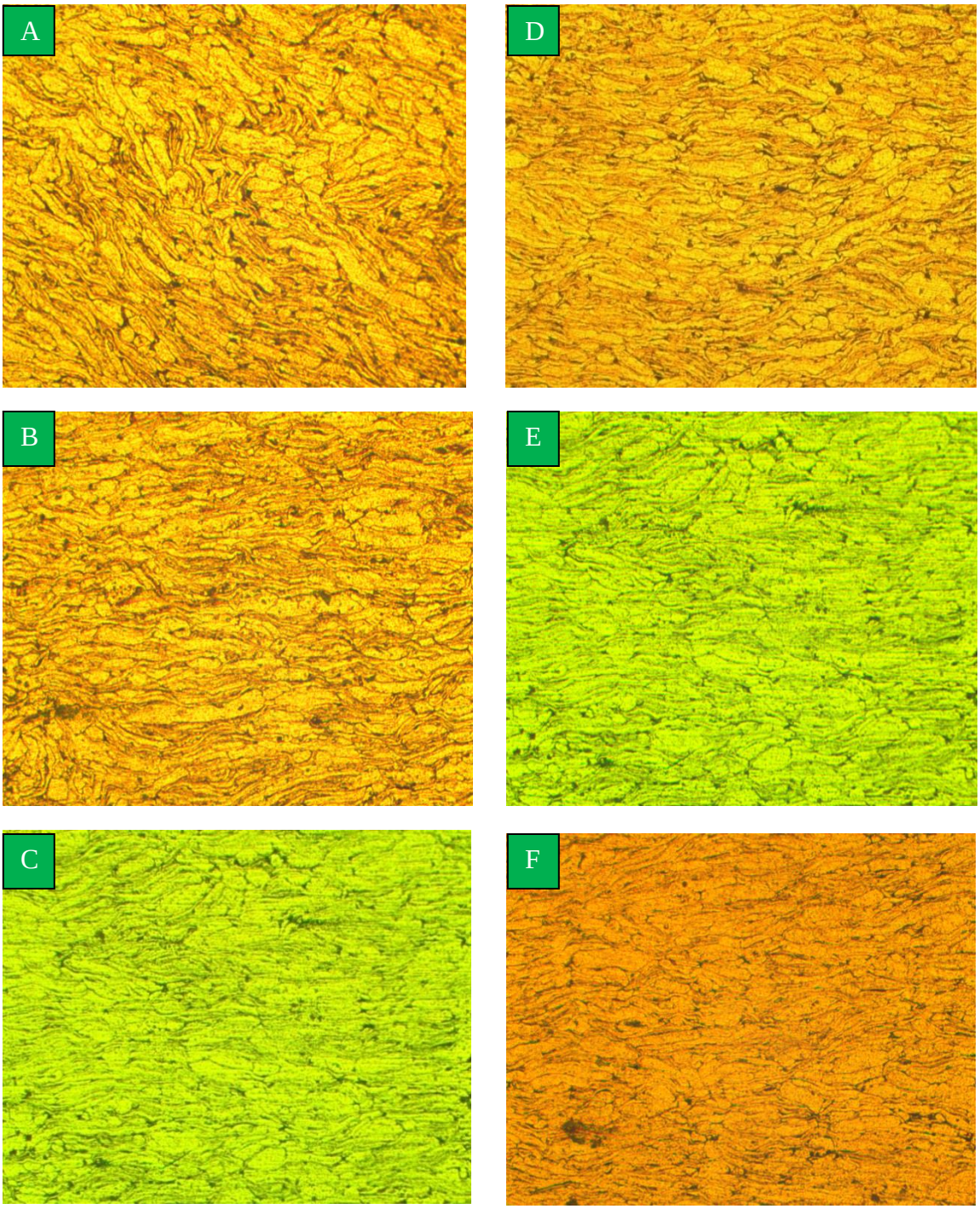


Fig. 4.20 Al -1wt% SiC sintered at (a) 20 MPa (b) 35 MPa (c) 50 MPa with other parameters, 550$^0$C, 5 min, 200$^0$C/min kept constant and at (d) 100$^0$C/min (e) 200$^0$C/min (f) 300$^0$C/min with other parameters, 550$^0$C, 5min, 50MPa, kept constant.

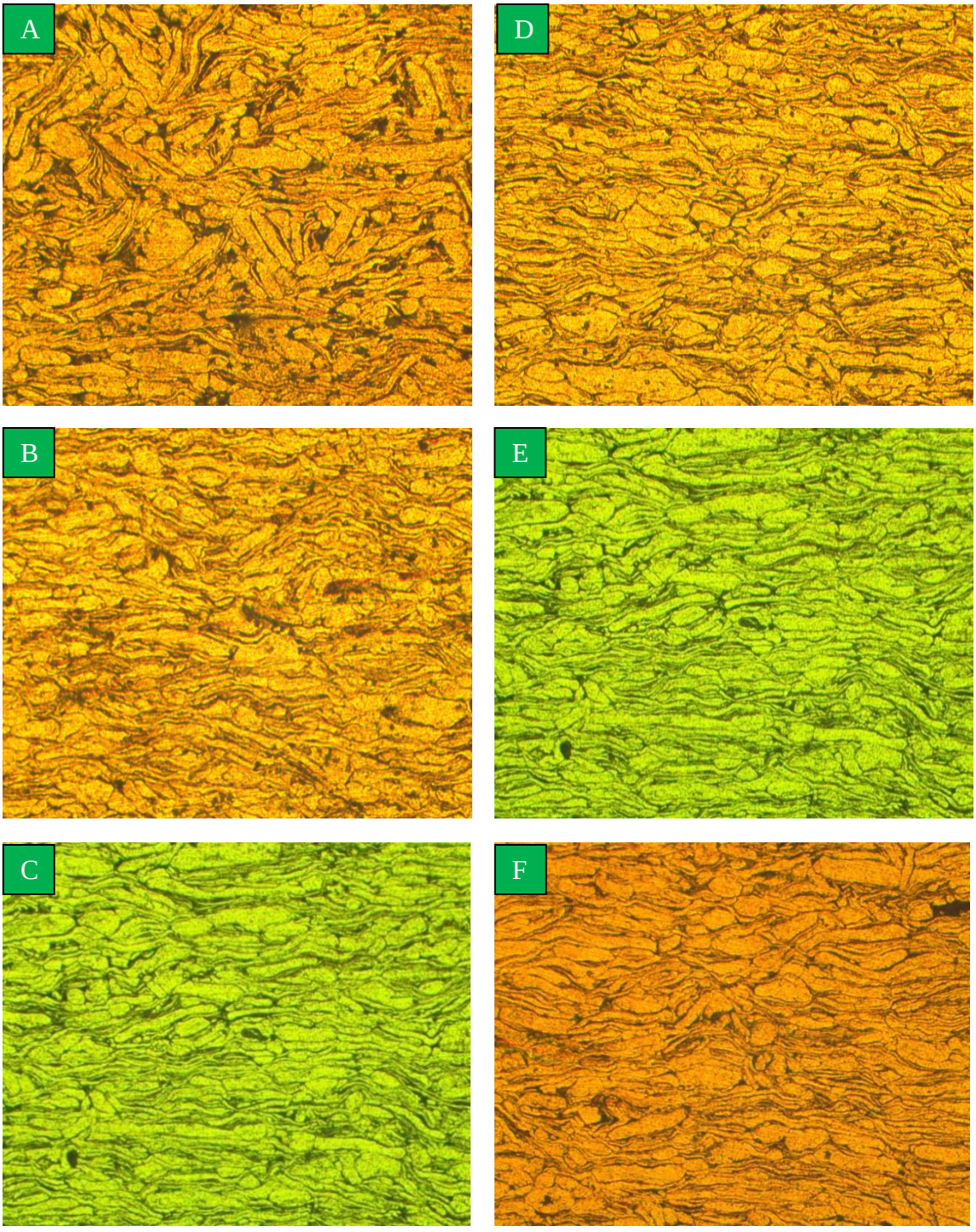


Fig. 4.21 Al -5wt% SiC sintered at (a) 20 MPa (b) 35 MPa (c) 50 MPa with other parameters, 550$^0$C, 5 min, 200$^0$C/min kept constant and at (d) 100$^0$C/min (e) 200$^0$C/min (f) 300$^0$C/min with other parameters, 550$^0$C, 5min, 50MPa, kept constant.

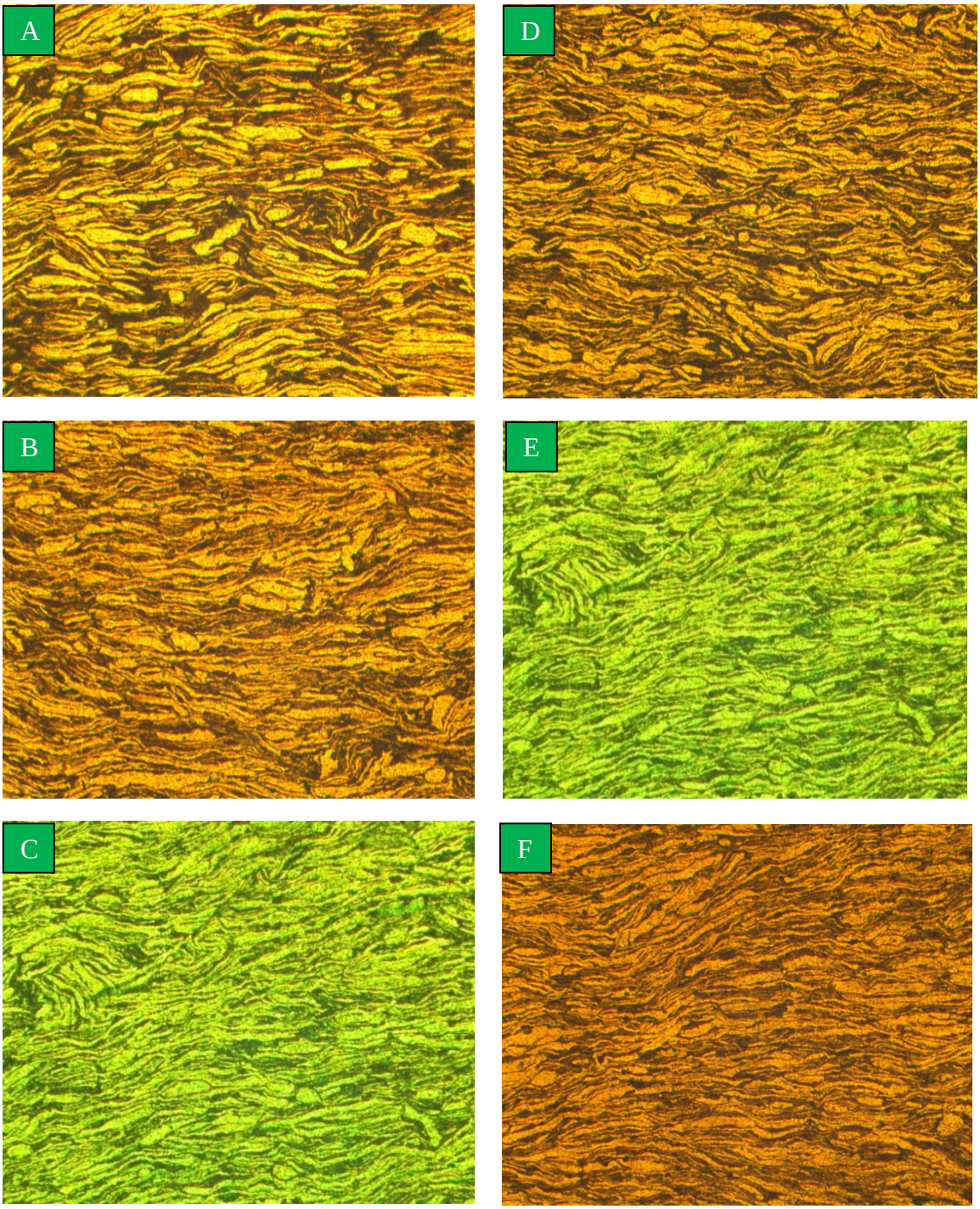


Fig. 4.22 Al -10wt% SiC sintered at (a) 20 MPa (b) 35 MPa (c) 50 MPa with other parameters, 550$^0$C, 5 min, 200$^0$C/min kept constant and at (d) 100$^0$C/min (e) 200$^0$C/min (f) 300$^0$C/min with other parameters, 550$^0$C, 5min, 50MPa, kept constant.

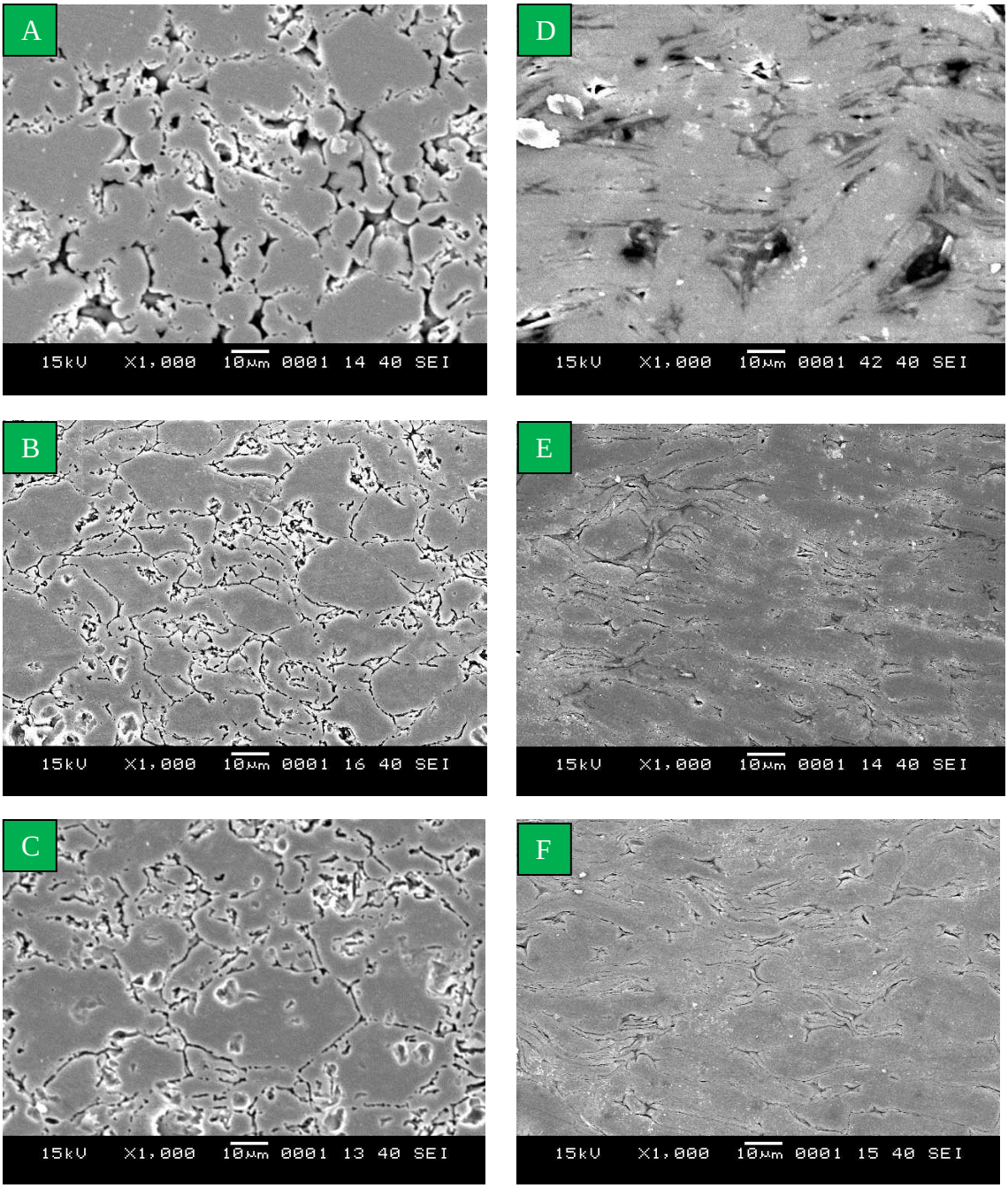


Fig. 4.23 Monolithic aluminium sintered at (a) $550^0$C, 5min, $200^0$C/min, 20MPa (b) $550^0$C, 5min, $200^0$C/min, 50MPa (c) $550^0$C, 5min, $300^0$C/min, 50MPa, Al -1wt% SiC sintered at (d) $550^0$C, 5min, $200^0$C/min, 20MPa (e) $550^0$C, 5min, $200^0$C/min, 50MPa (f) $550^0$C, 5min, $300^0$C/min, 50MPa

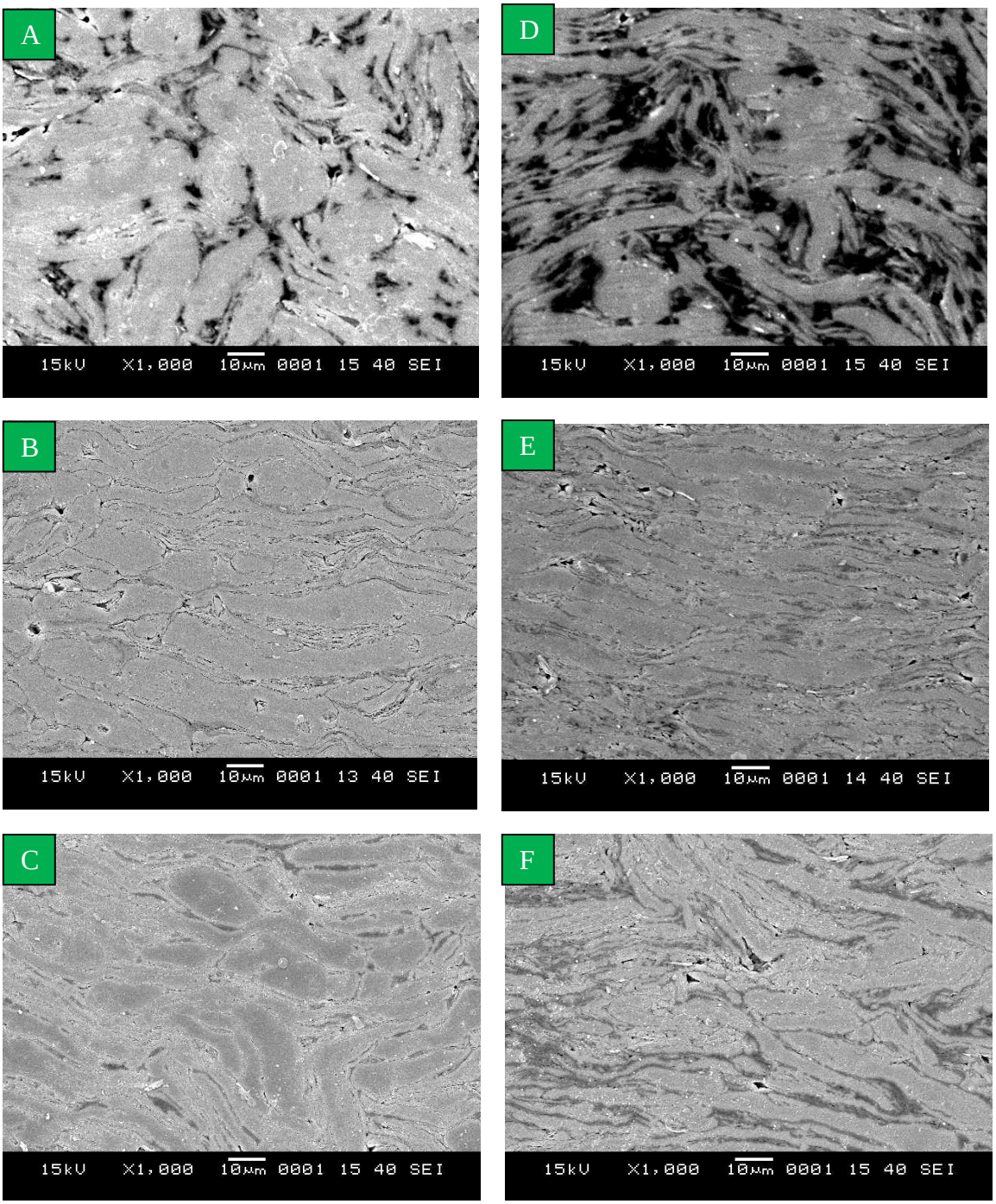


Fig. 4.24 Al -5wt% SiC sintered at (a) $550^0$C, 5min, $200^0$C/min, 20MPa (b) $550^0$C, 5min, $200^0$C/min, 50MPa (c) $550^0$C, 5min, $300^0$C/min, 50MPa, Al -10wt% SiC sintered at (d) $550^0$C, 5min, $200^0$C/min, 20MPa (e) $550^0$C, 5min, $200^0$C/min, 50MPa (f) $550^0$C, 5min, $300^0$C/min, 50MPa

For all the composites except pure (monolithic) Al, as pressure increase, microhardness increased at an appreciable rate. The microhardness profile tends to copy the density variation with sintering parameters meaning that higher hardness value can be attributed to higher density. This can only be so if other strength hindering factors, such as grain growth, are not favored with pressure increase. In Fig. 4.19 to Fig. 4.22 a, b and c of each figure shows that as pressure increases the grains become smaller except monolithic Al whose 50MPa grains are bigger than the 35 MPa grains. A clearer picture of this is seen in Fig. 4.23a, b, d, e and Fig. 4.24a, b, d, e. This justifies why there was a drop in hardness for Al between 35 and 50 MPa even when density increased between these points. The rate at which hardness increase with pressure at lower heating rate is higher than at higher heating rate, see Fig. 4.25. This is a sort of limiting behavior which implies that at higher heating rate increase in pressure will have less effect in enhancing microhardness. Monolithic Al microhardness drop can be attributed to absence of SiC. This is so because Kwon et al. [79] reported that SiC hinders or minimize Al matrix grain growth by pinning effect. Although some researchers [72, 77, 78] reported that Aluminium oxide prevented grain growth by pinning effect in SPSintered pure Al, the amount in this work may be too small to provide adequate pinning at 50 MPa for monolithic Al. In [77], linear white part that was not observed in this work was seen between some grains, indicating Al oxide. Also it seems as if 50 MPa exceeds the pressure at which grain growth is favored for pure Al at $550^0$C. very few or none of the reviewed research investigated the effect of pressure on microhardness of composites.

From the discussion of pressure effect on density and hardness it is observed that 50 MPa gave the highest density and hardness in most of the cases. This is because density and hardness keep increasing with pressure except at $300^0$C/min where a marginal behavior is seen. Hence 50 MPa is appropriate as the best sintering pressure for the composites. It has also been seen from samples' microstructures that higher pressure can impede grain growth.

Fig. 4.25 shows that as heating rate increases monolithic Al and composites' microhardness increases. However there are exceptions as the figure shows that after $200^0$C/min, Al -10wt% SiC (35 and 50 MPa) showed drop in hardness. Since the relative density graph (Fig. 4.18) for the same composites showed that density increases with heating rate when other parameters were kept constant, hardness is expected to follow similar trend. The variation of the grain sizes with heating rate in Fig. 4.19 to Fig. 4.22 d, e and f of each figure, also supports this observation. This agrees with some previous research [8, 56] that state that increase in heating rate results to smaller grains. The decrease that was observed in Al -10wt% SiC composites after $200^0$C/min can be attributed to fact that the composites has lower density and hence higher porosity at the said set of sintering parameters ($200^0$C/min, 35 and 50 MPa). A material should be fully densified in order to transfer load across the microstructure from the matrix to the reinforcement adequately.

In most cases, hardness and density of composites increases with heating rate throughout. Hence $300^0$C/min seems to be an best value. However some factors oppose its choice as an best value. First, density dropped after $200^0$C/min for Al -10wt% SiC while heating

rate increase from $200^0$C/min to $300^0$C/min only caused little improvement in monolithic Al and Al -1wt% SiC densities. Secondly, hardness dropped after $200^0$C/min for Al -10wt% SiC; the highest densification was obtained at $200^0$C/min. Finally, higher heating rate SP sintering is more difficult because it requires higher energy input. I especially experienced difficulties while sintering at $300^0$C/min.

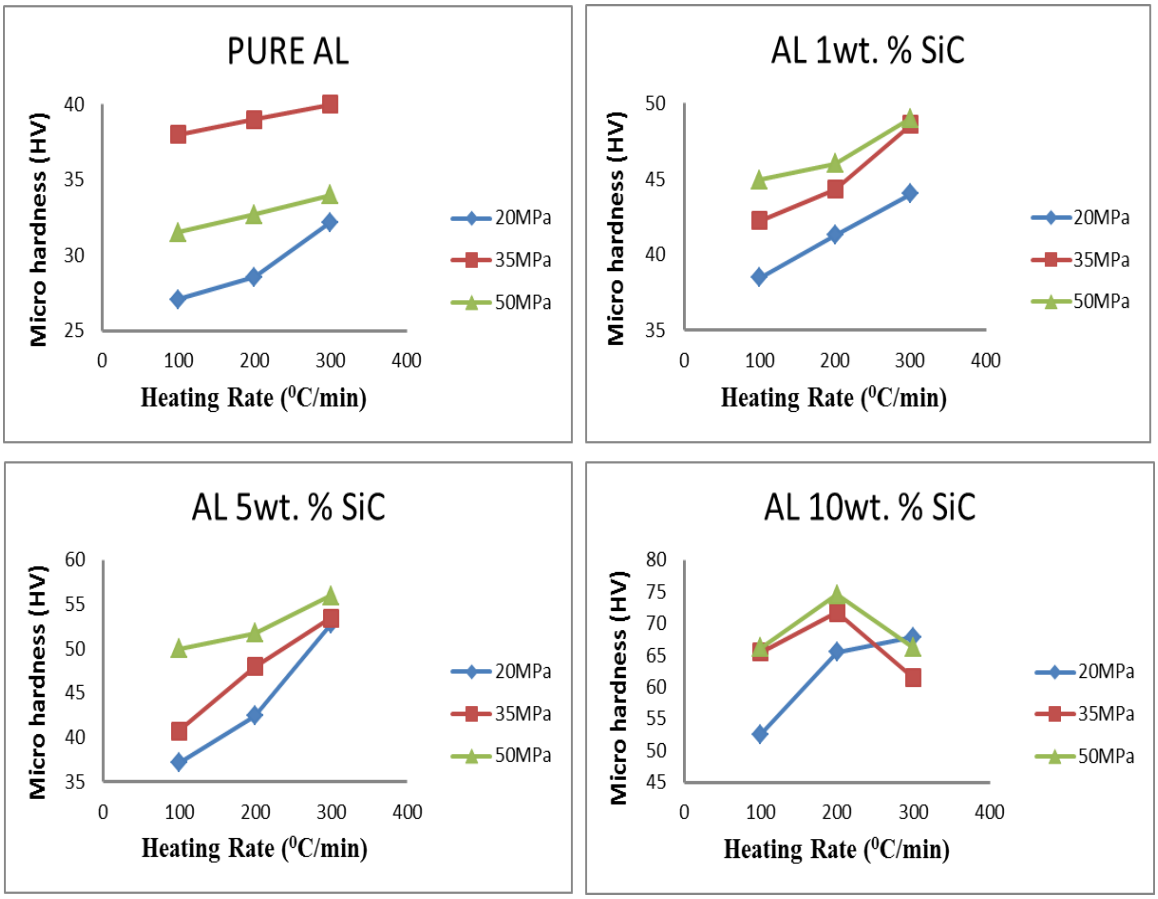


Fig. 4.25 Variation of micro-hardness with heating rate and pressure for monolithic aluminium and aluminium composites reinforced with 1, 5 and 10 wt% SiC.

### 4.2.2 Effect of Temperature and Time

In this section, the effect of sintering temperature on the relative density and then on the microhardness plus the effect of sintering time on the relative density and microhardness of sintered samples were investigated. The best pressure and heating rate (50 MPa and $200^0$C/min respectively) selected from section 4.2.1, were kept constant while temperature and time were varied, one after the other (Fig. 4.26 and Fig. 4.33).

The rate at which sintering temperature enhance the density of the sintered specimen is very high. Fig. 4.26 shows that for any holding time increase in temperature resulted in an increase in relative density of all the sintered composites including monolithic Aluminium. The optical micrographs of the composites shown in Fig. 4.27 to Fig. 4.30 (a, b and c of each figure) justify this; Porosity amount decreases with temperature while density increases. Furthermore, SEM micrographs, Fig. 4.31 and Fig. 4.32 (b, c, e, f of each figure) verified the same observation. A limiting trend of density variation with temperature is observed in pure Al and Al – 10 wt% SiC, as observed in [53, 67] where Al6061 and Al2124 were spark plasma sintered between 400 and $500^0$C. Al – 1 wt% SiC and Al – 5 wt% SiC showed uniform rate of relative density increase with temperature (Fig. 4.26). These observations agree with an explanation made in [59] where relationship between temperature and density was described by Eqn. 2.1.

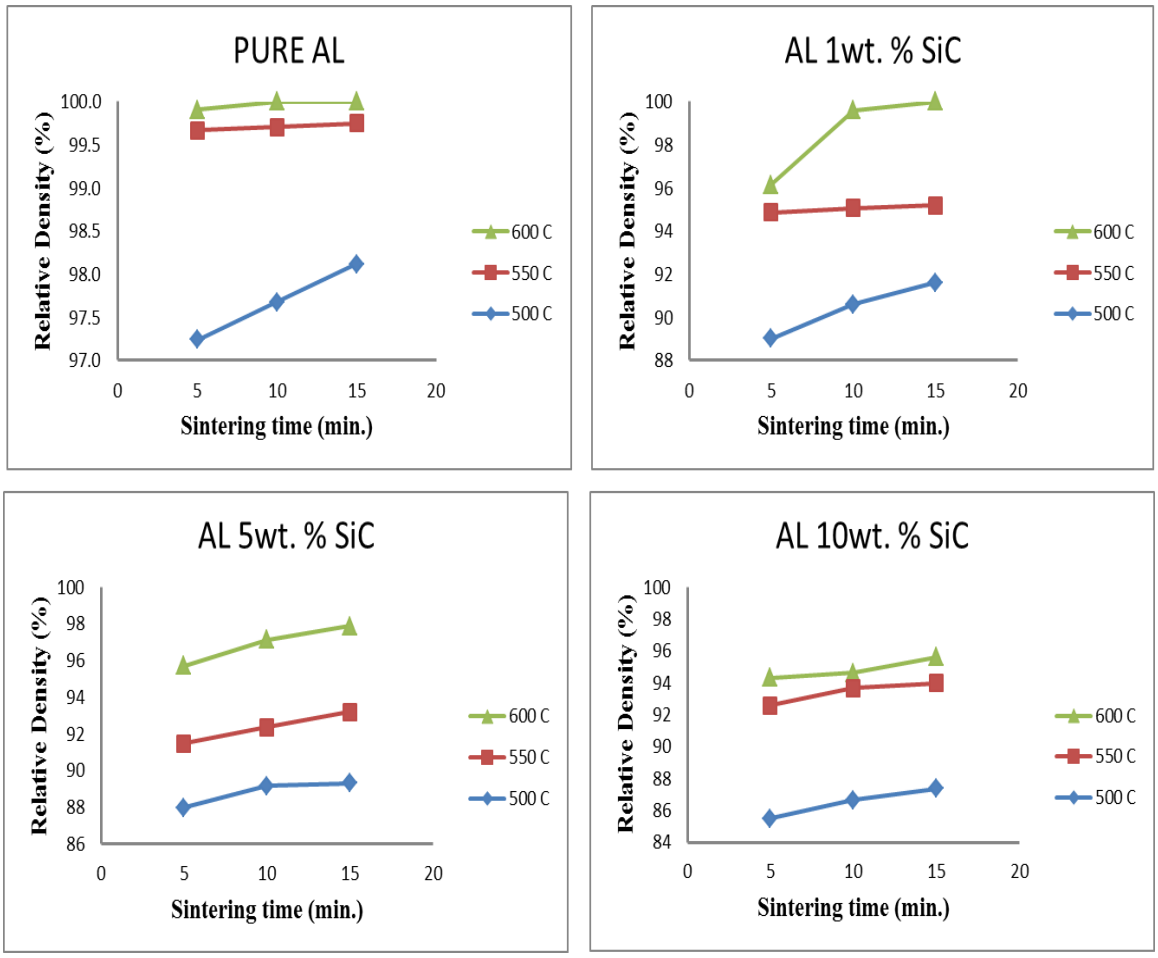


Fig. 4.26 Variation of relative density with sintering time and temperature for monolithic aluminium and aluminium composites reinforced with 1, 5 and 10 wt% SiC.

Over all the composites, relative density increases with increase in time. Similar observation was seen in [60]. However, the rate of increase is slight in some cases and marginal behavior is observed in most cases when sintering is done at $600^0$C (See Fig. 4.33). This agrees with was was reported in [17]. For pure Al, a temperature of $600^0$C can enable the attainment of full density in just 5 minutes. If sintering is done at $550^0$C, 15 minutes will be required to attain 100% relative density. This implies that the time required for adequate sintering is inversely proportional to sintering temperature [69].

As SiC amount increase, combination of $600^0$C and 15 minutes is required to obtain full densification. Full densification was obtained for Al – 1wt% SiC but it was not obtained for Al – 5 and 10wt% SiC, where 98 and 96 % relative densities were observed respectively. The increase in density with sintering time can be justified with the optical micrographs shown in Fig. 4.27 to Fig. 4.30 (d, e and f of each figure) and SEM images shown in Fig. 4.31 and Fig. 4.32 (a, b, d, and e of each figure).

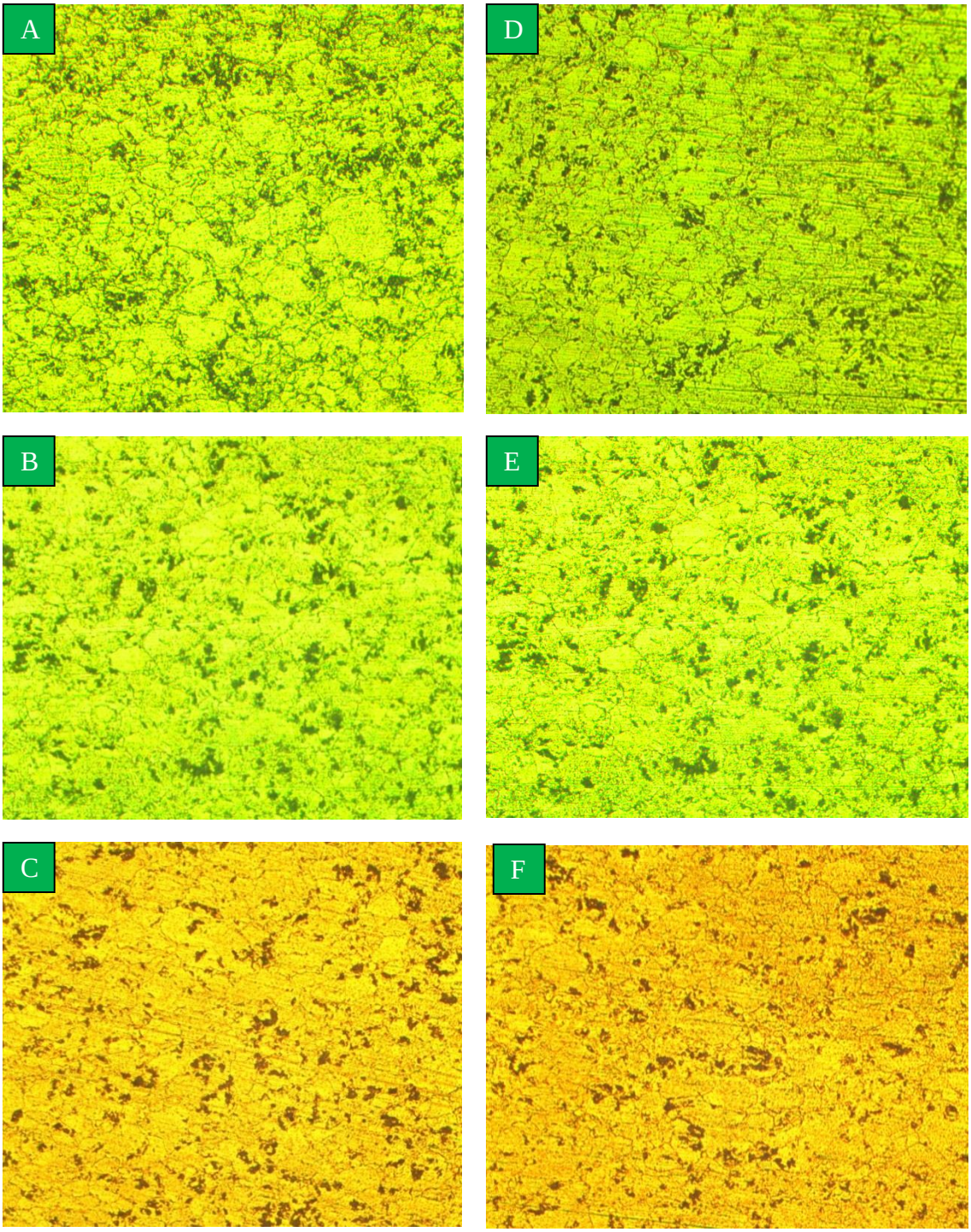


Fig. 4.27 Monolithic aluminium sintered at (a) $500^0$C (b) $550^0$C (c) $600^0$C with other parameters, 50MPa, $200^0$C/min, 10 min kept constant and at (d) 5 min. (e) 10 min. (f) 15 min. with other parameters, 50MPa, $200^0$C/min, $550^0$C kept constant.

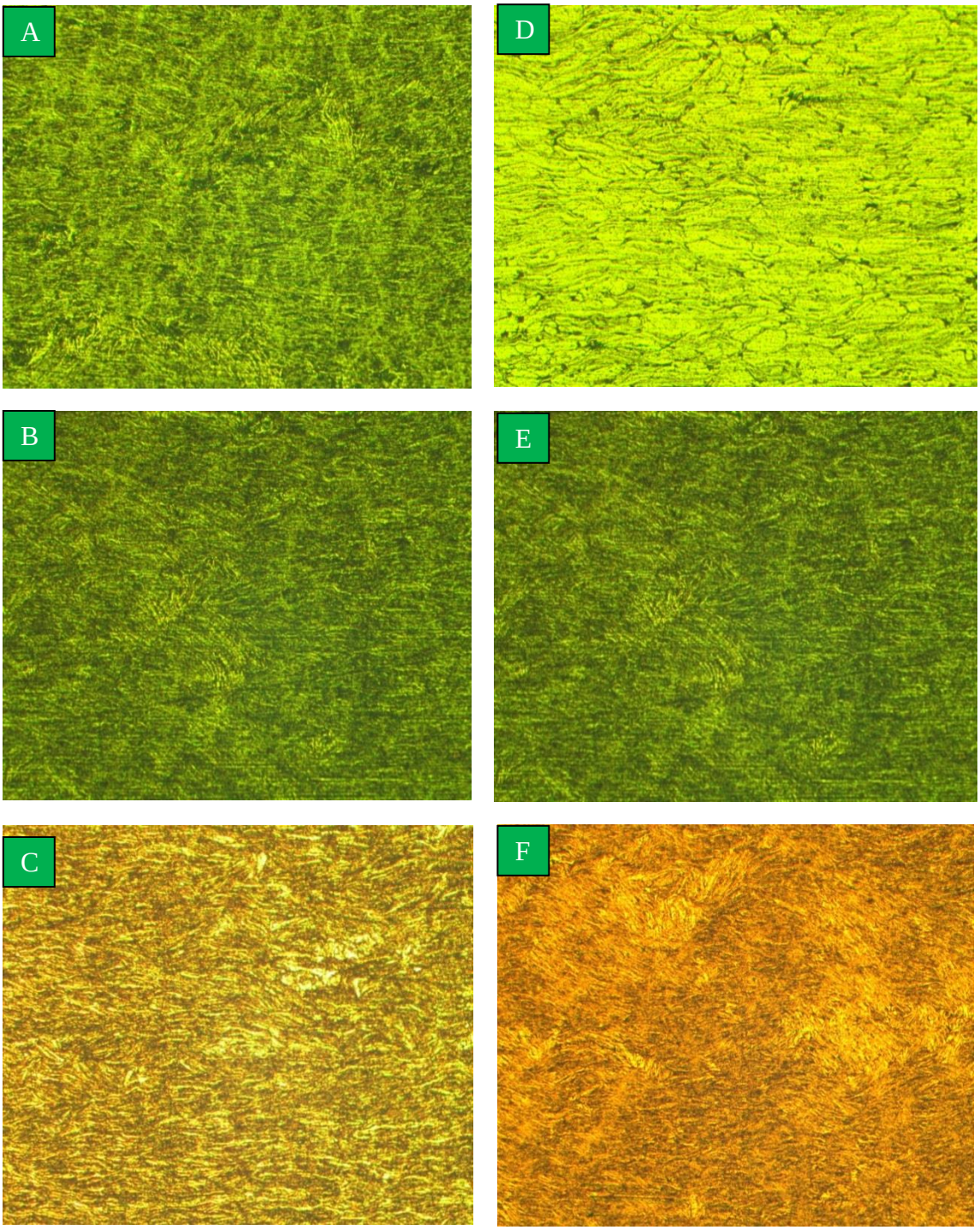


Fig. 4.28 Al -1wt% SiC sintered at (a) 500$^0$C (b) 550$^0$C (c) 600$^0$C with other parameters, 50MPa, 200$^0$C/min, 10 min kept constant and at (d) 5 min. (e) 10 min. (f) 15 min. with other parameters, 50MPa, 200$^0$C/min, 550$^0$C kept constant.

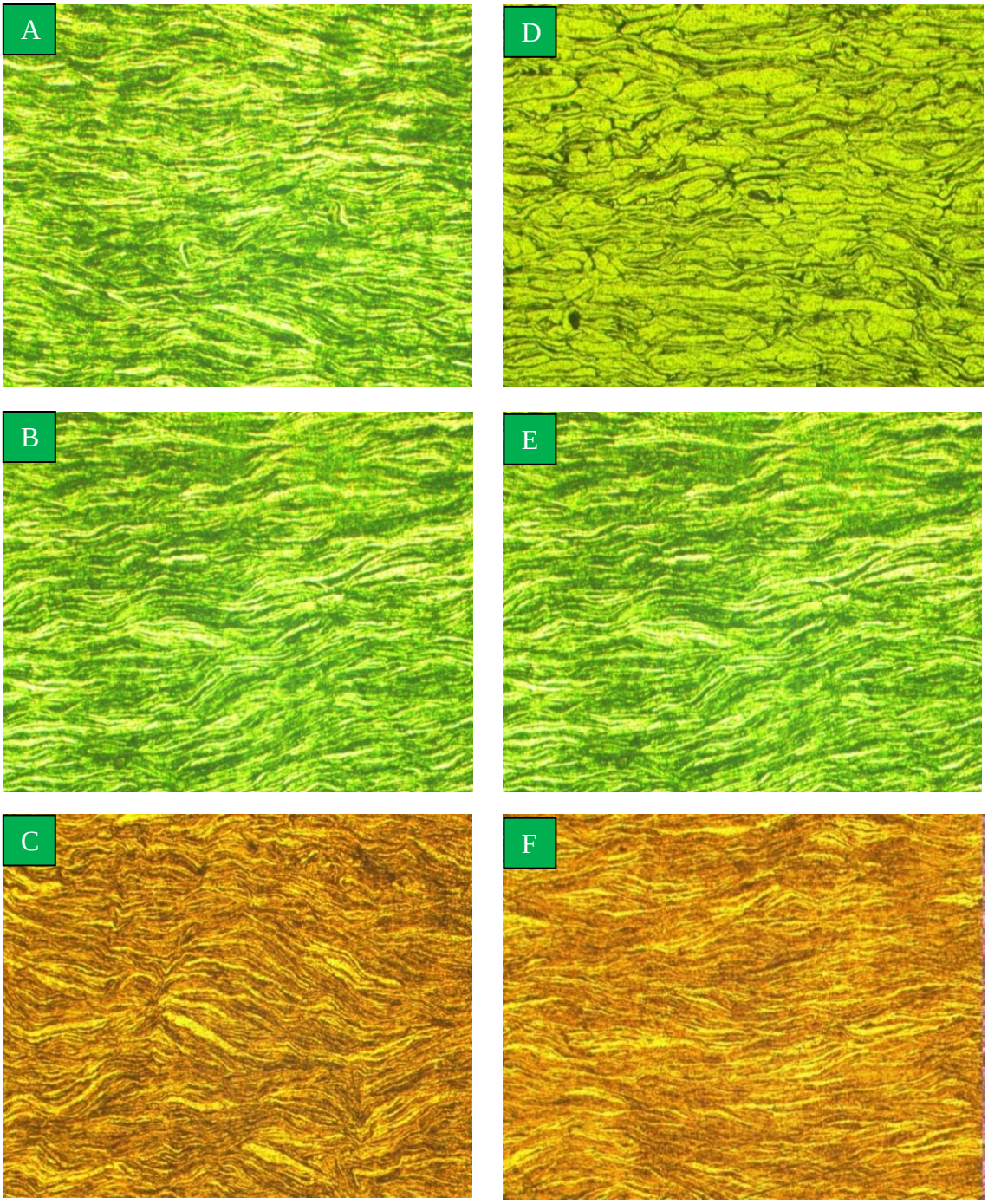


Fig. 4.29 Al -5wt% SiC sintered at (a) $500^0$C (b) $550^0$C (c) $600^0$C with other parameters, 50MPa, $200^0$C/min, 10 min kept constant and at (d) 5 min. (e) 10 min. (f) 15 min. with other parameters, 50MPa, $200^0$C/min, $550^0$C kept constant.

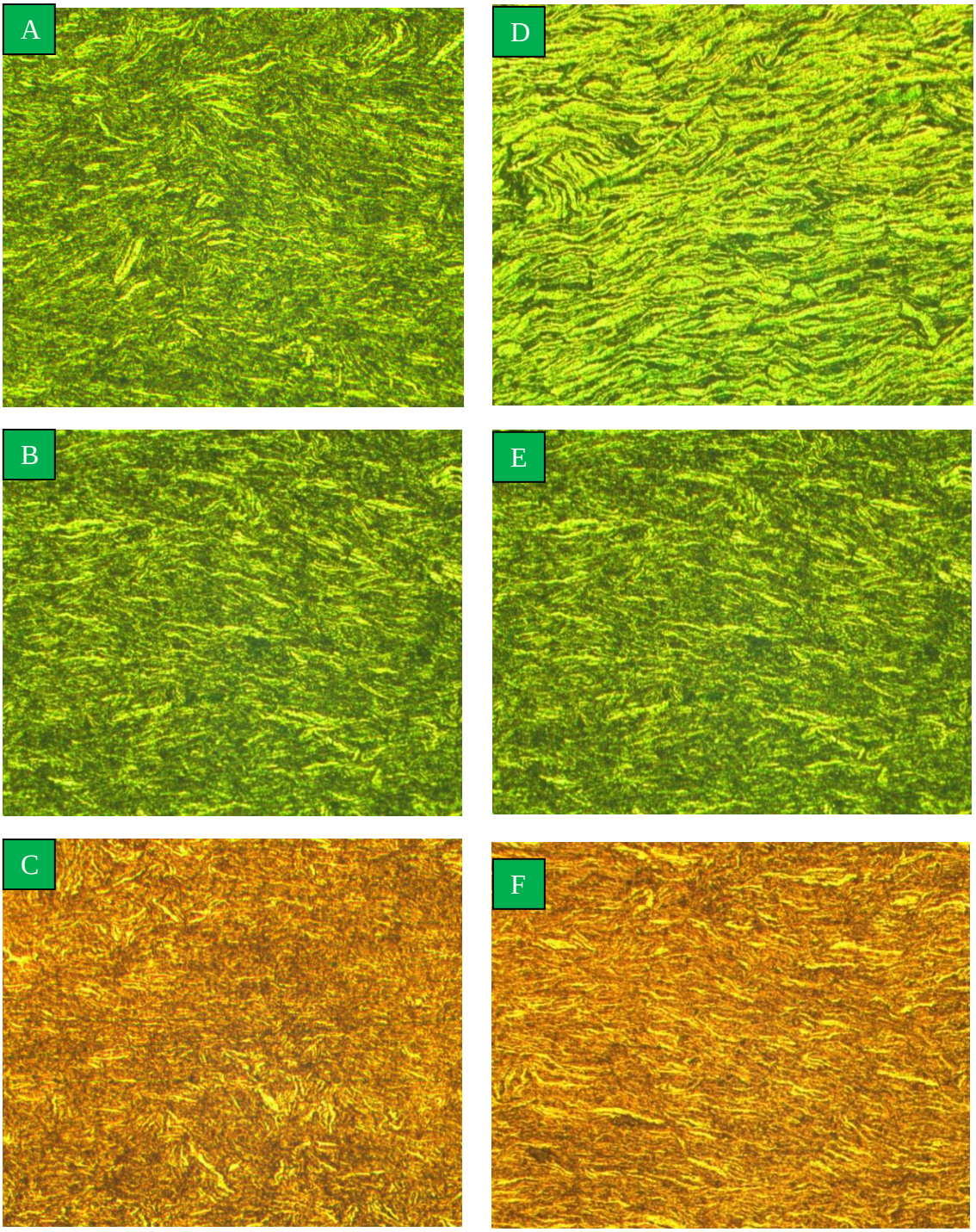


Fig. 4.30 Al -10wt% SiC sintered at (a) $500^0$C (b) $550^0$C (c) $600^0$C with other parameters, 50MPa, $200^0$C/min, 10 min kept constant and at (d) 5 min. (e) 10 min. (f) 15 min. with other parameters, 50MPa, $200^0$C/min, $550^0$C kept constant.

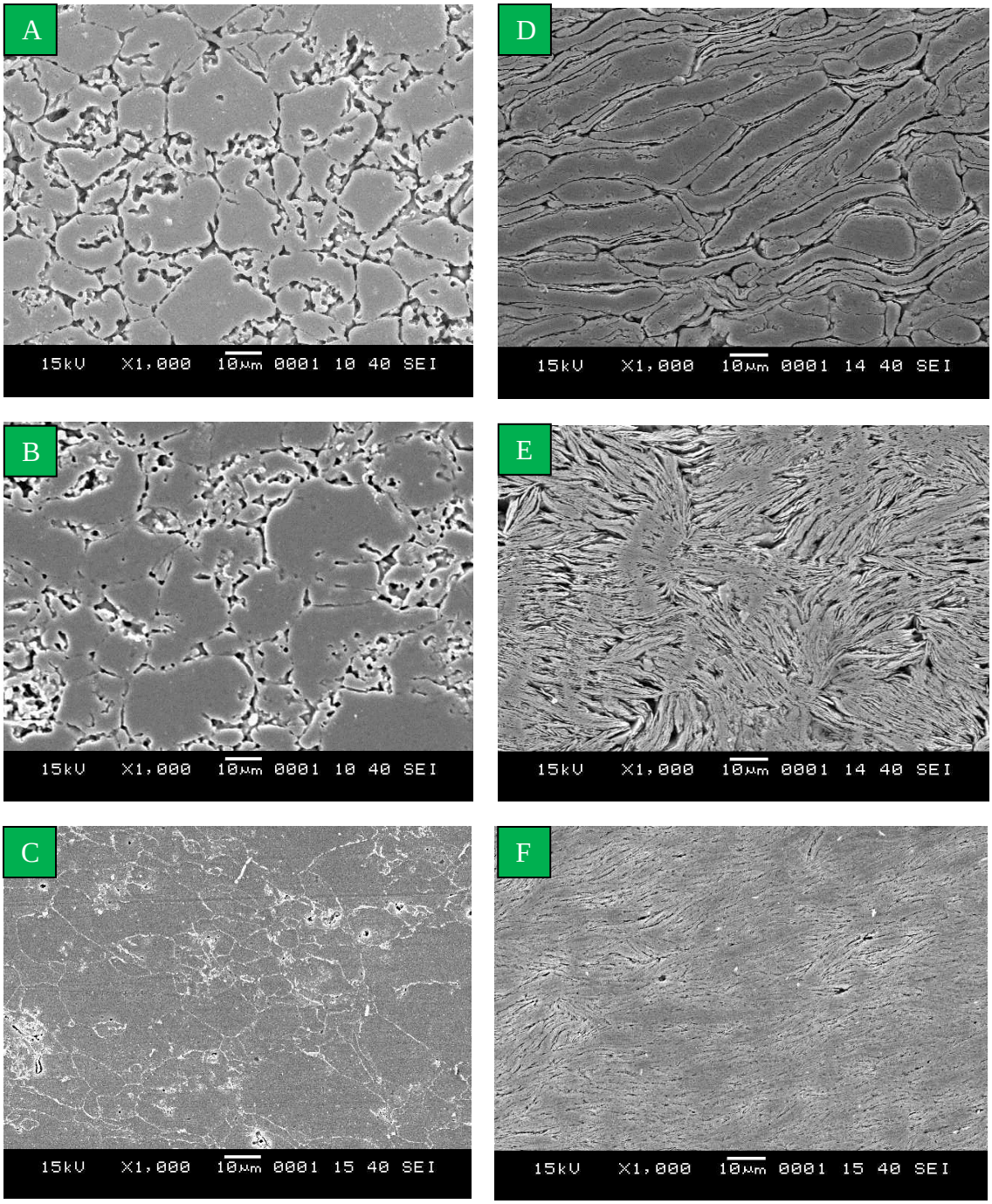


Fig. 4.31 Monolithic aluminium sintered at (a) $500^0$C, $200^0$C/min, 50MPa, 5min (b) $500^0$C, $200^0$C/min, 50MPa, 10min (c) $600^0$C, $200^0$C/min, 50MPa, 10min and Al -1wt% SiC sintered at (d) $500^0$C, $200^0$C/min, 50MPa, 5min (e) $500^0$C, $200^0$C/min, 50MPa, 10min (f) $600^0$C, $200^0$C/min, 50MPa, 10min

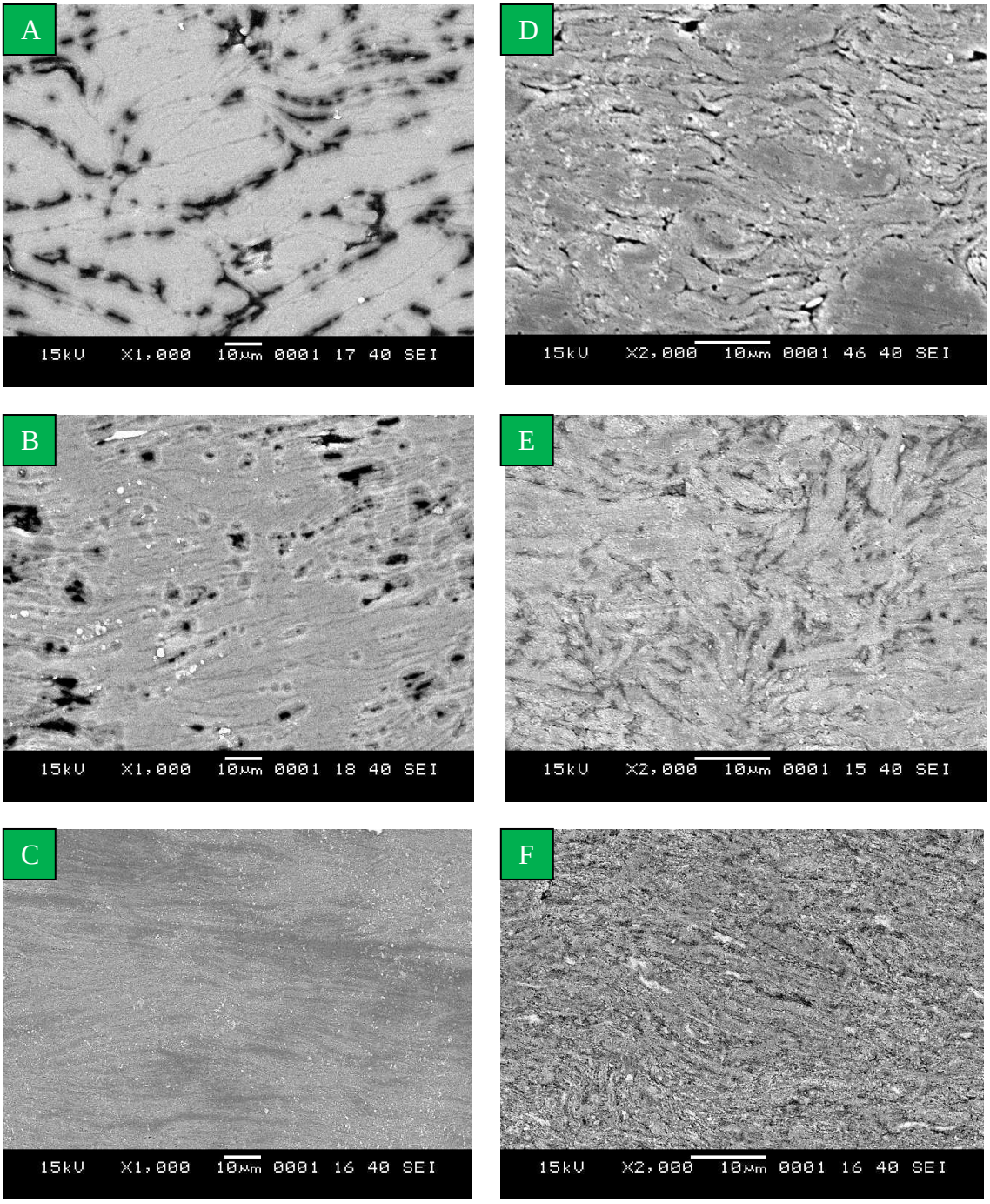


Fig. 4.32 Al -5wt% SiC sintered at (a) $500^0$C, $200^0$C/min, 50MPa, 5min (b) $500^0$C, $200^0$C/min, 50MPa, 10min (c) $600^0$C, $200^0$C/min, 50MPa, 10min and Al -10wt% SiC sintered at (d) $500^0$C, $200^0$C/min, 50MPa, 5min (e) $500^0$C, $200^0$C/min, 50MPa, 10min (f) $600^0$C, $200^0$C/min, 50MPa, 10min

Fig. 4.33 shows that increase in temperature resulted in decrease in hardness for monolithic Aluminium. Earlier on, we saw that increase in temperature increased relative density but with quick attainment of limiting trend. Hence it can be said that the drop in hardness is due to the increase in sintering temperature after full densification had been obtained which led to grain growth [55, 58]. This is hardly established with the optical microscope and SEM, comparing the Al sintered at various temperatures in Fig. 4.27 (a, b and c) and Fig. 4.31 (b and c). This may be attributed to the fact that the drop in hardness is not much; a maximum range of 1.3 HV. The observation of Kwon et al. [77] is in support of this. They sintered pure Al by SPS at temperatures varying from 280 to $540^0$C for 20 min. and found that there wasn't significant influence of temperature on microstructure. Grains had typical shape (about polygonal or irregular round shape) because powders were not milled as observed in this work. Black spots were called dust or grooves created by etching. For the SiC reinforced composites, increase in temperature led to increase in hardness. This should be so because the presence of SiC helps to impede grain growth which results from increase in temperature [79]. Hence the densification effect due to sintering temperature rise dominates. The equal hardness value seen in Al -1wt% SiC at $550^0$C and $600^0$C can be explained in similar way as done for Pure Al above at $500^0$C and $550^0$C. Al -1wt% SiC is almost close to pure Al. Fig. 4.33 suggests a sintering temperature of $550^0$C as in the case of pure Al. However $600^0$C stills proves better because it gave a composite of 99.6% relative density as compared to 95% and its hardness is still a bit higher than what was obtained from $550^0$C sintering. A limiting behavior is not observed in the effect of sintering temperature on Al -5wt% SiC

hardness; throughout the experiment, as temperature increase from $500^0$C to $600^0$C, microhardness increased too. This leaves $600^0$C to be chosen as the sintering temperature for Al -5wt% SiC. Similar observation is noted for Al -10wt% SiC but initial rate of hardness increase with temperature is very low compared to the final stage. This still favors the choice of $600^0$C as sintering temperature. The optical micrographs and SEM images for grain effects on hardness are shown in Fig. 4.27 to Fig. 4.30 (a, b and c of each figure), Fig. 4.31 and Fig. 4.32 (b, c, e, f of each figure) respectively.

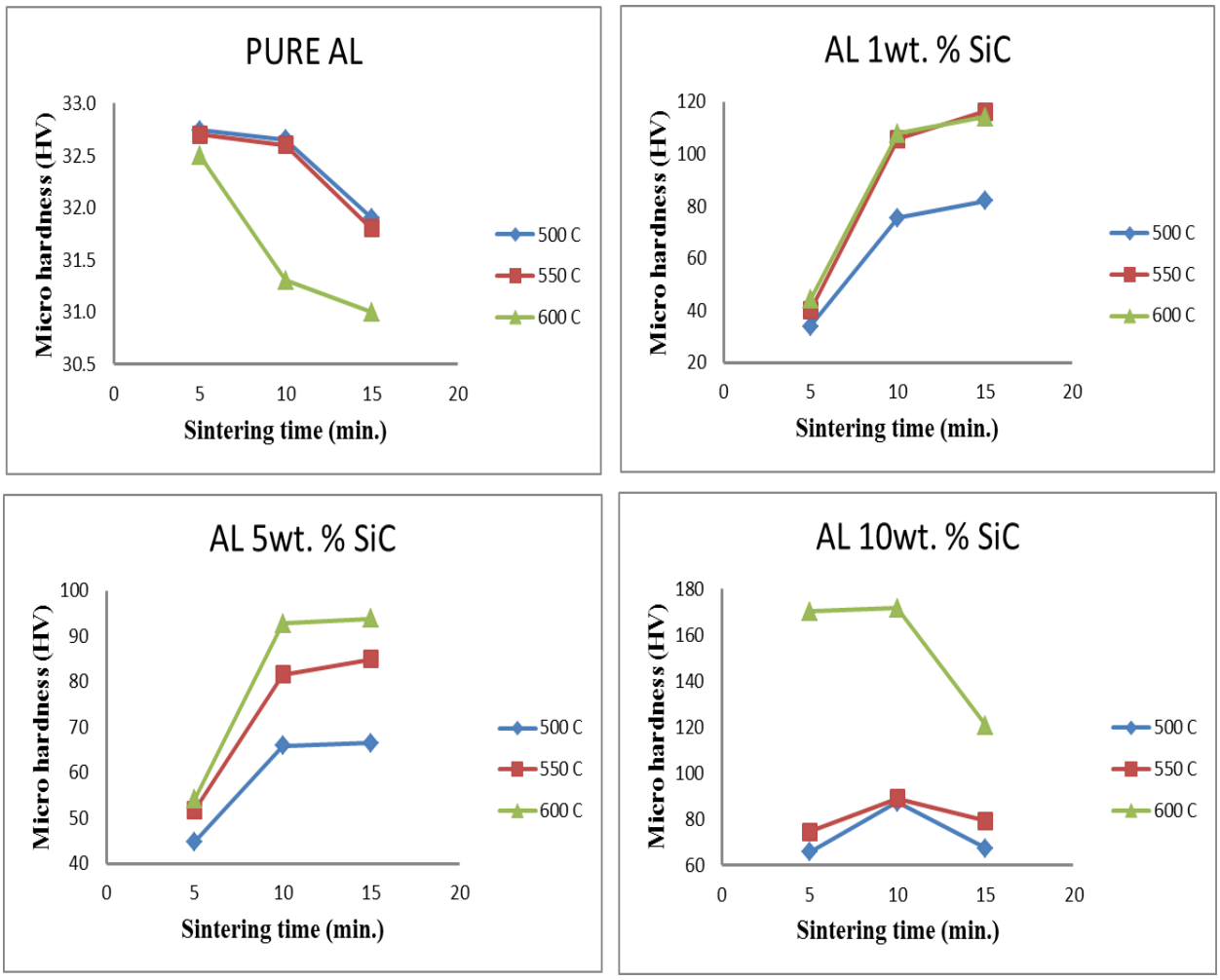


Fig. 4.33 Variation of micro hardness with sintering time and temperature for Monolithic Aluminium and Aluminium composites reinforced with 1, 5 and 10 wt% SiC.

For pure Al, at all sintering temperatures, increase in time led to decrease in hardness. This can be as a result of grain growth after full densification had been obtained [17]. Grain growth is easy for pure Al because of the absence of reinforcement that can serve as grain growth obstructer. The decrease in hardness of monolithic Aluminium with sintering time suggests that pure Al sintering time shouldn't exceed 5 minutes. However a 10 minute sintering time is preferred because it resulted in full densification of the material. For the three SiC reinforced composites, increase in holding time resulted in increase in hardness. Between 10 to 15 minutes holding time, "the rate of hardness increase with time" reduced. This effect increased as the SiC content increased such that there was fall in hardness between 10 to 15 minutes for Al – 10 wt% SiC composites. This implies that sintering time shouldn't exceed 10 minutes. There was a unique observation regarding the microstructure of most of the SiC reinforced composites sintered for 10 minutes or more. The grains are fine and needle like or elongated in shape; see Fig. 4.27 to Fig. 4.30 (d, e and f of each figure), Fig. 4.31 and Fig. 4.32 (a, b, d, and e of each figure). Similar microstructure of elongated grains or particles are seen in spark plasma sintered Al alloy nanocomposites in previous research [20, 68]. This probably helped to increase hardness against the traditional observation of grain growth with time [17, 69, 70].

The density and hardness of each composite at the best set of parameters are given in Table 4.1. Relatively low spark plasma sintering parameters are sufficient for full densification of pure Al; maximum densification was already attained in the first

sintering stage at ($550^0$C, 5 min.). Reference to [77], spark plasma sintering of pure Al resulted to full densification at $540^0$C. However, in a work carried out by Le et al. [78], full densification was not achieved at $550^0$C until $600^0$C (99.3 %) in the spark plasma sintering of pure Al at almost similar sintering parameters to the ones used in [77]. The densification of Pure Al was successful at relatively lower sintering parameters in this research. Despite being fully densified, the hardness of pure Al obtained is very low (40 HV). It appears that some properties of pure Al hardly improve without addition of reinforcement or milling of the powders even with spark plasma sintering. The traditional hardness of Al is about 15 to 30 HV [80]. Researchers have reported values ranging from 42 to 44 HV as hardness of un-milled pure Al by consolidation [79, 81]. However, milling of pure Al for 16 h at 250 rpm, led to a hardness value of up to 83 HV [72]. When reinforcement is introduced into Al, marked improvement in properties can be seen. With a density of 96 % Al – 10 wt% SiC gave a hardness value of 172 HV. This is 330 % increase in hardness compared to base Al (40 HV). The sintering of mechanically milled Al reinforced with 1.2, 6, and 8.2 wt% for 1.5 h at $640^0$C and 700 MPa by CIP gave microhardness of 105, 128 and 158 HV respectively [72]. The sintering was done at higher temperature and longer time hence, with grain growth, the hardness values are less compared to the one obtained by SPS in this research. Although 128 HV for 6 wt % SiC composite is higher than 94 HV obtained in this research for 5 wt % SiC composites. First, it has been seen that Al -5 wt% SiC gave a drop in hardness in this research due to reasons mentioned earlier. Also the amount of SiC in the referenced composite is more than 5 wt%. Kaftelen et al. [82] compared the properties of Al-4Cu-

15% TiC composite fabricated by casting to the one synthesized by hot pressing ($550^0$C, 70 MPa, 1 h). With casting, a hardness value of 113 HV was obtained. However hardness increased to 173 HV with hot pressing of Al-4Cu- 13 wt% TiC. Despite the fact that the amount of SiC (13wt%) is far more than the amount in Al -10wt% SiC developed by SPS in this research there hardness is almost equal (172 HV).

Table 4.1 Highest density and hardness of developed composites

| composite | Density (%) | hardness (HV) | % hardness increase |
|---|---|---|---|
| Al | 100 | 40 | 0 |
| AL 1wt. % SiC | 100 | 116 | 190 |
| AL 5wt. % SiC | 98 | 94 | 135 |
| AL 10wt. % SiC | 96 | 172 | 330 |

### 4.2.3 Composites Compositional Effect on Density and Hardness

Two stages of experiments have been performed to study the effect of process parameters on properties of sintered specimens. The first stage involved keeping temperature and time constant at varying pressure and heating rate. In the second stage, pressure and heating rate were kept constant while temperature and time were varied. In both stages, the relative density of composites has been found to decrease with SiC content as shown in Fig. 4.34 (a). This implies that the more the amount of SiC, in the matrix the higher the temperature required in obtaining adequate sintering. However, hardness generally increases with SiC amount in both stages except at 5 wt% SiC where hardness dropped as

shown in Fig. 4.34 (b). This fall might be due to a compromise made, during the choice of $200^0$C/min as the best heating rate against $300^0$C/min which seems to be better for 5weight composition. Number of previous researchers [8, 16, 20, 72] reported similar observation of increase in hardness against decrease in density. This behavior is likely due to the fact that SiC reinforcement strengthening effect out weights the negative effect of porosity.

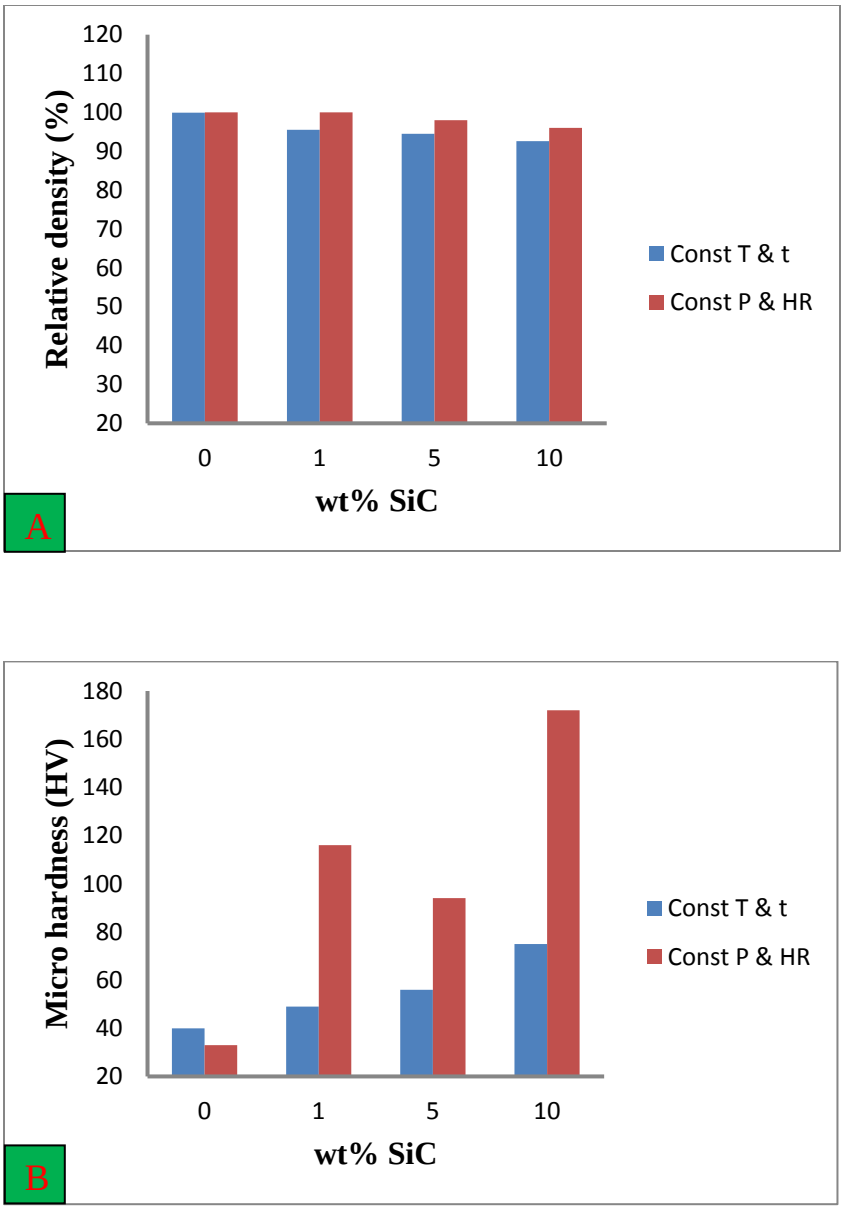


Fig. 4.34 (a) Relative density and (b) Microhardness variation with SiC amount in sintered Al nanocomposites

### 4.2.4 Crystallite Size and Lattice Strain

The XRD analysis of sintered samples was done to evaluate the crystallite size and strain variation with sintering parameters. Fig. 4.35 shows variation of crystallite size with pressure and heating rate for all the composite materials. Crystallite size increased with pressure and then drop after 35 MPa except for Al -5 wt% SiC in which there was continuous decrease in size. This is contrary to the claim that pressure increase caused grain growth as stated in [53]. The crystallite size analysis result has a partial agreement with the observation made in the optical and scanning electron microscope in which grain size decreased with sintering pressure in most of the cases. Hence 50 MPa is supported as the best sintering pressure since the composite has the smallest crystallite size at this pressure. The heating rate effect is not the same throughout the composites; in pure Al and Al -1 wt% SiC, there was an initial rise in crystallite size with increase in heating rate then a drop was observed after $200^0$C/min. A continuous decrease in crystallite size with heating rate was observed in Al -5 wt% SiC and Al -10 wt% SiC, however, a limiting behaviour was seen in Al -10 wt% SiC. This observation also partly agrees with the earlier results of density, hardness, optical and scanning electron microscope. In the micrographs, grains sizes decreased with increase in heating rate in some composites and some cases as explained in earlier sections (4.2.1 and 4.2.2).

It is rare to find XRD analysis for Al based composites on the effect of sintering parameters on crystallite size and strain. Those found only presented crystallite size without strain or investigation of process parameters effect. In this research a detail XRD

analysis is carried out to evaluate crystallite size, strain and investigate the effect of each sintering parameter on properties of sintered samples.

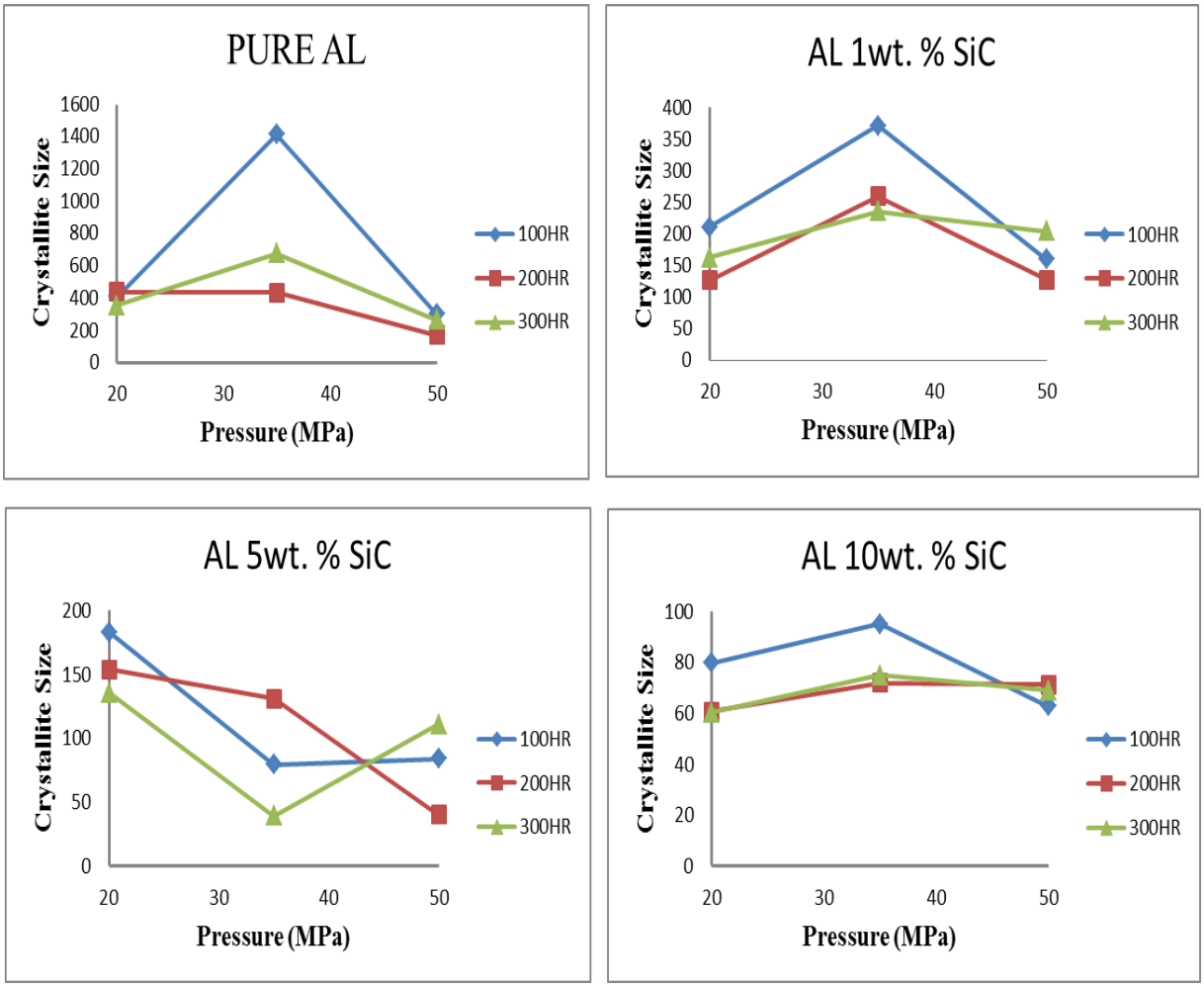


Fig. 4.35 Crystallite size of sintered composite plotted against pressure at different heating rate

The variation of lattice strain with pressure is seen in Fig. 4.36. Similar trend of increase and decrease at 35 MPa as in crystallite size plot is observed here too. This goes in contrary with the expectation of decrease then increase in lattice strain when crystallite size increased and then decrease (inverse proportion) as commonly reported. However, as the process in done under high temperature and pressure, increase in lattice strain can occur where a decrease is expected. The heating rate effect on lattice stain is not the same in all the composites for pure Al and Al -1 wt% SiC, there was an initial decrease in lattice strain with heating rate then a rise at $300^0$C/min. For Al -10 wt% SiC, lattice strain decreased with heating rate and became marginal at $200^0$C/min. for the Al -1 wt% SiC a random behaviour was seen. There was increase in lattice strain as heating rate increased at some pressure while decrease occurred at other pressure.

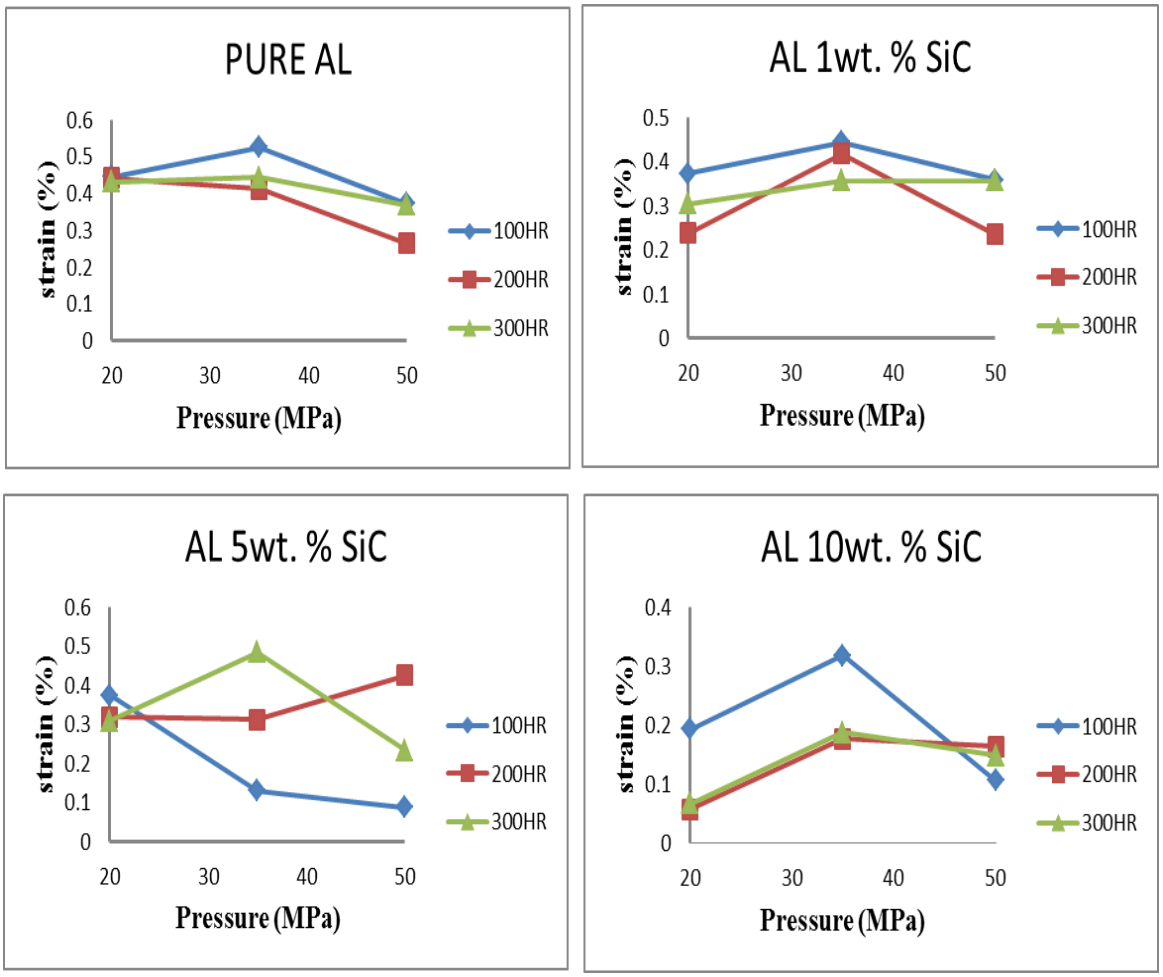


Fig. 4.36 Strain of sintered composite plotted against pressure at different heating rate.

In most cases, crystallite size increased with holding time (Fig. 4.37) but an increase then decrease was observed at $500^0$C, $600^0$C and $550^0$C for pure Al, Al -5 wt% SiC and Al -10 wt% SiC respectively. This is in agreement with the theory of grain growth and observations from previous research. However it goes in contrary with what was observed in the microstructures of the composite where a unique needle like or elongated grains were observed as time increased to 10 min. and 15 min. With respect to temperature effect a mixed observation was seen. In some cases crystallite size initially increased with temperature and later dropped while in others random variation was seen. Again no reference was found to compare the observation with, as effect of process parameters on crystallite size and strain was not reported. Studying the variation of strain with temperature, in some composites and cases, strain increased and then decreased after $550^0$C (Fig. 4.38). The observation tends to be similar to size variation with temperature. This is against the basic understanding of size-strain inverse proportion. However it might have occurred due to sintering at combination of high parameters. As the holding time increase the strain of pure Al and Al -10 wt% SiC increased and then decreased after 10 min (Fig. 4.38). Suitable analogy cannot be drawn when compared to the size variation of the two materials with time. For Al -1 wt% SiC predominantly increase in lattice strain with time was seen while decrease in crystallite size with time was observed for Al -5 wt% SiC. The crystallite size variation of Al -1 wt% SiC is similar to what has been observed for the lattice strain. References that studied the variation of strain with time and temperature have not been found to compare with this observation.

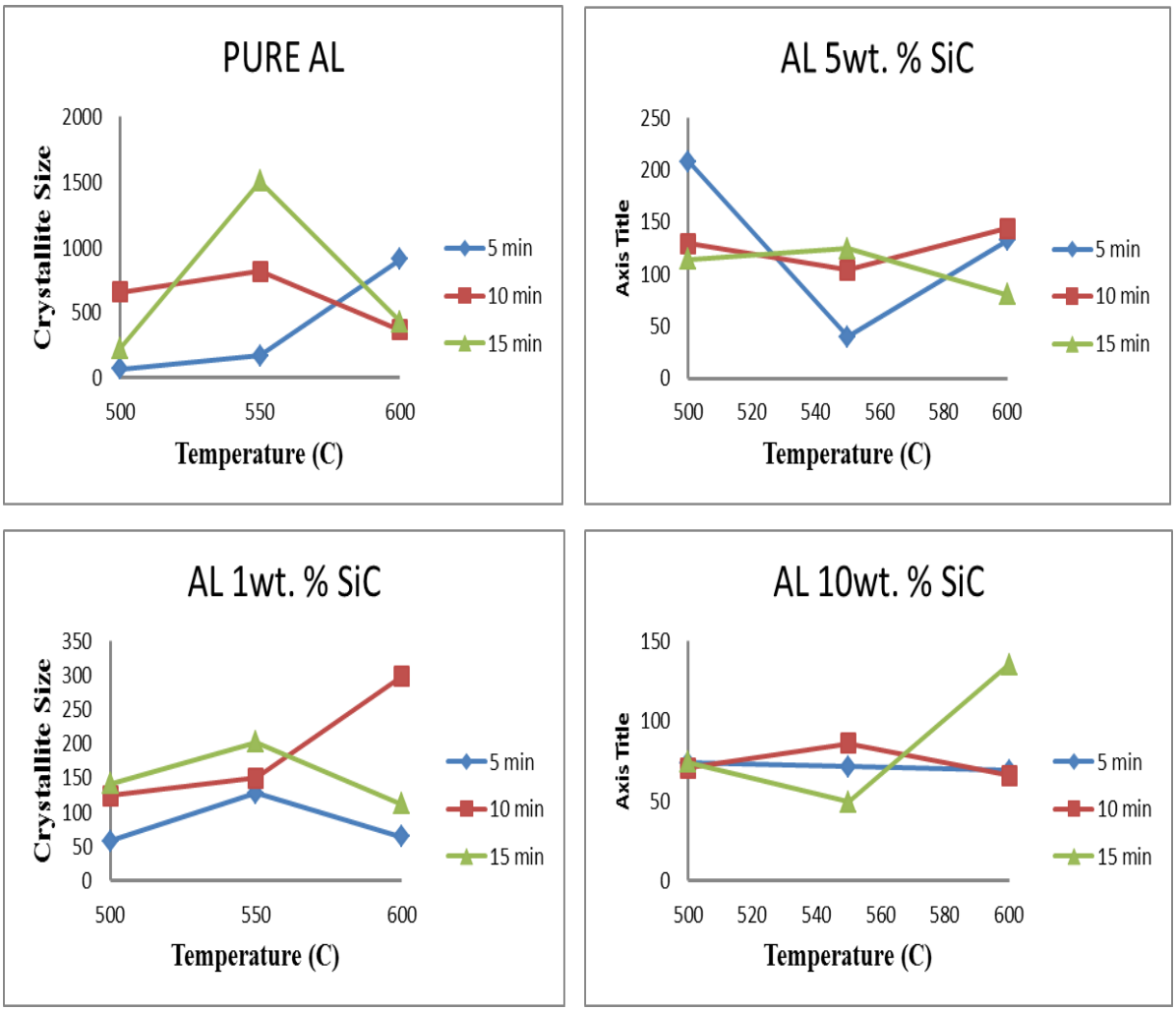


Fig. 4.37 Crystallite size of sintered composite plotted against temperature at different holding time

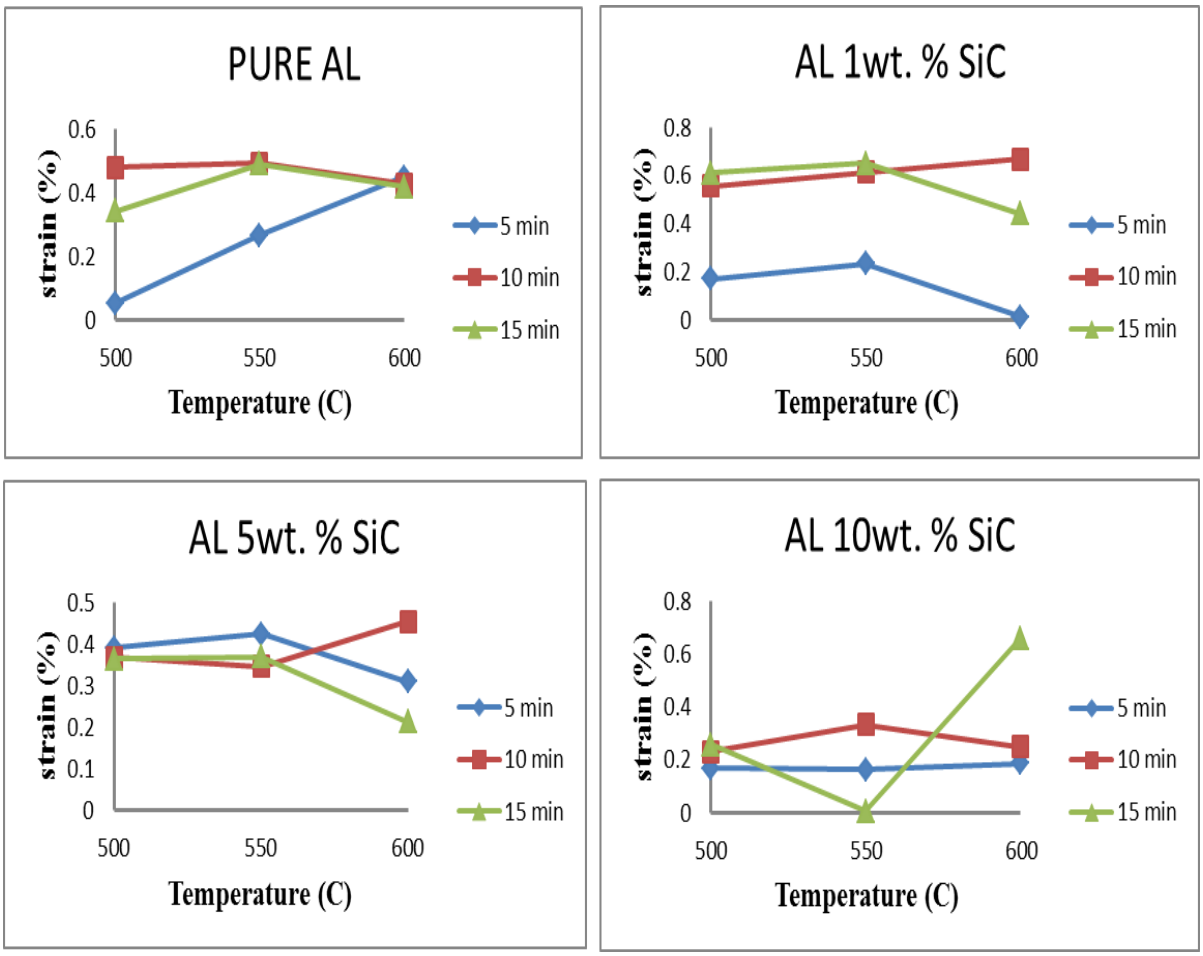


Fig. 4.38 Strain of sintered composite plotted against temperature at different holding time

The XRD analysis was focused on the composites sintered at the best set of parameters ($600^0$C, 50MPa, $200^0$C/min and 10 min.). The XRD spectra of these composites (Fig. 4.39) show that secondary phases were not formed due to sintering; the peaks are simply those of aluminium. A similar observation was seen in [20, 68, 83]. Phase composition remains unaltered after sintering at all parameters. It can be seen that only 10 wt % SiC composite spectra show, but very little peak of SiC (Fig. 4.39). A similar observation was seen in [83]. Similar observation was seen after milling. It is also seen from the spectra that as the amount of SiC increase the peaks intensity becomes shorter and broader. This implies that smaller crystallite size induced by SiC enhancement of mechanical milling is still maintained. The Crystallite size of composites sintered at the best set of parameters before and after sintering is shown in Table 4.2 along with some reference values.

Table 4.2 Crystallite size of sintered composite before and after sintering

| composites | Sintering condition | Crystallite size before sintering (nm) | Crystallite size after sintering (nm) | Ref. |
|---|---|---|---|---|
| Al -10 wt% SiC | SPS, 600 C, 50MPa, 10 min. | 32 | 66 | This work |
| Al -5 wt% SiC | SPS, 600 C, 50MPa, 10 min. | 50 | 144 | This work |
| Al -1 wt% SiC | SPS, 600 C, 50MPa, 10 min. | 140 | 298 | This work |
| Pure Al | SPS,600 C, 50MPa, 10 min. | 298 | 366 | This work |
| Al -6 wt% SiC | CIP, 640 C, 700MPa, 1 h. | 69 | 350 | [72] |
| Al -1.2 wt% SiC | CIP, 640 C, 700MPa, 1 h. | 63 | 150 | [72] |
| Al- 10 SiC-CNT, | Hot pressing for 1.5h, 550 C | 32 | 43 | [79] |
| Al- 5 SiC-CNT, | Hot pressing for 1.5h, 550 C | 34 | 45 | [79] |
| Pure Al | Hot pressing for 1.5h, 550 C | 141 | 183 | [79] |
| Al-5356/B4C | SPS, 500 C, 50MPa, 5 min | 36 | 92 | [69] |

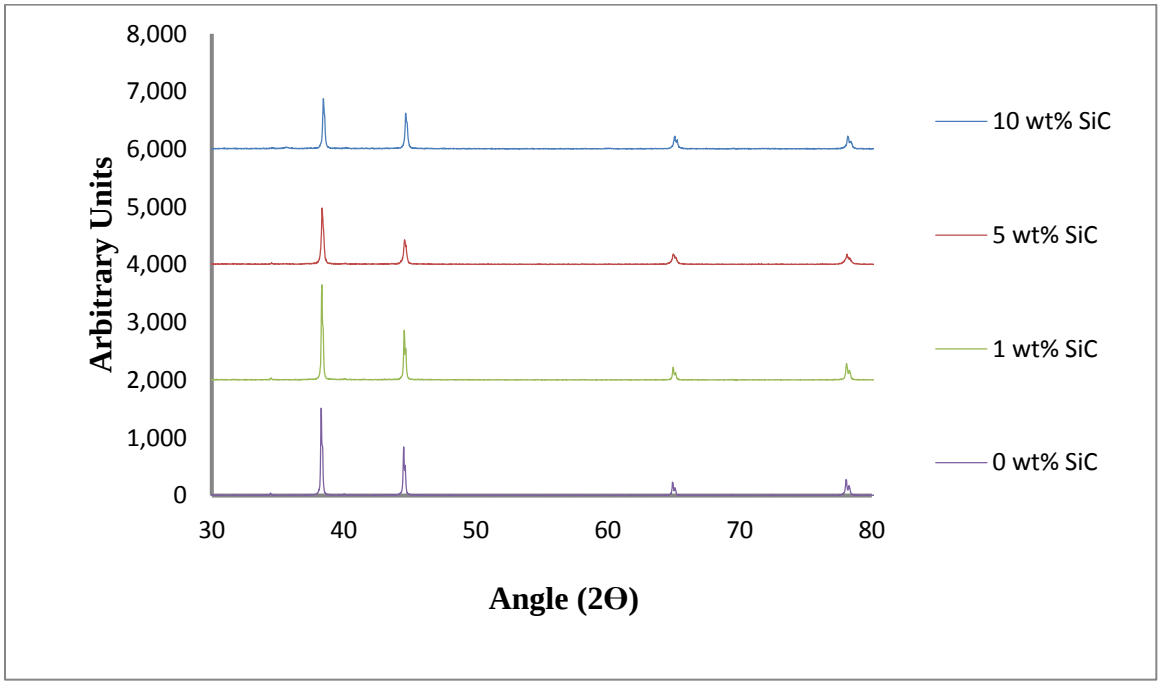


Fig. 4.39 XRD spectra of composites sintered at $600^0$C, 50MPa, $200^0$C/min and 10 min

### 4.2.5 SiC Dispersion

Samples with best sintering parameters have been selected for x-ray mapping to verify SiC dispersion in Al matrix. The uniform dispersion reported by x-ray mapping of milled powders remain so and confirmed by the mapping of sintered samples as can be seen in Fig. 4.40, Fig. 4.41 and Fig. 4.42. This implies that the sintering process didn't alter the uniform dispersion of SiC in Al matrix. A constant number of frames was maintained during mapping. That is why it is seen from the figures that as we move from Fig. 4.40 to Fig. 4.42, Si and C dots increase in agreement with the amount of SiC originally put into each composite; Al – 1wt% SiC, Al – 5wt% SiC and Al – 10wt% SiC respectively. This implies that SPS is highly better than the conventionl sintering techniques. For instance the consolidation of Al reinforced with 1.2, 6, and 8.2 wt% [72] by CIP led to particles clustering. The average reinforcement size became larger than its original value.

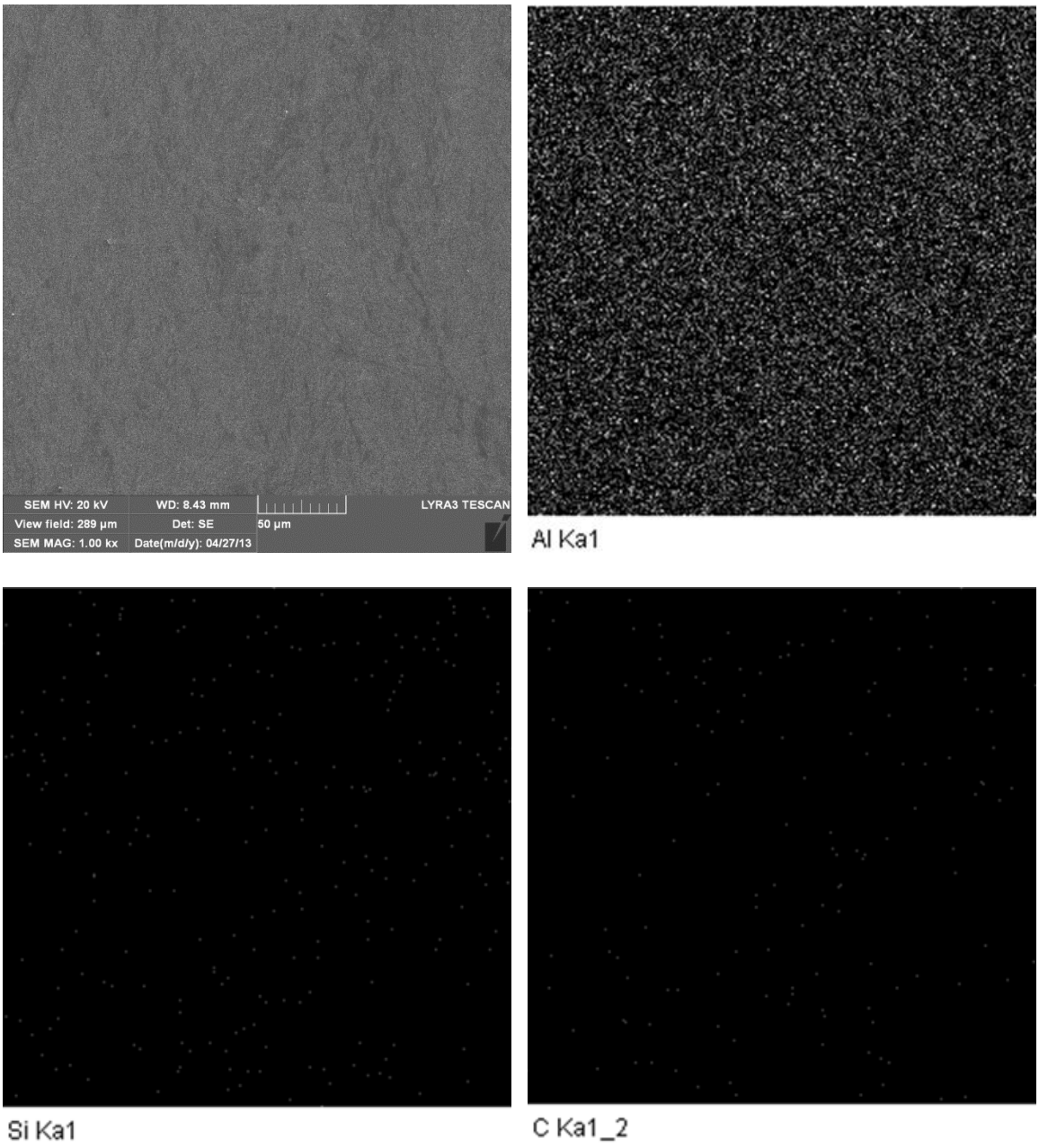


Fig. 4.40 X-ray mapping of Al – 1wt% SiC sintered at $600^0$C, 50MPa, $200^0$C/min for 10 minutes

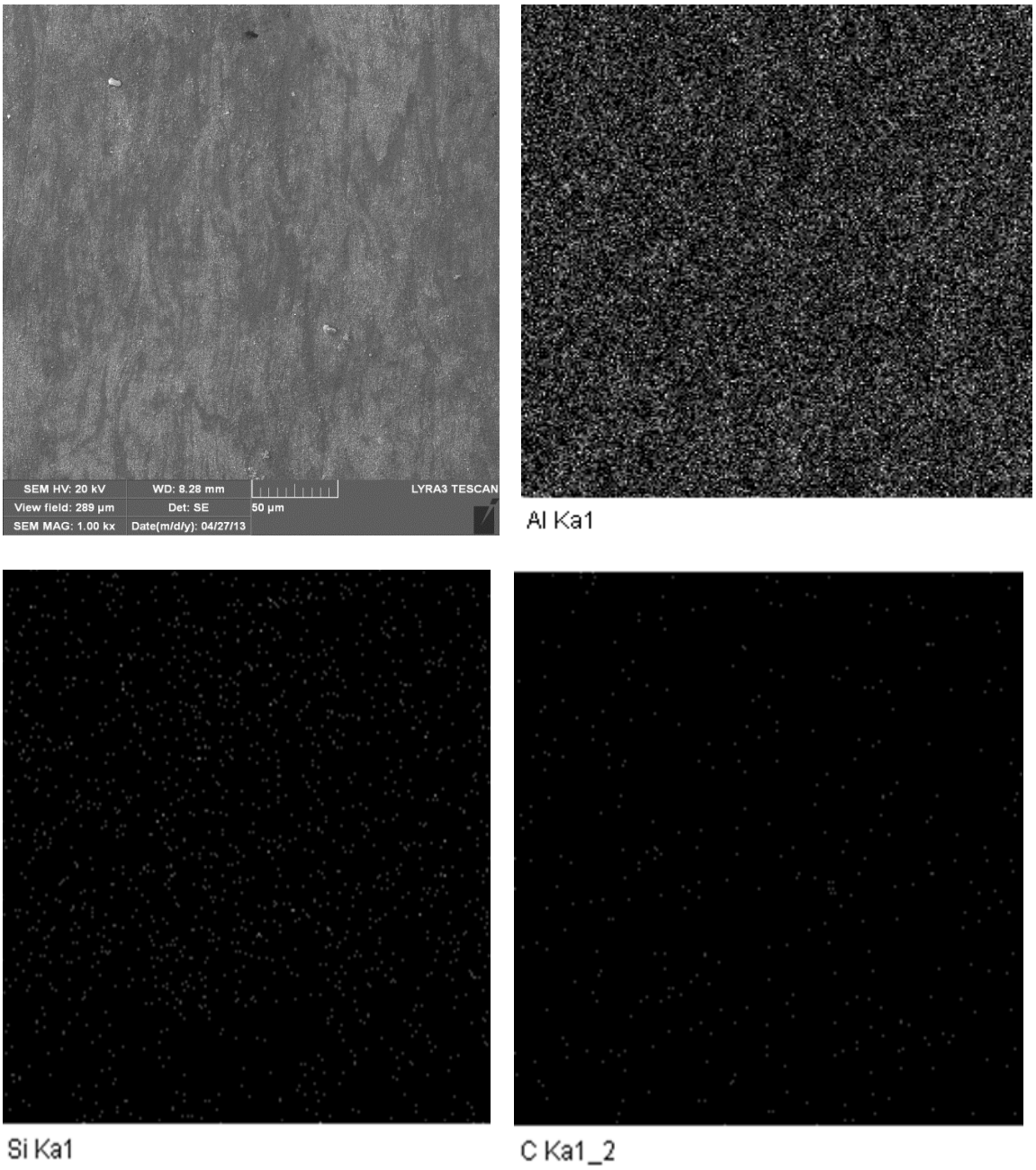


Fig. 4.41 X-ray mapping of Al – 5wt% SiC sintered at $600^0$C, 50MPa, $200^0$C/min for 10 minutes

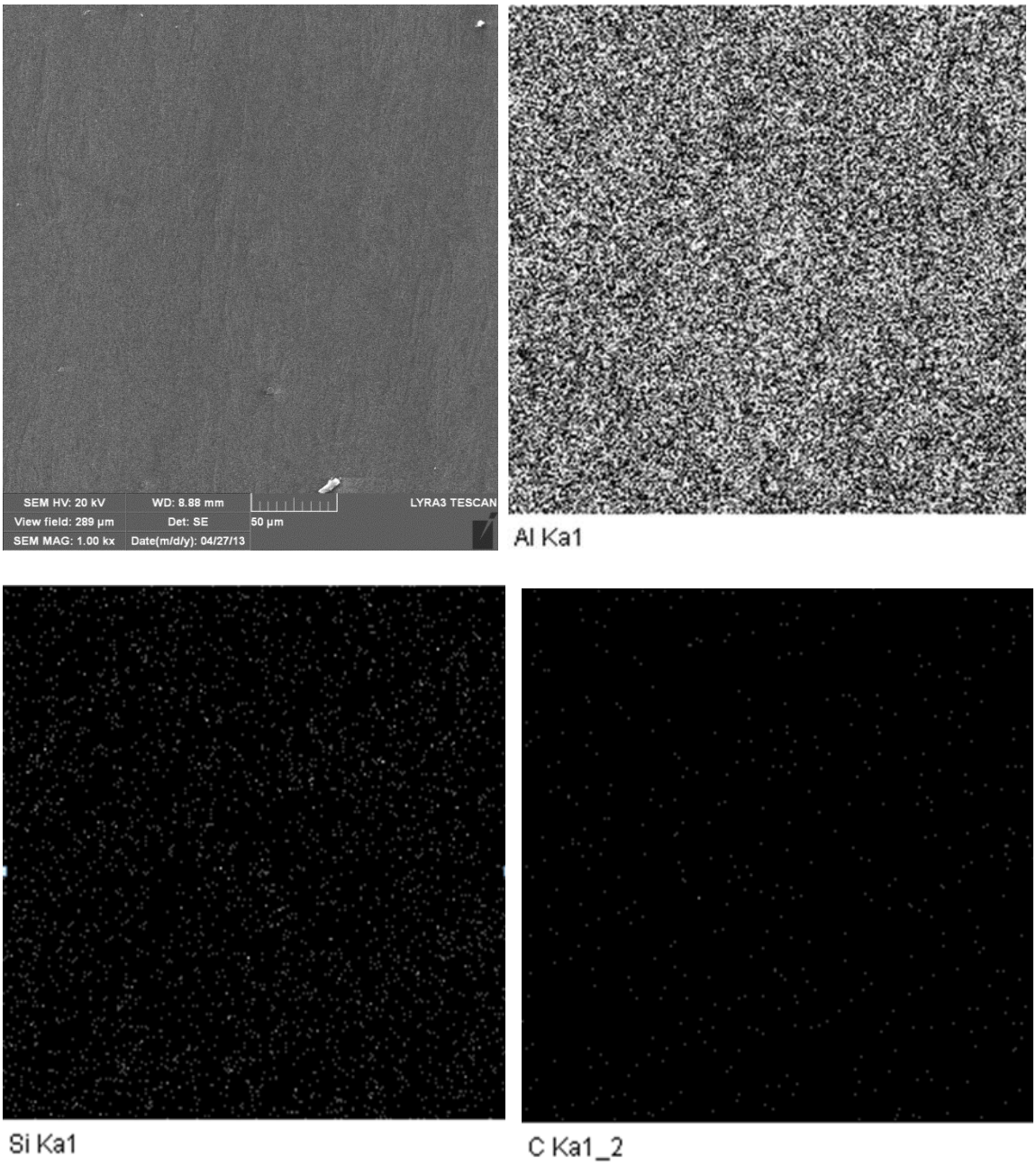


Fig. 4.42 X-ray mapping of Al – 10wt% SiC sintered at $600^0$C, 50MPa, $200^0$C/min for 10 minutes

### 4.2.6 Compressive Properties

The compressive properties of composites were estimated theoretically and measured experimentally. The best processing parameters i.e. sintering temperature of $600^0$C, sintering time of 10 minutes, pressure of 50MPa, and heating rate of $200^0$C/min were selected to prepare samples for compression test. However, challenges were faced sintering the composites because compressive test required samples with greater height than those used for previous characterization. Greater mass of powder samples and the chosen parameters made partial melting to occur. This led to die breakage and incomplete sintering. To overcome this problem, sintering temperature was limited to $550^0$C and time increased to 15 minutes. Axial compressive force was applied to every sample till it fractured. Increase in strength to about 200% was achieved with Al-10wt% SiC. See Fig. 4.43 and Table 4.3 for the compressive properties variation with composites' SiC content. Compressive strength, yield stress and elastic modulus show direct proportion with SiC amount. However a fall in these properties was observed at 5wt%, making the compressive properties of Al -1wt% SiC higher than that of Al -5wt% SiC. The drop in compressive properties at 5wt% is analogous to the drop in hardness earlier noticed and explained in section 4.2.3. The densities and micrographs of Al -5wt% SiC showed more porosities than that of Al -1wt% SiC. This might have led to a drop in mechanical properties of Al -5wt% SiC. It is quite established from Fig. 4.43 and Table 4.3 that addition of any amount of SiC led to improvement in compressive properties of

Aluminium. Fig. 4.43 shows that the compressive properties obtained from the compressive test are in agreement with the hardness test results.

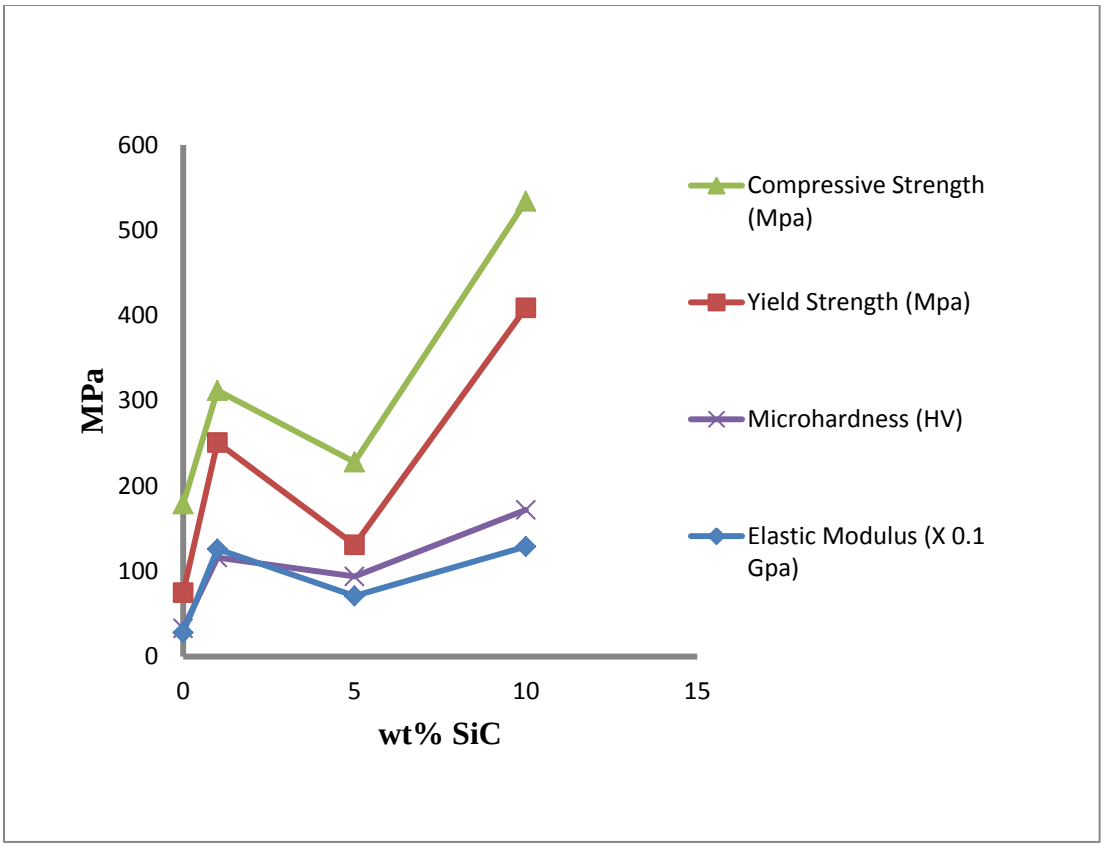


Fig. 4.43 Compressive properties as a function of SiC amount in the matrix of composites sintered at $550^0$C, 50MPa, $200^0$C/min for 15minutes.

Table 4.3 Compressive properties of composites including monolithic aluminium, sintered at $550^0$C, 50MPa, $200^0$C/min for 15minutes.

| Sample | Microhardness (HV) | E.Modulus (X 0.1Gpa) | Y.Strength (Mpa) | C. Strength (Mpa) | strain at failure(%) | % strength increase |
|---|---|---|---|---|---|---|
| Pure Al | 40 | 28 | 75 | 179 | - | 0 |
| Al-1wt% SiC | 116 | 126 | 251 | 312 | 7.5 | 74 |
| Al-5wt% SiC | 94 | 71 | 131 | 228 | 12 | 27 |
| Al-10wt% SiC | 172 | 129 | 409 | 534 | 7.2 | 198 |

There are several strengthening mechanisms in composites materials. As well, couple of theories have been put up by researchers to evaluate the strength of composites. However none of these theories include all the factors that enhance strengthening. Also only limited theories account for nanoscale composite materials. Some of the mechanisms of strengthening in composite include; solid solution strengthening , Orowan strengthening, strengthening due to grain size reduction (Hall Petch theory), and enhanced dislocation density strengthening [84]. Other means of strengthening include; load transfer from the matrix to the reinforcement and strain gradient-strengthening [85]. The effectiveness of the load transfer mechanism depends on the interfacial bonding between the matrix and the reinforcement (Al and SiC). Bathula et al [68] explained that the strengthening effect in Al-SiC nanocomposites is as a result of dislocation pile ups like Orowan grain boundaries strengthening effect. Indirect strengthening as a result of difference between the thermal conductivities of the metal matrix and reinforcement particles leads to formation of dislocations during thermal hardening processes [86]. With adequate interfacial bonding, SiC presence delay crack propagation. Uniform dispersion of SiC in the matrix is needed for

this mechanism to be efficient; Fig. 4.40 to Fig. 4.42 showed that dispersion is adequately achieved in the present work. Also milling of powders has led to successful grain size reduction as seen earlier. Hence the developed composites will be strengthened according to Hall Petch principle. The following are strengthening theories developed based on one or more of the mentioned mechanisms:

Orowan and Hall Petch theory combined in one equation: Kamrani etal. [72] used Eqn. 4.1 to evaluate the theoretical yield strength of Al (42μm) reinforced with SiC (50nm). The composites were fabricated by double stage CIP. The materials and size of the matrix and reinforcement used are almost similar to those used in this study. Hence same model and constants were used to evaluate the yield strength of the composites. It enables the effect of matrix size, reinforcement size and volume fraction on strengthening to be accounted for. The constants used are given in Table 4.4. The grain sizes of the sintered composites were used as the matrix size.

$$\sigma = \sigma_0 + kD^{-\frac{1}{2}} + \left(\frac{\pi}{6V_f} - \frac{2}{3}\right)^{-\frac{1}{2}} * \frac{Gbln(d/b)}{\pi d\sqrt{1-v}} \qquad \text{Eqn. 4.1}$$

Table 4.4 Parameters used for estimation of the yield strength of Al-SiC composites [72].

| Parameter | Nomenclature | unit | Value |
|---|---|---|---|
| Inherent friction stress | $\sigma_0$ | Mpa | 15.7 |
| Constant of Hall-Petch equation | $k$ | Mpa.m$^{0.5}$ | 0.0725 |
| Reinforcement volume fraction | $V_f$ | unitless | 0-0.1 |
| Shear modulus | G | GPa | 26.4 |
| Burger's vector | b (nm) | nm | 0.286 |
| Reinforcement particle size | d (nm) | nm | 50-200 |
| Poisson's ratio | v | unitless | 0.34 |

This theory can also be used to evaluate the compressive strength of the composite. Compressive strength can be taken as yield stress at a plastic strain were fracture occurs. $\sigma_0$ is assigned 179 MPa, the experimental compressive strength of pure Al fabricated by spark plasma sintering.

The Rule Of Mixture (ROM) for particulate reinforced composites: A basic ROM is given in [87] where certain properties of a coarse particulate composite are considered dependent only on the relative amounts and properties of the individual constituents. The ROM for elastic modulus is therefore expressed as;

$$E_c = V_p E_p + V_m E_m \qquad \text{Eqn. 4.2}$$

Where $E$ represents elastic modulus, $V$ volume fraction and the subscripts $p$, $m$ and $c$ stand for particle, matrix and composites respectively. The rule holds with an assumption that the reinforcement is perfect and intact [88]. However some researchers [88, 89] have ascribed Eqn. 4.2 to fiber reinforced composites. Moreover it is stated in [87] that the equation is for coarse reinforcement. For these reasons, a modified ROM (Eqn. 4.3) [88]

for particulate reinforced composites shall be considered. It should be noted that the nano scale of reinforcement is not considered by this equation.

$$E_c = \frac{E_m(1 + 2sqV_p)}{1 - qV_p} \qquad \text{Eqn. 4.3}$$

where $q = \frac{(E_p/E_m)-1}{(E_p/E_m)+2s}$ and *s* is the particles average aspect ratio.

Also there is no widely accepted ROM for nanocomposites. As such the elastic modulus is further evaluated based on a ROM that included a term "$\eta$" known as strengthening efficiency coefficient (Eqn. 4.4). $\eta$ is a function of reinforcement aspect ratio and an approximate value of 0.1 is used for nanocomposites [90]. *X* stands for the composite property which can be elastic modulus, strength etc. Therefore compressive yield and fracture strength are evaluated with Eqn. 4.4 for Al-1, 5 and 10wt% SiC.

$$E_c = \eta X_p E_p + X_m E_m \qquad \text{Eqn. 4.4}$$

Based on the thermal mismatch between reinforcement and matrix and dislocation strengthening, a strain gradient-strengthening law was developed using Tailor's equation [85]. However the model was used to evaluate microscale composites properties without the consideration of matrix size effect.

Table 4.5 gives the Elastic modulus of composites based on the two modified ROM (Eqn. 4.3 and Eqn. 4.4) discussed. The value obtained using the ROM that put nanocomposite into consideration is lower and inverse in proportion to the amount of SiC. This may be due to the fact that $\eta$ taken to be 0.1 for nanocomposite is an underestimation. The

experimentally obtained value is quite less than the two ROM values. However it tends to vary proportionally with SiC except for 5 wt%. The reason for this observation was mentioned earlier. A trend of increase in elastic modulus with SiC amount is also seen in [79] where Al-CNT composite reinforced with 10 and 5 wt% SiC gave a modulus of 123 and 101 GPa respectively. Also in this reference the experimental value is far less than the theoretical ROM values of 201 and 182 GPa respectively. The high experimental elastic modulus obtained in [79] can be attributed to the fact that the composite is a dual reinforcement phase composites. Experimental compressive moduli less than the values obtained in this research are also reported in [91]. The maximum modulus obtained for Al2124-CNT and Al6061-CNT nanocompistes are 9.5 and 3 GPa respectively compared to a value of 13 GPa obtained in this work.

Table 4.5 Theoretical and experimental values of the elastic modulus of composites

| composite | $V_f$ | E, Al (Gpa) | E, SiC (Gpa) | Aspect ratio | q | $E_c$ (Gpa) Eqn. 4.3 | $E_c$ (Gpa) Eqn. 4.4 | $E_c$ (Gpa) EXP. |
|---|---|---|---|---|---|---|---|---|
| Al-10wt% SiC | 0.085 | 69 | 410 | 10 | 0.1905 | 92.98 | 66.61 | 12.9 |
| Al-5wt% SiC | 0.042 | 69 | 410 | 15 | 0.1375 | 81.54 | 67.81 | 7.1 |
| Al-1wt% SiC | 0.008 | 69 | 410 | 13 | 0.1547 | 71.43 | 68.76 | 12.6 |

| Composite | Processing information | $E_c$ (Gpa) | Reference |
|---|---|---|---|
| Al-10vol% SiC-10vol%CNT | HP, $550^0$C, 1.5 h | 123 | [79] |
| Al-5vol% SiC-10vol%CNT | HP, $550^0$C, 1.5 h | 101 | [79] |
| Al2124-2wt% CNT | SPS, $450^0$C, 35 MPa, 15min. | 9.5 | [91] |
| Al2124-1wt% CNT | SPS, $450^0$C, 35 MPa, 15min. | 7.5 | [91] |
| Al2124 | SPS, $450^0$C, 35 MPa, 15min. | 4.5 | [91] |
| Al6061-2wt% CNT | SPS, $450^0$C, 35 MPa, 15min. | 3 | [91] |
| Al6061-1wt% CNT | SPS, $450^0$C, 35 MPa, 15min. | 3 | [91] |
| Al6061 | SPS, $450^0$C, 35 MPa, 15min. | 1.5 | [91] |

The theoretical and experimental compressive yield strength of composites are given in Table 4.6 where Eqn. 4.1 column is value obtained by combine Orowan and Hall Petch theory and Eqn. 4.4 column is for value obtained by modified ROM. The values obtained by ROM are very less compared to the orowan and Hall petch and the experimental values. Again $\eta$ taken to be 0.1 for nanocomposite is small. The experimental values find close comparison with the Orowan and Hall Petch theory results. 409 MPa for Al -10wt% SiC is a bit less than the theoretical value. This can be attributed to the fact that Al -10wt% SiC is not fully densified. Al -5wt% SiC yield stress is very lower than the theoretical value because of an observation that has been mentioned earlier. This observation is uniform throughout. As for Al -1wt% SiC the experimental value is higher than the theoretical value due to the fact that it is fully dense. Also the combined Orowan

and Hall Petch theory didn't include some other strengthening effect that might have increased the theoretical values.

Table 4.6 Theoretical and experimental values of the compressive yield strength of composites

| composite | $V_f$ | Grain size | $\sigma_y$ SiC (MPA) | $\sigma_y$ Al (MPA) | Y.S(Mpa) Eqn. 4.1 | Y.S(Mpa) Eqn. 4.4 | Y.S(Mpa) EXP. |
|---|---|---|---|---|---|---|---|
| Al-10wt% SiC | 0.085 | 4.90E-08 | 12500 | 75 | 474 | 175 | 409 |
| Al-5wt% SiC | 0.042 | 1.25E-07 | 12500 | 75 | 310 | 125 | 131 |
| Al-1wt% SiC | 0.008 | 2.01E-07 | 12500 | 75 | 216 | 85 | 251 |

| Composite | Processing information | Y.S (MPa) | Reference |
|---|---|---|---|
| Al-8.2wt% SIC | CIP, $640^0$C, 700 MPa, 1 h | 269 | [72] |
| Al-6wt% SIC | CIP, $640^0$C, 700 MPa, 1 h | 258 | [72] |
| Al-1.2wt% SIC | CIP, $640^0$C, 700 MPa, 1 h | 207 | [72] |

In Table 4.7, experimentally and theoretically evaluated compressive strength (σcs c) via two theories (combined Orowan and Hall Petch and ROM) are compared The values obtained from rule of mixture is a bit less than the ones obtained from combined Orowan and Hall Petch theory. They are also lower than the experimental results except for Al -5wt% SiC whose experimental value is lower than the two theories results. The Orowan and Hall Petch theory can be regarded to be more accurate because it takes into consideration several strengthening mechanism unlike the ROM which uses only material properties and volume fractions. The values obtained through combined Orowan and Hall Petch theory are compared with the experimental result. For Al -10wt% SiC, theoretical value is approximately equal to experimental value. Then for Al -5wt% SiC, theoretical

value is higher based on a uniform observation throughout this work. And for Al -1wt% SiC the experimental value is higher. This observation is expected for Al -10wt% SiC however, it didn't attain full densification like Al -1wt% SiC. The theory underestimated Al -1wt% SiC compressive strength because of some strengthening mechanisms (e.g strain gradient strengthening etc.) not accounted for by the combined Orowan and Hall Petch theory.

Table 4.7 Theoretical and experimental values of the compressive strength of composites

| composite | $V_f$ | Grain size | $\sigma_{cs}$ Al (MPa) | $\sigma_{cs}$ SiC (MPa) | $\sigma_{cs}$ c (MPa) Eqn. 4.1 | $\sigma_{cs}$ c (MPa) Eqn. 4.4 | $\sigma_{cs}$ c (MPa) Exp. |
|---|---|---|---|---|---|---|---|
| Al-10wt% SiC | 0.085 | 4.90E-08 | 3900 | 179 | 535 | 497 | 534 |
| Al-5wt% SiC | 0.042 | 1.25E-07 | 3900 | 179 | 372 | 337 | 228 |
| Al-1wt% SiC | 0.008 | 2.01E-07 | 3900 | 179 | 278 | 210 | 312 |

| Composite | Processing information | $\sigma_{cs}$ c, (MPa) | Reference |
|---|---|---|---|
| Al-8.2wt% SIC | CIP, 640 C, 700 MPa, 1 h | 448 | [72] |
| Al-6wt% SIC | CIP, 640 C, 700 MPa, 1 h | 436 | [72] |
| Al-1.2wt% SIC | CIP, 640 C, 700 MPa, 1 h | 385 | [72] |

For further investigation, the fractured surface images of the composites were taken with SEM (Fig. 4.44). All the structures can be said to fracture between brittle and dimple fracture mode; that is neither totally brittle nor ductile. The composites with greater compressive strength (Al -1 and 10wt% SiC) tend to have more brittle fracture surface (Fig. 4.44 a and c). Al -5wt% SiC has lower strength therefore its fracture surface is more ductile or dimple-like (See Fig. 4.44 b). It looks like shear ductile fracturing. The

microstructure of the three composites showed that the sample is fully sintered unlike what was observed in [78], where original powder morphology was observed on fractured surface of pure Al sintered at $550^0$C and below.

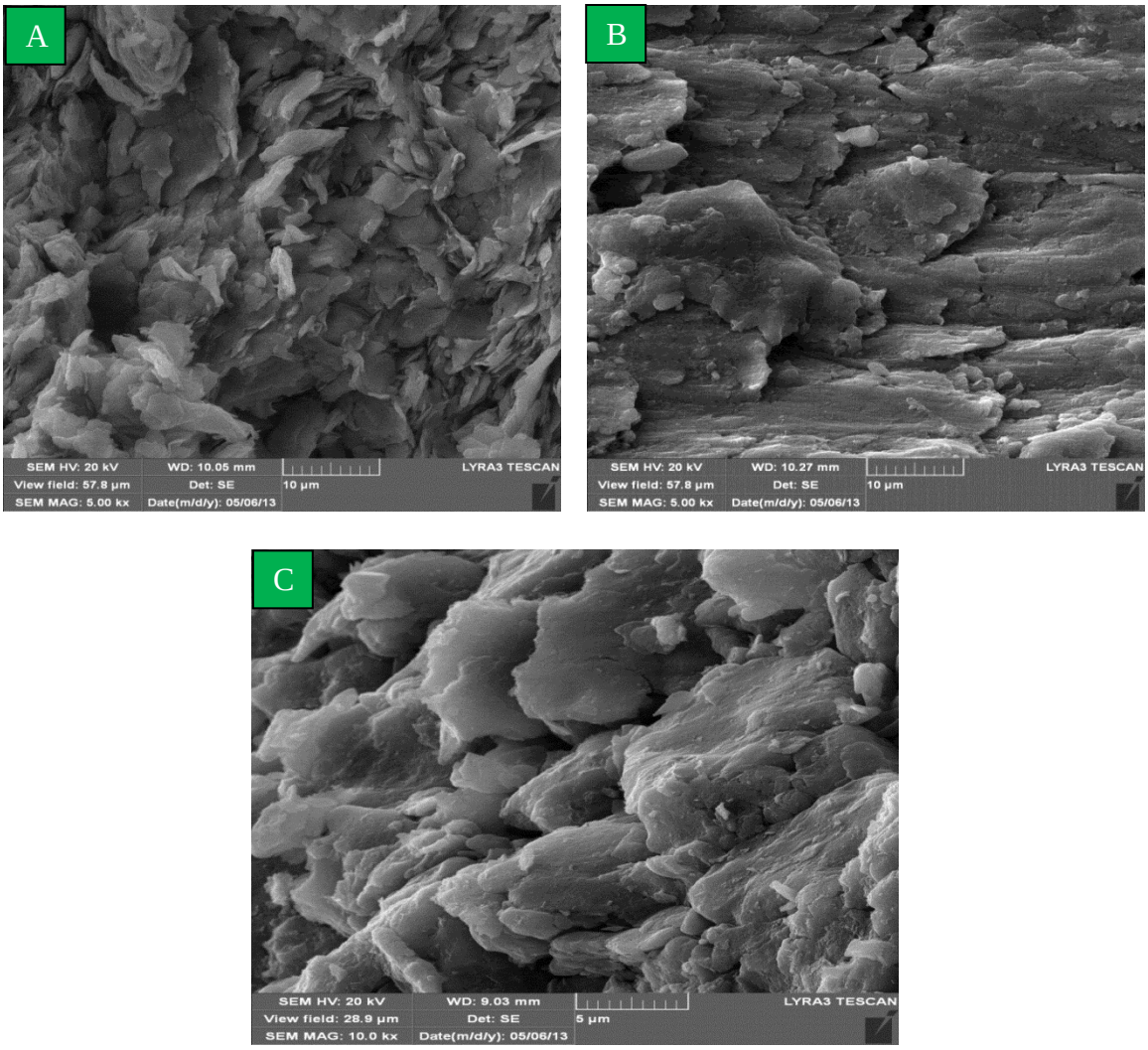


Fig. 4.44 SEM images showing fracture surfaces of (a) Al–1wt%SiC (b) Al–5wt%SiC and (c) Al–10wt%SiC composites, sintered at $550^0$C, 50MPa, $200^0$C/min for 15minutes.

# CHAPTER 5

# CONCLUSIONS AND RECOMMENDATIONS

## 5.1 Conclusions

Homogenous Al-SiC nanocomposite powders were developed through ball milling and consolidated through spark plasma sintering process. The effect of milling time on the crystallite size and lattice strain of the aluminum matrix and the dispersion of SiC nanoparticles in the ball milled nanopowders was investigated. The densification, microstructure, and mechanical properties of the consolidated nanocomposites were evaluated as function of SiC content and sintering parameters i.e. sintering pressure, temperature, and time; and heating rate. It was found that milling for 24 hours led to uniform dispersion of SiC nanoparticles in the Al matrix. Also, the presence and amount of SiC reinforcement enhanced the milling effect. Increasing milling time decreased the crystallite size and increased the lattice strain of the aluminum matrix. The uniform dispersion of SiC achieved by ball milling was maintained in sintered samples. XRD analysis showed that sintering pressure increase may not necessarily lead to grain growth since under some sintering conditions the crystallite size decreased as pressure was increased. For some of the composites, the crystallite size of the matrix decreased with the increase of the heating rate. The XRD spectra of the sintered nanocomposites did not reveal the formation of secondary phases. Sintering pressure and heating rate enhanced the densification and increased the hardness but the effect of heating rate was minor. The increase in sintering temperature and time led to the increase of density and hardness but

a drop occurred after 10 min. The highest microhardness and density were obtained at sintering pressure of 50MPa, sintering temperature of $600^0$C, sintering time of 10 minutes and heating rate of 2000 $^0$C/min. A microstructure with unique needle-like or elongated grains was observed in samples sintered at 50 MPa for 10 minutes regardless the values of sintering temperature and heating rate. The presence of SiC nanoparticles contributed to restricting grain growth. The increase of SiC to 10 wt% increased composite's hardness by 421%, compressive strength by 198%, yield strength by 445% and elastic modulus by 361%.

## 5.2 Recommendations

The present work led to the development of homogenous Al-SiC nanocomposites through ball milling and spark plasma sintering and characterization of their microstructure and mechanical properties. Further microstructural and mechanical characterization of the developed materials is recommended. This may include:

- TEM characterization of the microstructure to investigate the formation of secondary phases, interface between matrix and reinforcement and SiC dispersion.
- Further characterization of developed materials through XRD.
- Evaluation of mechanical properties as function of sintering parameters.
- Investigation of the wear and friction behaviors of the nanocomposites.

# REFERENCES


[1] P. Rohatgi and B. Schultz, "Lightweight Metal Matrix Nanocomposites-Stretching the Boundaries of Metals," *Material Matters,* vol. 2, pp. 16-19, 2007.

[2] T. Rostamzadeh, H. R. Shahverdi, A. Shanaghi, and T. Shahrabi, "EIS Study of Bulk Al-SiC Nanocomposite Prepared by Mechanical Alloying and the Hot Press Method," *Advanced Materials Research,* vol. 83-86, pp. 1297-1305, 2009.

[3] Z. Sadeghian, B. Lotfi, M. H. Enayati, and P. Beiss, "Microstructural and mechanical evaluation of Al–TiB2 nanostructured composite fabricated by mechanical alloying," *Journal of Alloys and Compounds,* vol. 509, pp. 7758-7763, 2011.

[4] C. Suryanarayana, "Synthesis of nanocomposites by mechanical alloying," *Journal of Alloys and Compounds,* vol. 509, pp. S229-S234, 2011.

[5] H. Yu, "Processing Routes for Aluminum based Nano-Composites," Worcester Polytechnic Institute, 2010.

[6] N. Ramakrishnan, "An analytical study on strengthening of particulate reinforced metal matrix composites," *Acta Materialia,* vol. 44, pp. 69-77, 1996.

[7] C. Borgonovo, D. Apelian, and M. Makhlouf, "Aluminum nanocomposites for elevated temperature applications," *JOM Journal of the Minerals, Metals and Materials Society,* vol. 63, pp. 57-64, 2011.

[8] V. Yadav, "Spark plasma sintering of aluminum matrix composites," Oklahoma State University, 2011.

[9] J. Lan, Y. Yang, and X. Li, "Microstructure and microhardness of SiC nanoparticles reinforced magnesium composites fabricated by ultrasonic method," *Materials Science and Engineering: A,* vol. 386, pp. 284-290, 2004.

[10] Y. Yang, J. Lan, and X. Li, "Study on bulk aluminum matrix nano-composite fabricated by ultrasonic dispersion of nano-sized SiC particles in molten aluminum alloy," *Materials Science and Engineering: A,* vol. 380, pp. 378-383, 2004.

[11] T. Rostamzadeh and H. Shahverd, "MICROSTRUCTURE STUDY ON AL-5% SiC NANOCOMPOSITE POWDERS," *Iranian Journal of Materials Science and Engineering,* vol. 8, pp. 32-39, 2011.

[12] Y. Saberi, S. Zebarjad, and G. Akbari, "On the role of nano-size SiC on lattice strain and grain size of Al/SiC nanocomposite," *Journal of Alloys and Compounds,* vol. 484, pp. 637-640, 2009.

[13] M. Singla, D. D. Dwivedi, L. Singh, and V. Chawla, "Development of aluminium based silicon carbide particulate metal matrix composite," *Journal of Minerals & Materials Characterization & Engineering,* vol. 8, pp. 455-467, 2009.

[14] C. Suryanarayana and N. Al-Aqeeli, "Mechanically alloyed nanocomposites," *Progress in Materials Science,* 2012.

[15] M. Sadeghi and J. Mahmoudi, "Experimental and Theoretical Studies on the Effect of Die Temperature on the Quality of the Products in High-Pressure Die-Casting Process," *Advances in Materials Science and Engineering,* vol. 2012, 2012.

[16] K. A. Gujba," Development and characterization of carbon nanotubes (CNTs) and silicon carbide (SiC) reinforced al-based nanocomposites," ProQuest Dissertations and Theses, pp. 156. 2012.

[17] U. Anselmi-Tamburini, J. Garay, Z. Munir, A. Tacca, F. Maglia, and G. Spinolo, "Spark plasma sintering and characterization of bulk nanostructured fully

stabilized zirconia: Part I. Densification studies," *Journal of materials research*, vol. 19, pp. 3255-3262, 2004.

[18] A. Khalil, " Synthesis and wear behavior of aluminum 6061 alloy reinforced with carbon nanotubes," ProQuest Dissertations and Theses, pp. 129. 2012.

[19] A. Csanády, I. Sajó, J. Lábár, A. Szalay, K. Papp, G. Balaton, and E. Kálmán, "Al–Pb nanocomposites made by mechanical alloying and consolidation," *Current Applied Physics*, vol. 6, pp. 131-134, 2006.

[20] N. Al-Aqeeli, K. Abdullahi, A. Hakeem, C. Suryanarayana, T. Laoui, and S. Nouari, "Synthesis, characterisation and mechanical properties of SiC reinforced Al based nanocomposites processed by MA and SPS," 2012.

[21] A. M. K. Esawi, K. Morsi, A. Sayed, M. Taher, and S. Lanka, "Effect of carbon nanotube (CNT) content on the mechanical properties of CNT-reinforced aluminium composites," *Composites Science and Technology*, vol. 70, pp. 2237-2241, 2010.

[22] J. Zhang, L. Wang, L. Shi, W. Jiang, and L. Chen, "Rapid fabrication of Ti3SiC2–SiC nanocomposite using the spark plasma sintering-reactive synthesis (SPS-RS) method," *Scripta Materialia*, vol. 56, pp. 241-244, 2007.

[23] J. Zhang, T. Wu, L. Wang, W. Jiang, and L. Chen, "Microstructure and properties of Ti3SiC2/SiC nanocomposites fabricated by spark plasma sintering," *Composites Science and Technology*, vol. 68, pp. 499-505, 2008.

[24] Y. Yang and X. Li, "Ultrasonic cavitation-based nanomanufacturing of bulk aluminum matrix nanocomposites," *Journal of manufacturing science and engineering*, vol. 129, pp. 252-255, 2007.

[25] M. Gupta, M. O. Lai, and C. Y. Soo, "Effect of type of processing on the microstructural features and mechanical properties of Al-Cu/SiC metal matrix composites," *Materials Science and Engineering: A*, vol. 210, pp. 114-122, 1996.

[26] L. Lü and M. O. Lai, *Mechanical alloying*: Kluwer Academic Publishers, 1998.

[27] H. Zoz, D. Ernst, and R. Reichardt, "High Energy Milling/Mechanical Alloying/Reactive Milling," 1998.

[28] M. Flores-Zamora, C. Martínez-Pérez, M. García-Guaderrama, I. Estrada-Guel, F. Espinosa-Magaña, and R. Martínez-Sánchez, "Comparative study of Al-Ni-Mo alloys obtained by mechanical alloying in different ball mills," *Rev. Adv. Mater. Sci*, vol. 18, pp. 301-304, 2008.

[29] D. L. Zhang, "Processing of advanced materials using high-energy mechanical milling," *Progress in Materials Science,* vol. 49, pp. 537-560, 2004.

[30] C. Suryanarayana, "Mechanical alloying and milling," *Progress in Materials Science,* vol. 46, pp. 1-184, 2001.

[31] J. S. Benjamin, "Mechanical alloying—A perspective," *Metal powder report,* vol. 45, pp. 122-127, 1990.

[32] http://www.imim-phd.edu.pl/contents/multifunctional.php [Online].

[33] D. Amador, "Morphological and microstructural characterisation of low-alloying Fe powder obtained by mechanical attrition," *Journal of Materials Processing Technology,* vol. 143-144, pp. 776-780, 2003.

[34] L. Di and H. Bakker, "Phase transformation of the compound V3Ga induced by mechanical grinding," *Journal of Physics: Condensed Matter,* vol. 3, p. 3427, 1991.

[35] A. A. El-Daly, M. Abdelhameed, M. Hashish, and W. M. Daoush, "Fabrication of silicon carbide reinforced aluminum matrix nanocomposites and characterization

of its mechanical properties using non-destructive technique," *Materials Science and Engineering: A,* vol. 559, pp. 384-393, 2013.

[36] J. Zhang, H. Shi, M. Cai, L. Liu, and P. Zhai, "The dynamic properties of SiCp/Al composites fabricated by spark plasma sintering with powders prepared by mechanical alloying process," *Materials Science and Engineering: A,* vol. 527, pp. 218-224, 2009.

[37] E. Mostaed, H. Saghafian, A. Mostaed, A. Shokuhfar, and H. R. Rezaie, "Investigation on preparation of Al–4.5%Cu/SiCp nanocomposite powder via mechanical milling," *Powder Technology,* vol. 221, pp. 278-283, 2012.

[38] D. R. Askeland, P. P. Fulay, and W. J. Wright, *The Science and Engineering of Materials: Si Edition*: Cl-Engineering, 2011.

[39] R. Orrù, R. Licheri, A. M. Locci, A. Cincotti, and G. Cao, "Consolidation/synthesis of materials by electric current activated/assisted sintering," *Materials Science and Engineering: R: Reports,* vol. 63, pp. 127-287, 2009.

[40] J. S. Moya, C. Baudín, and P. Miranzo, "Sintering," in *Encyclopedia of Physical Science and Technology (Third Edition)*, A. M. Editor-in-Chief: Robert, Ed., ed New York: Academic Press, 2003, pp. 865-878.

[41] J. R. Groza and A. Zavaliangos, "Sintering activation by external electrical field," *Materials Science and Engineering: A*, vol. 287, pp. 171-177, 2000.

[42] P. Figiel, M. Rozmus, and B. Smuk, "Properties of alumina ceramics obtained by conventional and non-conventional methods for sintering ceramics," *Journal of Achievements in Materials and Manufacturing Engineering*, vol. 48, 2011.

[43] M. Nygren and Z. Shen, "On the preparation of bio-, nano- and structural ceramics and composites by spark plasma sintering," *Solid State Sciences*, vol. 5, pp. 125-131, 2003.

[44] K. Vanmeensel, A. Laptev, O. Van der Biest, and J. Vleugels, "Field assisted sintering of electro-conductive ZrO2-based composites," *Journal of the European Ceramic Society*, vol. 27, pp. 979-985, 2007.

[45] D. P. Butt and B. Jaques, "Synthesis and Optimization of the Sintering Kinetics of Actinide Nitrides," United States, 2009.

[46] M. Omori, "Sintering, consolidation, reaction and crystal growth by the spark plasma system (SPS)," *Materials Science and Engineering: A*, vol. 287, pp. 183-188, 2000.

[47] http://sps.fdc.co.jp/whats/whats1.html [Online].

[48] B. S. Murty, P. Shankar, B. Rath, and J. Murday, *Textbook of Nanoscience and Nanotechnology*: Springer, 2012.

[49] W. Chen, U. Anselmi-Tamburini, J. E. Garay, J. R. Groza, and Z. A. Munir, "Fundamental investigations on the spark plasma sintering/synthesis process: I. Effect of dc pulsing on reactivity," *Materials Science and Engineering: A*, vol. 394, pp. 132-138, 2005.

[50] V. Mamedov, "Spark plasma sintering as advanced PM sintering method," *Powder Metallurgy*, vol. 45, pp. 322-328, 2002.

[51] D. M. Hulbert, A. Anders, D. V. Dudina, J. Andersson, D. Jiang, C. Unuvar, U. Anselmi-Tamburini, E. J. Lavernia, and A. K. Mukherjee, "The absence of plasma in “spark plasma sintering”," *Journal of Applied Physics*, vol. 104, pp. 033305-033305-7, 2008.

[52] U. Anselmi-Tamburini, S. Gennari, J. E. Garay, and Z. A. Munir, "Fundamental investigations on the spark plasma sintering/synthesis process," *Materials Science and Engineering: A,* vol. 394, pp. 139-148, 2005.

[53] A. Khalil, A. S. Hakeem, and N. Saheb, "Optimization of Process Parameters in Spark Plasma Sintering Al6061 and Al2124 Aluminum Alloys," *Advanced Materials Research,* vol. 328-330, pp. 1517-1522, 2011.

[54] N. Saheb, Z. Iqbal, A. Khalil, A. S. Hakeem, N. Al Aqeeli, T. Laoui, A. Al-Qutub, and R. Kirchner, "Spark Plasma Sintering of Metals and Metal Matrix Nanocomposites: A Review," *Journal of Nanomaterials,* vol. 2012, 2012.

[55] R. Ohser-Wiedemann, U. Martin, H. J. Seifert, and A. Müller, "Densification behaviour of pure molybdenum powder by spark plasma sintering," *International Journal of Refractory Metals and Hard Materials,* vol. 28, pp. 550-557, 2010.

[56] Z. A. Munir, U. Anselmi-Tamburini, and M. Ohyanagi, "The effect of electric field and pressure on the synthesis and consolidation of materials: A review of the spark plasma sintering method," *Journal of Materials Science,* vol. 41, pp. 763-777, 2006.

[57] S. Grasso, Y. Sakka, and G. Maizza, "Pressure Effects on Temperature Distribution during Spark Plasma Sintering with Graphite Sample," *Materials Transactions,* vol. 50, pp. 2111-2114, 2009.

[58] L.-h. Chai, Y.-y. Chen, L.-q. Zhang, and J.-p. Lin, "Effect of spark plasma sintering temperature on microstructure and mechanical properties of melt-spun TiAl alloys," *Transactions of Nonferrous Metals Society of China,* vol. 22, pp. 528-533, 2012.

[59] J. E. Garay, "Current-Activated, Pressure-Assisted Densification of Materials," *Annual review of materials research,* vol. 40, pp. 445-468, 2010.

[60] L. Wang, W. Jiang, L. Chen, and S. Bai, "Rapid reactive synthesis and sintering of submicron TiC/SiC composites through spark plasma sintering," *Journal of the American Ceramic Society,* vol. 87, pp. 1157-1160, 2004.

[61] L. Stanciu, V. Kodash, and J. Groza, "Effects of heating rate on densification and grain growth during field-assisted sintering of α-Al2O3 and MoSi2 powders," *Metallurgical and Materials Transactions A,* vol. 32, pp. 2633-2638, 2001.

[62] Y. Zhou, K. Hirao, Y. Yamauchi, and S. Kanzaki, "Effects of heating rate and particle size on pulse electric current sintering of alumina," *Scripta materialia,* vol. 48, pp. 1631-1636, 2003.

[63] Z. Shen, M. Johnsson, Z. Zhao, and M. Nygren, "Spark plasma sintering of alumina," *Journal of the American Ceramic Society,* vol. 85, pp. 1921-1927, 2002.

[64] H. Kwon and A. Kawasaki, "Effect of Spark Plasma Sintering in Fabricating Carbon Nanotube Reinforced Aluminum Matrix Composite Materials," *Advances in Composite Materials for Medicine and Nanotechnology*, ***Dr. Brahim Attaf (Ed.)***, pp. 429-444, 2011.

[65] Z. Sadeghian, B. Lotfi, M. Enayati, and P. Beiss, "Fabrication of bulk Al-TiB2 nanocomposite by spark plasma sintering of mechanically alloyed powder," in *Technical Proceedings of the NSTI Nanotechnology Conference and Expo, NSTI-Nanotech (Nanotech'10)*, 2010, pp. 107-110.

[66] F. C. Robles Hernández and H. A. Calderon, "Nanostructured Al/Al4C3 composites reinforced with graphite or fullerene and manufactured by mechanical milling and spark plasma sintering," *Materials Chemistry and Physics,* vol. 132, pp. 815-822, 2012.

[67] S. Nouari, "Spark Plasma Sintering of Al6061 and Al2124 Alloys," *Advanced Materials Research,* vol. 284, pp. 1656-1660, 2011.

[68] S. Bathula, R. C. Anandani, A. Dhar, and A. K. Srivastava, "Microstructural features and mechanical properties of Al 5083/SiCp metal matrix nanocomposites produced by high energy ball milling and spark plasma sintering," *Materials Science and Engineering: A,* vol. 545, pp. 97-102, 2012.

[69] R. Vintila, A. Charest, R. A. L. Drew, and M. Brochu, "Synthesis and consolidation via spark plasma sintering of nanostructured Al-5356/B4C composite," *Materials Science and Engineering: A,* vol. 528, pp. 4395-4407, 2011.

[70] B. Mouawad, M. Soueidan, D. Fabrègue, C. Buttay, V. Bley, B. Allard, and H. Morel, "Full Densification of Molybdenum Powders Using Spark Plasma Sintering," *Metallurgical and Materials Transactions A,* vol. 43, pp. 3402-3409, 2012.

[71] B. Prabhu, C. Suryanarayana, L. An, and R. Vaidyanathan, "Synthesis and characterization of high volume fraction Al–Al2O3 nanocomposite powders by high-energy milling," *Materials Science and Engineering: A,* vol. 425, pp. 192-200, 2006.

[72] S. Kamrani, R. Riedel, S. M. Seyed Reihani, and H. J. Kleebe, "Effect of Reinforcement Volume Fraction on the Mechanical Properties of Al--SiC Nanocomposites Produced by Mechanical Alloying and Consolidation," *Journal of Composite Materials,* vol. 44, pp. 313-326, 2009.

[73] A. A. El-Daly, M. Abdelhameed, M. Hashish, and A. M. Eid, "Synthesis of Al/SiC nanocomposite and evaluation of its mechanical properties using pulse echo overlap method," *Journal of Alloys and Compounds,* vol. 542, pp. 51-58, 2012.

[74] K. H. Chung, J. He, D. H. Shin, and J. M. Schoenung, "Mechanisms of microstructure evolution during cryomilling in the presence of hard particles," *Materials Science and Engineering: A,* vol. 356, pp. 23-31, 2003.

[75] O. M. Lemine, "Microstructural characterisation of nanoparticles using, XRD line profiles analysis, FE-SEM and FT-IR," *Superlattices and Microstructures*, vol. 45, pp. 576-582, 2009.

[76] S. A. Khadem, S. Nategh, and H. Yoozbashizadeh, "Structural and morphological evaluation of Al–5vol.%SiC nanocomposite powder produced by mechanical milling," *Journal of Alloys and Compounds,* vol. 509, pp. 2221-2226, 2011.

[77] H. Kwon, D. H. Park, Y. Park, J. F. Silvain, A. Kawasaki, and Y. Park, "Spark plasma sintering behavior of pure aluminum depending on various sintering temperatures," *Metals and Materials International,* vol. 16, pp. 71-75, 2010.

[78] G. Le, A. Godfrey, and N. Hansen, "Structure and strength of aluminium with sub-micrometer/micrometer grain size prepared by spark plasma sintering," *Materials & Design,* 2013.

[79] H. Kwon, S. Cho, M. Leparoux, and A. Kawasaki, "Dual-nanoparticulate-reinforced aluminum matrix composite materials," *Nanotechnology,* vol. 23, p. 225704, Jun 8 2012.

[80] A. Livesey, *The Repair of Vehicle Bodies*: Routledge, 2013.

[81] M. Kubota, "Properties of nano-structured pure Al produced by mechanical grinding and spark plasma sintering," *Journal of Alloys and Compounds,* vol. 434, pp. 294-297, 2007.

[82] H. Kaftelen, N. Ünlü, G. Göller, M. Lütfi Öveçoğlu, and H. Henein, "Comparative processing-structure–property studies of Al–Cu matrix composites reinforced with TiC particulates," *Composites Part A: Applied Science and Manufacturing,* vol. 42, pp. 812-824, 2011.

[83] S. Bathula, R. Anandani, A. Dhar, and A. Srivastava, "Synthesis and characterization of Al-alloy/SiCp nanocomposites employing high energy ball milling and spark plasma sintering," *Advanced Materials Research*, vol. 410, pp. 224-227, 2012.

[84] M. Munoz-Morris, C. Garcia Oca, and D. Morris, "An analysis of strengthening mechanisms in a mechanically alloyed, oxide dispersion strengthened iron aluminide intermetallic," *Acta Materialia*, vol. 50, pp. 2825-2836, 2002.

[85] L. Dai, Z. Ling, and Y. Bai, "A strain gradient-strengthening law for particle reinforced metal matrix composites," *Scripta materialia*, vol. 41, pp. 245-252, 1999.

[86] N. Chawla and Y.-L. Shen, "Mechanical behavior of particle reinforced metal matrix composites," *Advanced Engineering Materials*, vol. 3, pp. 357-370, 2001.

[87] D. R. Askeland, P. P. Fulay, and W. J. Wright, *The science and engineering of materials*: Thomson Engineering, 2011.

[88] C. Cayron, *TEM Study of Interfacial Reactions and Precipitation Mechanisms in Al 2O 3 Short Fiber Or High Volume Fraction SiC Particle Reinforced Al-4Cu-1Mg-0.5 Ag Squeeze-cast Composites*: Empa, 2001.

[89] F. L. Matthews and R. D. Rawlings, *Composite materials: engineering and science*: Woodhead Publishing, 1999.

[90] M. Kuo, C. Tsai, J. Huang, and M. Chen, "PEEK composites reinforced by nano-sized SiO< sub> 2</sub> and Al< sub> 2</sub> O< sub> 3</sub> particulates," *Materials Chemistry and Physics*, vol. 90, pp. 185-195, 2005.

[91] N. Saheb, "Compressive Behavior of Spark Plasma Sintered CNT Reinforced Al2124 and Al6061 Nanocomposites," *Advanced Materials Research*, vol. 652-654, pp. 33-37, 2013.

# VITAE

| | |
|---|---|
| **Name** | **ISMAILA KAYODE ALIYU** |
| **Nationality** | **Nigerian** |
| **Date of Birth** | 18/05/1980 |
| **Email** | ismaaelei@yahoo.com<br><br>ismaaelei@gmail.com |
| **Academic Background** | **M.Sc.(Mechanical Engineering), May, 2013**<br><br>*Specialized in Materials and Manufacturing.*<br><br>King Fahd University of Petroleum and Minerals (KFUPM), Dhahran, Saudi Arabia.<br><br>**B.Eng.(Mechanical Engineering), November, 2007**<br><br>*Specialized in Design and Production.*<br><br>University of Ilorin, Ilorin, Nigeria. |